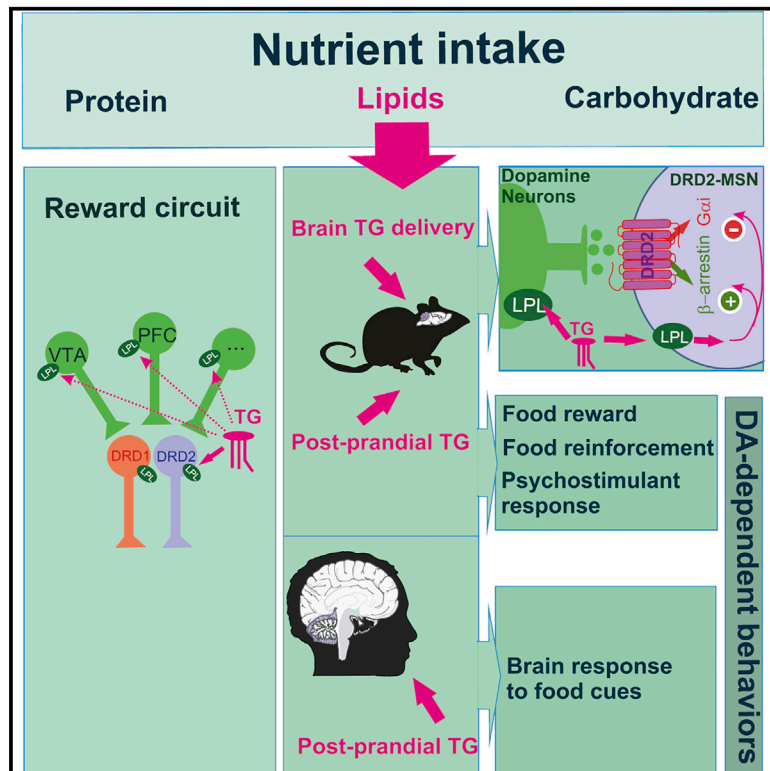


# Cell Metabolism

## Circulating Triglycerides Gate Dopamine-Associated Behaviors through DRD2-Expressing Neurons

### Graphical Abstract



### Authors

Chloé Berland, Enrica Montalban, Elodie Perrin, ..., Dana M. Small, Giuseppe Gangarossa, Serge H. Luquet

### Correspondence

giuseppe.gangarossa@u-paris.fr (G.G.),  
serge.luquet@univ-paris-diderot.fr (S.H.L.)

### In Brief

Dietary triglycerides (TGs) can gate dopamine receptor type 2 (DRD2)-expressing neurons' activity and dopamine-dependent behaviors. These results highlight a new physiological mechanism by which nutritional inputs can directly tune reward-associated behaviors and provide a new basis by which energy-rich diets may lead to (mal) adaptations in brain circuits that underlie compulsive behavior.

### Highlights

- Dopamine receptor type 2 (DRD2)-expressing neurons respond to dietary triglycerides (TGs)
- Dietary TGs modulate dopamine-dependent behaviors
- Lipoprotein lipase participates in the action of TGs on the reward circuit
- In humans, plasma TGs influence brain responses to food



# Circulating Triglycerides Gate Dopamine-Associated Behaviors through DRD2-Expressing Neurons

Chloé Berland,<sup>1,2</sup> Enrica Montalban,<sup>1</sup> Elodie Perrin,<sup>3,15</sup> Mathieu Di Miceli,<sup>4,15</sup> Yuko Nakamura,<sup>5,6,15</sup> Maud Martinat,<sup>4,15</sup> Mary Sullivan,<sup>5,6</sup> Xue S. Davis,<sup>5,6</sup> Mohammad Ali Shenasa,<sup>7</sup> Claire Martin,<sup>1</sup> Stefania Tolu,<sup>9</sup> Fabio Marti,<sup>9</sup> Stephanie Caille,<sup>8</sup> Julien Castel,<sup>1</sup> Sylvie Perez,<sup>3</sup> Casper Gravesen Salinas,<sup>11</sup> Chloé Morel,<sup>1</sup> Jacob Hecksher-Sørensen,<sup>10,11</sup> Martine Cador,<sup>8</sup> Xavier Fioramonti,<sup>4</sup> Matthias H. Tschöp,<sup>2,12,13</sup> Sophie Layé,<sup>4</sup> Laurent Venance,<sup>3</sup> Philippe Faure,<sup>9</sup> Thomas S. Hnasko,<sup>7,14</sup> Dana M. Small,<sup>5,6</sup> Giuseppe Gangarossa,<sup>1,16,\*</sup> and Serge H. Luquet<sup>1,5,16,17,\*</sup>

<sup>1</sup>Université de Paris, BFA, UMR 8251, CNRS, F-75014 Paris, France

<sup>2</sup>Helmholtz Diabetes Center, Helmholtz Zentrum München, German Research Center for Environmental Health, München, Neuherberg, Germany

<sup>3</sup>Center for Interdisciplinary Research in Biology, College de France, INSERM U1050, CNRS UMR 7241, Labex Memolife, 75005 Paris, France

<sup>4</sup>Université Bordeaux, INRA, Bordeaux INP, NutriNeuro, UMR 1286, F-33000 Bordeaux, France

<sup>5</sup>The Modern Diet and Physiology Research Center, New Haven, CT, USA

<sup>6</sup>Department of Psychiatry, Yale University School of Medicine, New Haven, CT, USA

<sup>7</sup>Department of Neurosciences, University of California, San Diego, La Jolla, CA, USA

<sup>8</sup>Université Bordeaux, Institut de Neurosciences Cognitives et Intégratives d'Aquitaine, CNRS, UMR5287, 33076 Bordeaux, France

<sup>9</sup>Sorbonne Université, CNRS UMR 8246, INSERM, Neurosciences Paris Seine, Institut de Biologie Paris-Seine, Paris, France

<sup>10</sup>Global Research, Novo Nordisk A/S, Måløv, Denmark

<sup>11</sup>Gubra ApS, Hørsholm Kongevej 11B, 2970 Hørsholm, Denmark

<sup>12</sup>Division of Metabolic Diseases, TUM, Munich, Germany

<sup>13</sup>Institute for Advanced Study, TUM, Munich, Germany

<sup>14</sup>Research Service VA San Diego Healthcare System, San Diego, CA 92161, USA

<sup>15</sup>These authors contributed equally

<sup>16</sup>Senior author

<sup>17</sup>Lead Contact

\*Correspondence: [giuseppe.gangarossa@u-paris.fr](mailto:giuseppe.gangarossa@u-paris.fr) (G.G.), [serge.luquet@univ-paris-diderot.fr](mailto:serge.luquet@univ-paris-diderot.fr) (S.H.L.)  
<https://doi.org/10.1016/j.cmet.2020.02.010>

## SUMMARY

Energy-dense food alters dopaminergic (DA) transmission in the mesocorticolimbic (MCL) system and can promote reward dysfunctions, compulsive feeding, and weight gain. Yet the mechanisms by which nutrients influence the MCL circuitry remain elusive. Here, we show that nutritional triglycerides (TGs), a conserved post-prandial metabolic signature among mammals, can be metabolized within the MCL system and modulate DA-associated behaviors by gating the activity of dopamine receptor subtype 2 (DRD2)-expressing neurons through a mechanism that involves the action of the lipoprotein lipase (LPL). Further, we show that in humans, post-prandial TG excursions modulate brain responses to

food cues in individuals carrying a genetic risk for reduced DRD2 signaling. Collectively, these findings unveil a novel mechanism by which dietary TGs directly alter signaling in the reward circuit to regulate behavior, thereby providing a new mechanistic basis by which energy-rich diets may lead to (mal)adaptations in DA signaling that underlie reward deficit and compulsive behavior.

## INTRODUCTION

Feeding results from a complex and dynamic integration of signals reflecting metabolic needs, but also cognitive, appetitive, and emotional drives, which collectively contribute to adaptive strategies to maintain caloric intake and body weight. The

### Context and Significance

The release of dopamine in the reward circuit is involved in the hedonic and motivational aspects of feeding. In susceptible individuals, the hedonic drive to consume palatable food can contribute to the obesity epidemic by promoting compulsive eating beyond metabolic needs. However, the physiological basis linking nutritional inputs to reward deficits is still unclear. In this work, we show that dietary triglycerides (TGs) can alter cell-type-specific processes within the reward circuit, thereby regulating food reward-related behaviors. This finding allows to directly bridge plasma lipids with the activity of dopamine-sensitive neurons in the reward circuit, hence providing new insights in the understanding of why and how lipid-rich food or chronically elevated plasma lipids may promote reward deficits and compulsive behaviors.



mesocorticolimbic dopamine (MCL-DA) circuitry encodes the reinforcing and motivational properties of food (Dallman et al., 2005; Di Chiara and Imperato, 1988; Volkow et al., 2012). DA neurons in the ventral tegmental area (VTA) and substantia nigra pars compacta represent a major source of DA in the dorsal and ventral striatum, where DA binds to receptors located on striatal medium-sized spiny neurons (MSNs). The DA receptors are G-coupled receptors associated with the  $G_{s\alpha/olf}$  protein for the D1 family (DRD1), or with the  $G_i$  protein for the D2 family (DRD2), thus forming two distinct populations, notably the DRD1- and DRD2-MSNs (Baik, 2013; Gerfen et al., 1990; Jackson and Westlind-Danielsson, 1994), which also dynamically integrate inputs from prefrontal cortex, thalamus, and limbic structures. DA release and signaling within the MCL system plays a pivotal role in reward prediction errors (Schultz, 2016), associative learning (Frank and Fossella, 2011), motor-planning, decision-making, and the attribution of incentive salience to reward-related stimuli (Berridge, 2009).

Converging lines of evidence have now clearly established that both overconsumption of palatable food and metabolic syndrome (obesity) drive maladaptive modifications within the MCL system. These dysfunctions lead to impulsivity (Adams et al., 2015; Babbs et al., 2013; Guo et al., 2014), altered hedonic and motivational drive, uncontrolled craving, and, ultimately, compulsive and addictive-like feeding (Johnson and Kenny, 2010; Michaelides et al., 2012; Vucetic and Reyes, 2010; Wang et al., 2001). For instance, high-fat-diet-induced impulsivity in rodents correlates with the magnitude of reduction in DRD2 but not DRD1 signaling (Adams et al., 2015), and genetic downregulation of striatal DRD2 leads to a reward-deficit state and compulsive eating in rats exposed to high-fat food (Johnson and Kenny, 2010). In humans, body mass index (BMI) is associated with striatal DRD2 redistribution and opportunistic eating behavior (Guo et al., 2014). Additionally, the inheritable genetic polymorphism TaqIA A1, which correlates in humans with a ~30%–40% decrease of striatal DRD2 abundance, creates a favorable substrate for uncontrolled feeding and obesity (Ritchie and Noble, 2003; Stice et al., 2015; Stice et al., 2008). Several observations suggest that nutritional fat might directly alter DA transmission independently of adiposity and BMI. Indeed, high-fat diet was shown to reduce DRD2 expression and DA turn-over, leading to decreased reward-seeking behaviors (Davis et al., 2008; Hryhorczuk et al., 2016; South and Huang, 2008), reduced cognitive function (Farr et al., 2008), and increased impulsivity (Adams et al., 2015). Triglycerides (TGs) represent a major source of available lipid substrates, and the transient increase of TG-rich particles after a meal is a naturally occurring physiological phenomenon. However, TGs are chronically high in obesity (Ruge et al., 2009). Post-prandial plasma TG levels predict body weight gain and uncontrolled feeding in rodents (Karatyayev et al., 2009) and promote cognitive impairments in obese mice (Farr et al., 2008). In humans, brain imaging studies have highlighted a correlation between circulating TGs and neuronal response to food reward (Sun et al., 2014). Several experiments using radio-labeled FFAs (free fatty acids) or TGs confirmed that both TGs and TG-rich particles cross the blood-brain barrier, being transported and locally metabolized in the brain (Banks et al., 2018; Cansell

et al., 2014). Collectively, these observations suggest that plasma TGs potentially act on DA signaling substrates to modulate reward. Finally, the rate-limiting enzyme of TG metabolism, the lipoprotein lipase (LPL), is expressed in rodents' brains (Ben-Zeev et al., 1990; Bessesen et al., 1993; Eckel and Robbins, 1984; Goldberg et al., 1989; Paradis et al., 2004). The activity of central LPL has been associated with body weight control and reward-drive behavior (Cansell et al., 2014; Picard et al., 2013; Wang et al., 2011). These observations raise the possibility that post-prandial LPL-mediated hydrolysis of TG-rich particles in the MCL could play a role in high-fat-diet-induced adaptations within the reward circuitry (Berland et al., 2016).

Here, we provide evidence supporting a key role of dietary TG-induced adaptations in DRD2-expressing neurons. First, in both human and mouse brains, *Lpl* mRNA is present in the mesocorticolimbic structures, including in VTA DA neurons and striatal MSNs. Second, using *in vivo* brain-specific TG delivery and *ex vivo* whole-cell patch-clamp recordings, we provide multiple lines of evidence indicating that circulating TGs act within the reward system to gate the excitability and cellular responses of DRD2-expressing neurons. Third, central TGs can act as a direct reinforcer and regulate reward-seeking and other dopamine-dependent behaviors. Fourth, we use functional magnetic resonance imaging (fMRI) to show that TG levels are associated with altered region-specific brain activity to food-related cues. Importantly, and in line with our mouse data, these associations are sensitive to genetic variations affecting DRD2-dependent signaling. Collectively, these findings reveal a previously unappreciated mechanism by which dietary TGs can act directly in the MCL system to regulate DRD2-expressing neurons' activity and reward-seeking behaviors.

## RESULTS

### The TG-Processing Enzyme Lipoprotein Lipase Is Expressed in Both Mouse and Human Mesocorticolimbic Structures

Pioneering studies have shown that *Lpl* mRNA is expressed in rodent brains (Ben-Zeev et al., 1990; Bessesen et al., 1993; Goldberg et al., 1989; Paradis et al., 2004). Here, we wondered whether *Lpl* mRNA was present in reward-related structures, namely the dorsal striatum (DS), the nucleus accumbens (NAc), and the VTA. Using fluorescent *in situ* hybridization we observed that *Lpl* mRNA co-localizes with a large portion of *Drd1*- and *Drd2*-expressing MSNs in the DS (Figure 1A) and the NAc, as well as in VTA *Th*-neurons (Figure S1B). *Lpl* mRNA expression data from available single-cell RNA sequencing atlas (Zeisel et al., 2018) or cell-type transcriptomic characterization of striatal neurons (Doyle et al., 2008) revealed that, in midbrain and striatal structures, *Lpl* mRNA was enriched in VTA DA neurons compared to local inhibitory neurons (Figure S1C), and in striatal DRD1- and DRD2-MSNs compared to striatal cholinergic interneurons (Figure 1B). In addition, expression data from the rodent and human Allen Brain Atlas (Hawrylycz et al., 2012; Lein et al., 2007) revealed that *Lpl* mRNA is expressed in the MCL of both species (Figures S1A and S1D).

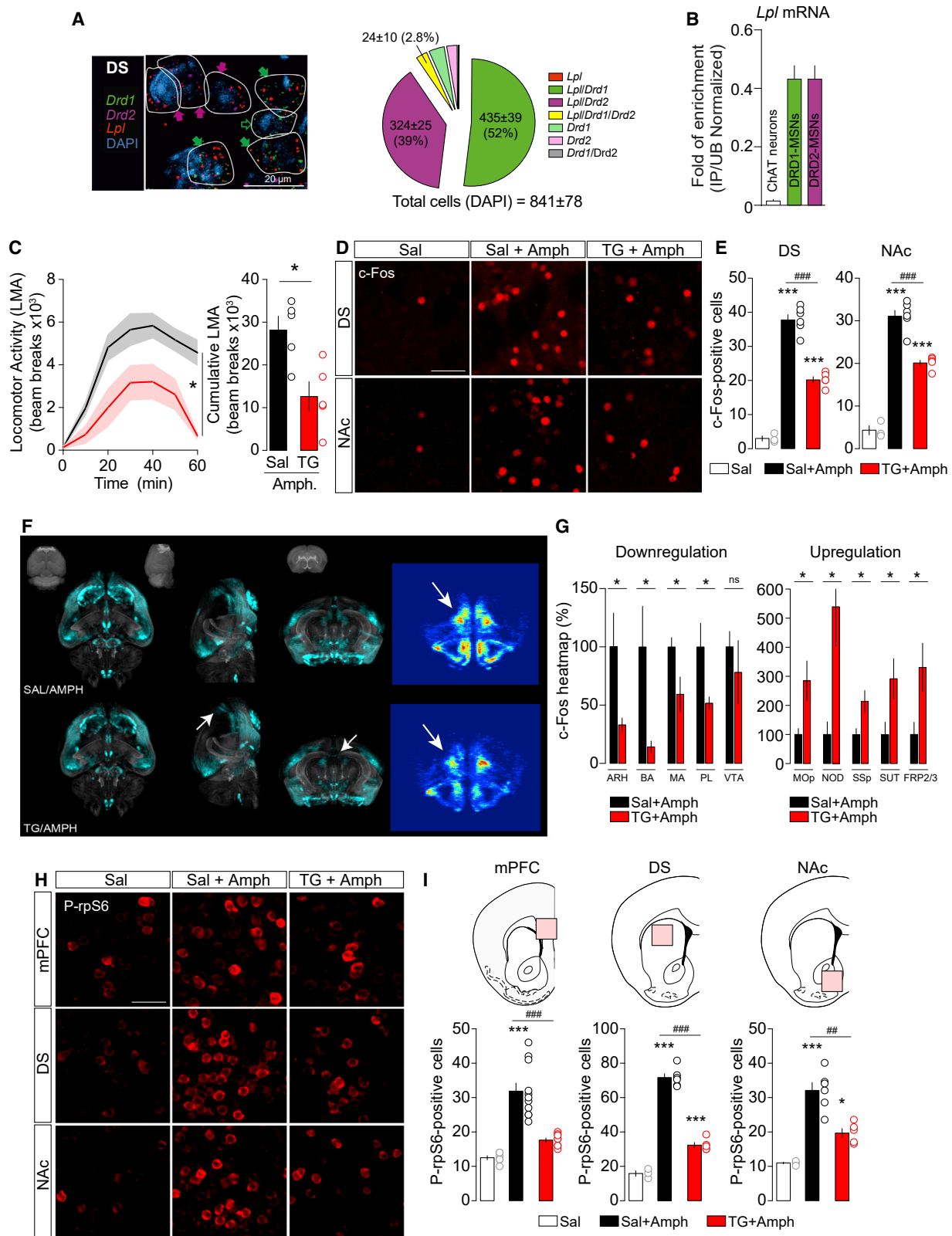


**Figure 1. Striatal TG Metabolism Decreases Amphetamine-Induced Behavioral and Molecular Adaptations**

(A) Representative photomicrographs and semiquantitative analysis of RNAscope fluorescence *in situ* hybridization (FISH) signal for Lipoprotein lipase (*Lpl*, red), dopamine receptor 1 and 2 (*Drd1* green, *Drd2* violet) in the dorsal striatum (DS). DAPI (blue) was used to identify cells. Scale bars: 20  $\mu$ m. The white lines represent

(legend continued on next page)



### Striatal TG Metabolism Decreases Amphetamine-Induced Behavioral and Molecular Adaptations

To decipher the central action of TGs respecting the physiological route by which nutrients access the brain, mice were perfused with TGs through an indwelling catheter into the carotid artery in the direction of the brain (Cansell et al., 2014). Here, we investigated whether TGs, or any derived metabolites, could be detected in the mouse striatum. C57Bl6/J mice received a 6 h saline or TG perfusion (0.1  $\mu$ l/min, Figure S2A), after which striata were dissected out for lipidomic analysis. Brain TG delivery significantly increased striatal content of TGs and metabolites (Figure S2B, Table S1, striatal FFAs and glycolipids content in Data S1 and S2), hence confirming that our experimental setting efficiently reproduces blood-to-brain TG entry and access to MCL structures.

Next, we investigated whether TG modulate the molecular activations induced by amphetamine (3 mg/kg). As we previously described (Cansell et al., 2014), TGs blunted the hyperlocomotor effects of amphetamine (Figure 1C), but also reduced the cellular c-Fos response evoked by amphetamine in both dorsal striatum and NAc (Figures 1D and 1E). In order to have a more global view of central TG-responsive structures, we also performed whole-brain c-Fos immunostaining using the iDISCO method (immunolabeling-enabled 3D imaging of solvent-cleared organs) coupled with light sheet microscopy (Figure 1F). Whole-brain heatmaps of c-Fos signal revealed a modulatory action of brain TG delivery on neural responses to amphetamine in anatomically distinct structures. In particular, whereas brain TG delivery enhanced neural responses to amphetamine in fronto-cortical regions, a blunted c-Fos induction was observed in several subcortical areas (Figure 1G). In line with the pattern of c-Fos activation, amphetamine-induced activation of the ribosomal protein S6 (rpS6 phosphorylation, Ser<sup>235/236</sup>), a marker of translational activity, was also dramatically decreased in the prefrontal cortex (mPFC), dorsal striatum, and the NAc (Figures 1H and 1I). Altogether, these results show that brain TG delivery inhibits amphetamine-induced neuronal activation and protein translation in reward-related structures.

### TGs Exert Modulatory Actions onto Dopamine Signaling and Behaviors

The above-mentioned results reveal that TGs may alter the ability of MSNs to integrate DA-dependent signals. We thus explored

whether central TG sensing was accompanied by alterations of key molecular pathways known to shape MSNs activity and be strongly modulated by DA (Beaulieu and Gainetdinov, 2011). Western blot analysis of striatal tissues revealed that brain TG delivery decreased p70S6K and rpS6 phosphorylation, at both mitogen-activated protein kinases (MAPK)-dependent (Ser<sup>235/236</sup>) and mammalian target of rapamycin (mTOR)-dependent (Ser<sup>240/244</sup>) sites, as well as extracellular signal-regulated kinase (ERK1/2) phosphorylation (Figures 2A and 2B). In addition, we found a reduction of phosphorylated DARPP-32<sup>Thr34</sup>, a direct protein kinase A (PKA)-dependent target. Interestingly, we also observed reduced levels of tyrosine hydroxylase (TH) phosphorylation, indicating a reduction in TH activity in the DA terminals that innervate the striatum (Lew et al., 1999; Salvatore et al., 2016) (Figures 2A and 2B).

Because DA signaling in MSNs can also trigger the PKB/Akt-GSK3 pathway, we explored Akt/GSK-3 $\beta$  signaling phosphorylation as a proxy for  $\beta$ -arrestin recruitment (Figures 2C and 2D). Akt phosphorylation remained unchanged at Thr<sup>308</sup>, but was significantly decreased at Ser<sup>473</sup>, while GSK-3 $\beta$  phosphorylation at Ser<sup>9</sup> was reduced (Figures 2E and 2F), indicating that this signaling pathway is activated following TG delivery (Beaulieu et al., 2004, 2005; Peterson et al., 2015). Indeed, a significant modulation of key phospho-proteins (p-rpS6, p-ERK1/2, p-DARPP-32, p-TH, and p-GSK-3 $\beta$ ) was also observed following multiple comparison corrections (see Table S5). Altogether, these results reveal that striatal TG sensing modulates MSNs signaling by decreasing canonical PKA-, MAPK-, and mTOR-dependent signaling while promoting  $\beta$ -arrestin-dependent Akt/GSK-3 $\beta$  signaling.

Next, to explore whether brain TG delivery exhibits an action on either DRD2- or DRD1-dependent behaviors, we assessed the consequences of brain TG delivery on behavioral and cellular responses triggered by pharmacological manipulation of DRD1 and DRD2 receptors. The hyperlocomotion triggered by a first or second injection of the DRD1 agonist SKF38393 (10 mg/kg) was similar between saline- or TG-perfused mice (Figure 2G). However, brain TG delivery was still fully efficient in reducing amphetamine-induced hyperlocomotion assessed on the same animals after the 2 consecutive days of SKF38393 treatment (Day 3, Figure 2H). Consistently, DRD1-dependent increase in striatal c-Fos remained unaffected by

the cellular limits. Filled and empty arrows within representative photomicrographs indicate co-expression or absence, respectively, of *Lpl* according to the presence of *Drd1* (green arrows) and *Drd2* (violet arrows) transcripts.

(B) Translating ribosome affinity purification (TRAP) technique (Doyle et al., 2008) reveals a specific enrichment of *Lpl* mRNA in medium spiny neurons (MSNs) as compared to cholinergic neurons in the striatum. Each immunoprecipitation (IP) is compared to the average of unbound (UB) samples from the same tissue to calculate a ratio of IP/UB as a measure of enrichment. IP/UB are represented for cholinergic, DRD1-, and DRD2-expressing MSNs.

(C) Amphetamine (Amph)-induced locomotor activity (LMA) and cumulative LMA after a 6-h saline (Sal, *n* = 5) or TG (TG, *n* = 5) central perfusion followed by amphetamine administration (3 mg/kg). Statistics: \**p* < 0.05 Sal versus TG.

(D and E) Representative confocal photomicrographs and quantification of c-Fos-positive cells in the dorsal striatum (DS) and the nucleus accumbens (NAc) of animals infused with saline and injected with saline (Sal, *n* = 3) or amphetamine (Sal+Amph, *n* = 6) and animals infused with TG and injected with amphetamine (TG+Amph, *n* = 5). Scale bars: 50  $\mu$ m. Statistics: \*\*\**p* < 0.001 Sal versus Sal+Amph or Sal versus TG+Amph; ###*p* < 0.001 Sal+Amph versus TG+Amph).

(F and G) Representative pictures showing whole-brain c-Fos-based signal and heatmaps quantification of brain structures in which central TG perfusion (TG/AMPH, *n* = 5) negatively or positively affect amphetamine-induced c-Fos response compared to controls (Sal/AMPH, *n* = 5). ARH: Arcuate hypothalamic nucleus, BA: Bed nucleus of the accessory olfactory tract, MA: Magnocellular nucleus, PL: Prelimbic area, VTA: Ventral tegmental area, Mop: Primary motor area, NOD: Nodulus (X), SSP: Primary somatosensory area, SUT: supratrigeminal nucleus, FRP2/3: Frontal pole, layer 2/3. Statistics: \**p* < 0.05 TG+Amph versus Sal+Amph.

(H and I) Representative confocal photomicrographs and quantification of phosphorylated ribosomal protein S6 (Ser<sup>235/236</sup>)-positive cells in the medial prefrontal cortex (mPFC), dorsal striatum (DS), and nucleus accumbens (NAc) of animals infused with saline and injected with saline (Sal, *n* = 3) or amphetamine (Sal+Amph, *n* = 6) and animals infused with TG and injected with amphetamine (TG+Amph, *n* = 5). Statistics: \*\*\**p* < 0.001 Sal versus Sal+Amph; ###*p* < 0.001 TG+Amph versus Sal+Amph, ##*p* < 0.01 TG+Amph versus Sal+Amph). For statistical details, see Table S5.

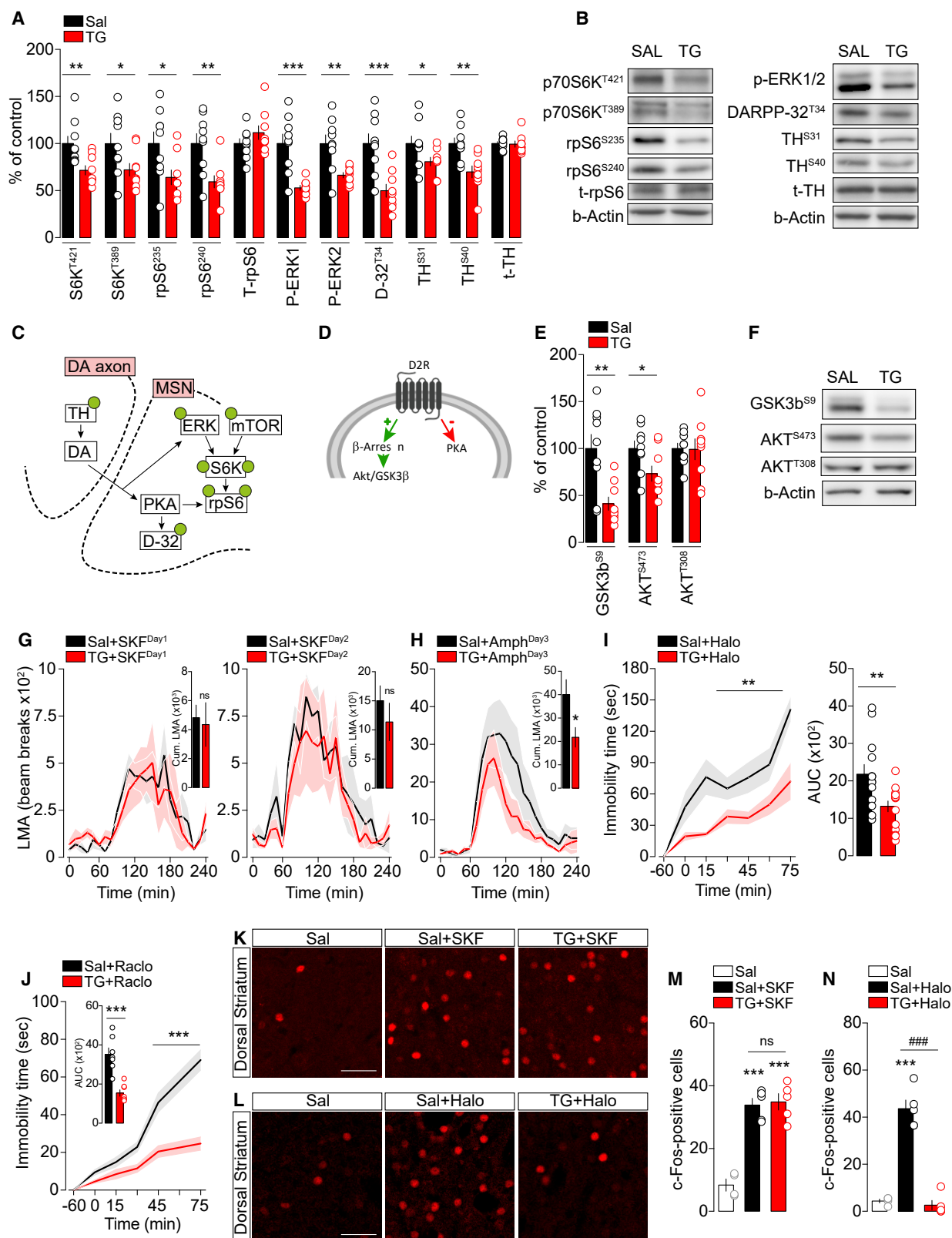


**Figure 2. Central TG Delivery Blunts DRD2-Dependent Striatal Signaling Pathways**

(A and B) Protein quantifications (A) and representative western blots (B) of signaling cascades classically downstream to dopamine receptors in the striatum after a 6-h central delivery of triglycerides (TG,  $n = 9$ ) or saline (Sal,  $n = 9$ ). Nomenclature: p70S6K (p70 ribosomal S6 kinase), rpS6 (ribosomal protein S6), t-rpS6 (total-

(legend continued on next page)

central TG delivery on a separate cohort of mice (Figures 2K and 2M).

In sharp contrast, brain TG delivery drastically reduced the cataleptic response triggered by two well-characterized DRD2 antagonists: haloperidol (0.5 mg/kg) or raclopride (0.6 mg/kg) (Figures 2I and 2J). As previously described (Bertran-Gonzalez et al., 2008), pharmacological blockade of DRD2 robustly increased the number of c-Fos- and rpS6-Ser<sup>235/236</sup>-positive neurons (putative DRD2-MSNs) in saline-treated animals, while this molecular response was dramatically reduced in mice receiving brain TG delivery (Figures 2L, 2N, S3A, and S3B). These results demonstrate that within the striatum, TGs preferentially impact DRD2-neuronal responses, possibly by reducing DRD2 signaling and/or DRD2-neurons excitability.

### Triglycerides Alter Excitability of DRD2-MSNs

The behavioral and cellular pharmacological responses mentioned above point to a particular role for DRD2-expressing neurons in sensing and/or responding to circulating TGs. To explicitly test this hypothesis, we used whole-cell patch-clamp recordings to determine active and passive membrane properties of both DRD1-MSNs (in *Drd1a*-tdTomato transgenic mice) and DRD2-MSNs (in *Drd2*-eGFP transgenic mice) in response to bath application of vehicle or triglyceride triolein at a concentration (4  $\mu$ M, 0.35 mg/dl) within the physiological range of cerebrospinal TGs (0.65  $\pm$  0.06 mg/dl, Banks et al., 2018). We assessed neuronal excitability in both the dorsal striatum and the NAc, and MSNs were recognized according to (1) fluorescence (tdTomato or eGFP, Figure 3A), (2) hyperpolarized resting membrane potentials, and (3) characteristic spiking profiles in response to current injections such as a marked inward rectification of the I/V relationship (Figure 3B).

Strikingly, in both striatal and accumbal structures, bath-applied triolein (~15–20 min, 4  $\mu$ M) further hyperpolarized the resting membrane potential (RMP) (Figures 3C and 3E) and increased the action potential rise time in DRD2-MSNs without significant influence in DRD1-MSNs (Figures 3D and 3F). Other parameters (for full list, see Tables S2 and S3) such as the membrane time constant and the action potential half width were modulated by triolein in striatal DRD2-MSNs (Figure S4, Table S2). Altogether, these results demonstrate that TGs selectively reduce the excitability of DRD2-MSNs.

To test whether DRD2-MSNs show reduced activity *in vivo*, we used fiber photometry to record real-time calcium transients in DRD2 neurons of behaving mice. Prior work has demonstrated

that DRD2-MSNs are transiently activated during action initiation (Cui et al., 2013). We thus used Cre-dependent expression of GCaMP6f in *Drd2*-Cre mice together with brain TG delivery in mice placed into a novel environment (new cage) (Figures 3G and 3H). We first used separate groups of C57BL/6 mice to assess the exact time window at which brain TG delivery started to inhibit spontaneous locomotor activity following exposure to a new cage. We found that the increase in exploratory drive to a new cage was similar between saline- or TG-perfused animals within the first ~10 min, becoming significantly reduced over the following 60 min (Figure S5). Therefore, in order to fully dissociate the action of TGs onto spontaneous locomotor activity from their effects on DRD2-MSNs calcium activity to novelty-induced exploration, we chose a 3-min window of exploration, which corresponds to the most intense period of activity in both experimental groups (Figure S5). Since DRD2-MSNs are transiently activated during action initiation (Cui et al., 2013), GCaMP-encoded calcium fluorescence was measured during the first 50 s of exploration. Transfer to a new cage was associated with a rapid and significant increase in DRD2-neurons calcium activity in saline-perfused mice (Figure 3I). Such increase was not significant in TG-perfused animals (Figure 3J). We then decided to analyze the dynamics of calcium transients during different temporal intervals (10 s/bin) of exploration (Figure 3K) and observed that the initial increase in exploration-evoked calcium signal in DRD2 neurons (B2 versus B1, TG-mice) decayed more rapidly in TG-perfused animals compared to control mice (Figure 3L). These *in vivo* results agree with the reduced excitability of DRD2-MSNs following *ex vivo* TG application, and further indicate that central TG delivery gates striatal DRD2-MSNs responses during behavior.

### Triglycerides Dynamically Influence Dopamine Neuron Activity

The above-mentioned results reveal that TGs rapidly influence DRD2-MSNs by modulating their activity and associated behavioral outputs. However, *Lpl* is also expressed in VTA DA neurons (Figure S1), thereby raising the question whether TGs may also modulate DA neurons. To test this hypothesis, we performed single-unit recordings of VTA DA neurons in anaesthetized mice during acute (<30 min) and long-term (6 h) brain TG delivery. We found that 10 min (Figure 4A) acute brain TG delivery did not affect the *in vivo* electrical activity of VTA DA neurons (Figure 4A). However, prolonged TG perfusion (5–6 h) led to a significant decrease in DA-neurons firing rate and burst activity

ribosomal protein S6), ERK (Extracellular-signal Regulated Kinase), DARPP-32 (32 kDa dopamine and cAMP regulated phosphoprotein), TH (tyrosine hydroxylase), t-TH (total-Tyrosine hydroxylase). Statistics: \* $p < 0.05$ , \*\* $p < 0.01$  and \*\*\* $p < 0.001$  TG versus Sal.

(C and D) Post-synaptic molecular signaling induced by DA in MSNs (C) and DRD2-specific signaling (D).

(E and F) Protein quantification (E) and representative western blots (F) of the Akt/GSK-3 $\beta$  pathway in the striatum. Nomenclature: GSK-3 $\beta$  (glycogen synthase kinase 3 $\beta$ ). Statistics: \* $p < 0.05$  and \*\* $p < 0.01$  TG versus Sal.

(G and H) Locomotor activity (LMA) induced by the DRD1 agonist SKF38393 (10 mg/kg) (G) and by amphetamine (3 mg/kg) (H) on 3 consecutive days after 6 h of central delivery of saline (Sal,  $n = 6$ ) or triglycerides (TG,  $n = 6$ ). Statistics: \* $p < 0.05$  TG+Amph<sup>Day3</sup> versus Sal+Amph<sup>Day3</sup>.

(I and J) Quantification of immobility time and area under the curve (AUC) induced by administration of haloperidol (0.5 mg/kg) (I) or raclopride (0.6 mg/kg) (J) after 6 h of central delivery of saline (Sal,  $n = 13$  for haloperidol,  $n = 7$  for raclopride) or triglycerides (TG,  $n = 15$  for haloperidol,  $n = 7$  for raclopride). Statistics: haloperidol (\*\* $p < 0.01$  TG+Halo versus Sal+Halo), raclopride (\*\*\* $p < 0.001$  TG+Raclo versus Sal+Raclo).

(K–N) Representative confocal photomicrographs in the dorsal striatum (K and L) and quantification of c-Fos-positive cells (M and N) 1 h after administration of the DRD1 agonist SKF38393 (K and M) or the DRD2 antagonist haloperidol (L and N) in saline- (Sal/SKF,  $n = 6$ , Sal/Halo,  $n = 5$ ) and TG-perfused mice (TG/SKF,  $n = 5$ , TG/Halo,  $n = 5$ ) compared to saline-treated animals (Sal/Sal,  $n = 3$ ). Scale bars: 50  $\mu$ m. Statistics: SKF38393 (\*\*\* $p < 0.001$  Sal+SKF or TG+SKF versus Sal), haloperidol (\*\*\* $p < 0.001$  Sal+Halo versus Sal, ### $p < 0.001$  TG+Halo versus Sal+Halo). For statistical details, see Table S5.

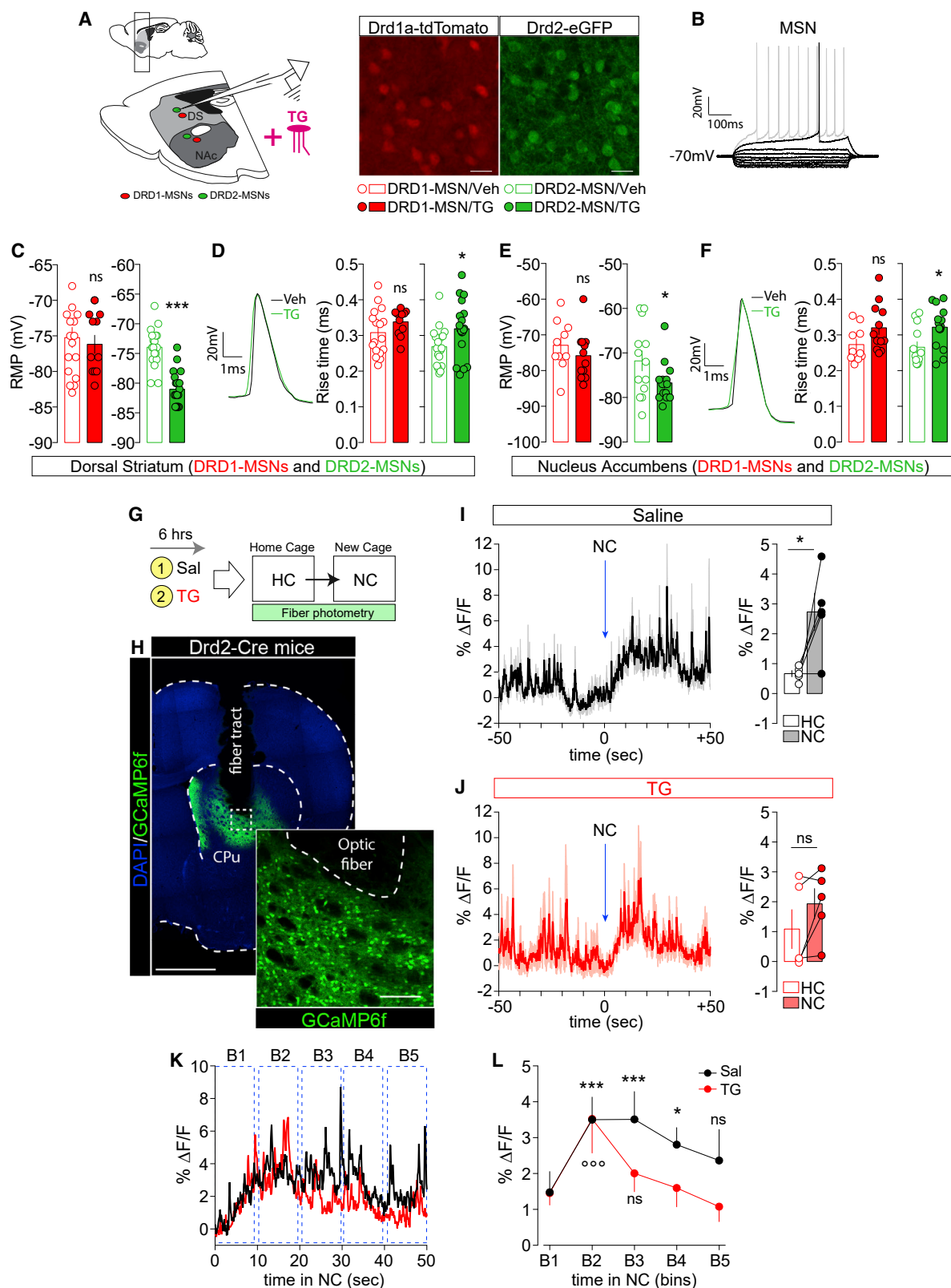


**Figure 3. Nutritional TGs Gate D2R-MSNs Activity In Vitro and In Vivo**

(A) Drawing indicates the sagittal slice used for whole-cell patch-clamp recording in Drd1a-tdTomato and Drd2-eGFP transgenic mice. Confocal images show DRD1-MSNs (red) and DRD2-MSNs (green) in the dorsal striatum (DS). Scale bars: 50  $\mu$ m.

(legend continued on next page)



(Figure 4B). This decrease in DA-neurons activity is consistent with the decreased phosphorylation of TH (Lindgren et al., 2001) observed in the striatum of TG-perfused mice (Figures 2A and 2B). These data show that sustained increase in TGs can reduce VTA DA-neurons activity in anaesthetized mice.

Next, we compared the consequences of acute and long-term (6 h) brain TG delivery on amphetamine-induced hyperlocomotion. Our results reveal that acute brain TG delivery decreased amphetamine-induced hyperlocomotion to a similar extent as observed following long-term brain TG delivery (Figures 4C and 4D). This result supports a mechanism by which central actions of TGs occur first in striatal structures, with later impacts on midbrain DA neurons.

### Central Triglycerides Can Act as Reinforcer and Modulate Food-Seeking Behavior

Given the time-dependent modulatory action of TGs onto pre- and post-synaptic components of the reward system, we next explored the rewarding properties of short- and long-term brain TG delivery. We first used the conditioned-place preference test (CPP) to assess whether short-term brain TG delivery could be reinforcing. We used an unbiased apparatus-biased protocol in which animals were first allowed to explore two defined compartments (pre-test) before enduring 8 days of conditioning sessions. The least-preferred compartment (pre-test) was associated with a 1-h brain TG delivery or saline control (Figure 5A). Following conditioning, animals were allowed to explore the two compartments during the post-test session. Importantly, the pre- and post-test sessions were performed without any central TG administration, so that exploration of the complete apparatus was not affected by the treatment. Animals conditioned with 1-h brain TG delivery displayed a significant preference for the compartment associated with TGs (Figure 5B). This result shows that central detection of TGs can serve as a direct positive reinforcer.

In order to further establish the reinforcing properties of centrally delivered TGs, we next used a self-administration paradigm for intracarotid TG delivery. Since self-administration paradigms generally require rapid perception of the reinforcer, we used a faster delivery of central TGs (each active nose-poke led to delivery of 10  $\mu$ l intracarotid TG bolus over 60 s compared to 0.1–0.3  $\mu$ l/min prior). We first verified that the increased rate of TG perfusion did not perturb general brain hemodynamics. Using photoacoustic imaging, we found no

major modifications in oxygenated hemoglobin and cerebral blood flow at rates of 1 or 10  $\mu$ l/min (data not shown). Thus, animals were placed in operant chambers equipped with two nose-poke holes, the active hole being paired with central infusion of TGs or saline, and the inactive hole without consequence (Figure 5C). While TG and saline groups exhibited equivalent discrimination scores, mice receiving TG infusions performed more active nose-poke visits in both food-sated and 24-h-deprived conditions compared to control animals (Figure 5D). These similar results observed in both sated and food-deprived conditions support the idea that the positive reinforcement of centrally detected TGs is not solely contingent on caloric demands.

Overall, both the CPP and self-administration data support the hypothesis that short-term TGs can act in the brain to support positive reinforcement.

Because plasma TGs typically rise during the post-prandial period, TGs acting on the mesocorticolimbic circuit may modify food perception and/or reward properties; for example, serving as a satiating or reward signal. Therefore, we next explored whether brain TG delivery could modulate the reinforcing properties of high-fat high-sucrose diet (HFHS). We used a CPP paradigm similar to that described above, but each conditioning chamber was now paired to either regular or HFHS food. Before food-conditioning sessions, mice received long-term brain TG delivery or saline (6 h) (Figure 5E). Compared to controls, TG-mice spent significantly more time in the HFHS-paired compartment during the post-test session (Figure 5F). Notably, in this experiment, mice were not food-restricted in order to maximize reward-driven food preference over metabolic demands, perhaps explaining why HFHS pairing was not sufficient to drive a strong place preference in saline-perfused mice. Interestingly, cumulative HFHS consumption during the conditioning session was significantly greater in saline group compared to TG group (5.51 kcal  $\pm$  0.34 versus 4.30  $\pm$  0.34 in saline versus TG group respectively,  $p$  = 0.0039), thereby indicating that the TG group required less palatable food to produce a CPP. These results reveal that central TG sensing potentiates the reinforcing aspects of palatable food and, since a stronger preference was achieved with less HFHS consumption, brain TG delivery may enhance reward sensitivity by lowering the threshold at which reward and/or satiety is achieved.

(B–F) Characteristic voltage response of a striatal MSN to a series of 500-ms current pulses with current steps increasing by 10 pA (B). Resting membrane potential (RMP) in dorso-striatal (C) and accumbal (E) DRD1- (red) and DRD2-MSNs (green) with (TG) and without (Veh) bath-applied triolein (4  $\mu$ M). Statistics: \* $p$  < 0.05 and \*\*\* $p$  < 0.001 TG versus Veh. Traces indicate one action potential in striatal (D) and accumbal (F) DRD2-MSNs with (TG, green trace) and without (Veh, black trace) bath-applied triolein. Histograms indicate the action potential rise time (in ms) in dorso-striatal (D) and accumbal (F) DRD1- (red) and DRD2-MSNs (green). Statistics: \* $p$  < 0.05 TG versus Veh.

(G) Drawing indicates the behavioral protocol used to elicit environmental stimuli-evoked calcium transients. HC = home cage, NC = new cage.

(H) Confocal image of cell-type-specific expression of GCaMP6f in the dorsal striatum of Drd2-Cre mice. Scale bars: 1 mm (mosaic, DAPI/GCaMP6f) and 150  $\mu$ m (inset, GCaMP6f).

(I and J) Dynamics of averaged calcium traces in saline- (I) and TG-perfused mice (J) over a period of 100 s (50 s in the home cage and 50 s in the new cage). Time 0 corresponds to the moment when the animal is placed in the new cage (NC). Data are represented as the percent change in fluorescence over the mean fluorescence (%  $\Delta F/F$ ). Histograms (I and J) indicate the overall %  $\Delta F/F$  in both home cage (HC) and new cage (NC) in saline- and TG-perfused mice. Statistics: \* $p$  < 0.05 NC versus HC in saline-perfused mice.

(K) Temporal dynamics of evoked calcium events (%  $\Delta F/F$ ) during exploration of the new cage (0 to 50 s) with temporal subdivision in bins (B1 to B5, each bin is 10 s).

(L) Curves show averaged calcium signals (saline in black and TG in red) during each temporal bin. Statistics: \*\*\* $p$  < 0.001 (B2 and B3 versus B1 for saline-mice), \* $p$  < 0.05 (B4 versus B1 for saline-mice) and °°° $p$  < 0.001 (B2 versus B1 for TG-mice). For statistical details, see Table S5.

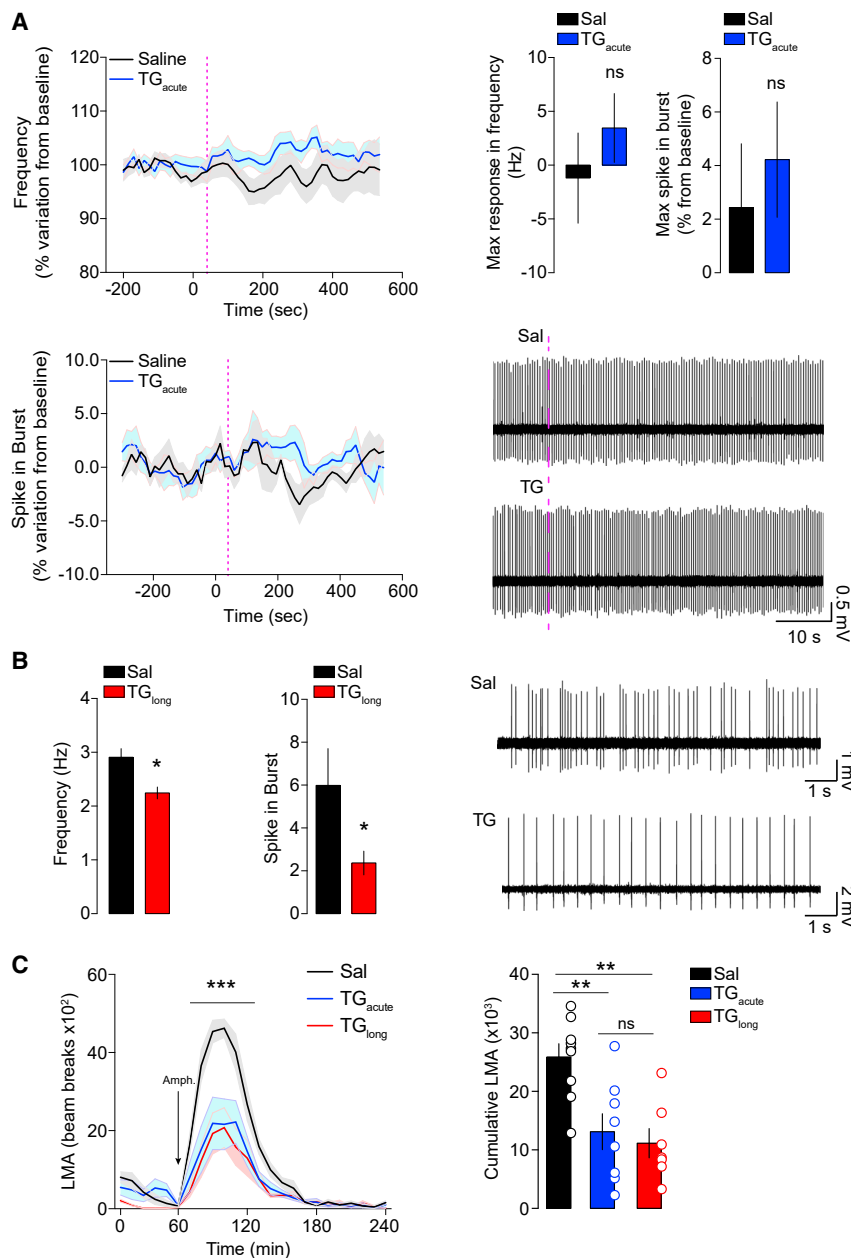


**Figure 4. Centrally Delivered TGs Exert a Time- and Dose-Dependent Action on Pre-Synaptic Dopaminergic Neurons**

(A) Data show single-cell extracellular electrophysiological recordings of dopaminergic neurons in the VTA of anaesthetized animals receiving Sal or TG injections through the carotid artery, with a follow-up of neuronal frequency and firing for 10 min. Histograms display the maximum frequency recorded for each neuron and the maximal spike in burst.

(B) Animals were centrally infused for 6 h with Sal or TG then anaesthetized, and dopaminergic neurons of the VTA were recorded. Data show representative traces of DA-neurons recordings as well as average frequencies and spikes observed during the recordings. Statistics: \* $p < 0.05$  TG<sub>long</sub> versus Sal for each independent comparison.

(C) Locomotor activity (LMA) profile and cumulative LMA following amphetamine (3 mg/kg) administration in animals receiving brain delivery of acute TG ( $n = 8$ ), long-term TG ( $n = 7$ ), or saline ( $n = 9$ ). Statistics: C \*\*\* $p < 0.001$  (TG<sub>acute</sub> or TG<sub>long</sub> versus Sal groups), D \*\* $p < 0.01$  (TG<sub>acute</sub> or TG<sub>long</sub> versus Sal groups). For statistical details, see Table S5.

received a 6-h brain TG delivery or saline prior to access to the palatable drink (Figure 5H). TG-perfused mice reduced binge consumption by ~50% (Figure 5H). This result shows that central TGs can oppose compulsive eating in line with a putative role for TG sensing in enhancing reward sensitivity such that animals require less palatable food. It is also possible that increased TGs may counterbalance the decreased *Lpl* expression in NAc.

### Lpl Gates DRD2-MSN Excitability and Reward-Associated Behavior

Using complementary approaches, we next explored neuronal TG sensing by directly manipulating LPL in the reward system. Using virally Cre-delivered strategy, we deleted *Lpl* in the ventral striatum (NAc) and the midbrain (VTA) of *Lpl*<sup>lox/lox</sup>

Finally, we explored how brain TG delivery modulates food consumption in a context of altered reward sensitivity in a compulsive binge-eating behavioral model (Kessler et al., 2016; Valdivia et al., 2015). *Ad libitum*-fed mice were exposed to intermittent, restricted access (1 h/day) to fat and sugar mixture (10% sucrose and 20% lipids from Intralipid) for 10 days. In that setting, mice rapidly maximized their intake during the first 5 days (Figure 5H). We first observed that a 9-day binge regimen led to a significant decrease in *Lpl* mRNA expression in the NAc but not in the dorsal striatum (Figure 5G), while no major modifications in *Drd1* or *Drd2* mRNA expressions were detected in either region. We then tested whether centrally delivered TGs were able to modulate binge-like behavior. On day 10 of our binge protocol, mice

mice (Figures 5I and 5M). Disruption of *Lpl* in the nucleus accumbens (NAc-*Lpl*<sup>Δ/Δ</sup>; or control mice referred to as NAc-*Lpl*<sup>lox/lox</sup>) led to increased operant responding for food rewards (Figures 5J–5L), as previously reported (Cansell et al., 2014). Strikingly, disruption of *Lpl* in the midbrain (VTA-*Lpl*<sup>Δ/Δ</sup>, Figure 5M) had the opposite consequence and decreased operant performance for food-pellet rewards (Figures 5N–5P). These results suggest that TG sensing may play opposite roles at pre- and post-synaptic sides of the dopamine circuit, underscoring the complexity of bimodal actions of TGs on the reward system.

Since our data point toward DRD2 neurons as privileged targets for TG sensing, and since TGs reduce DRD2-MSNs excitability, we investigated the functional role of LPL as a regulatory component of DRD2-expressing neurons activity. We

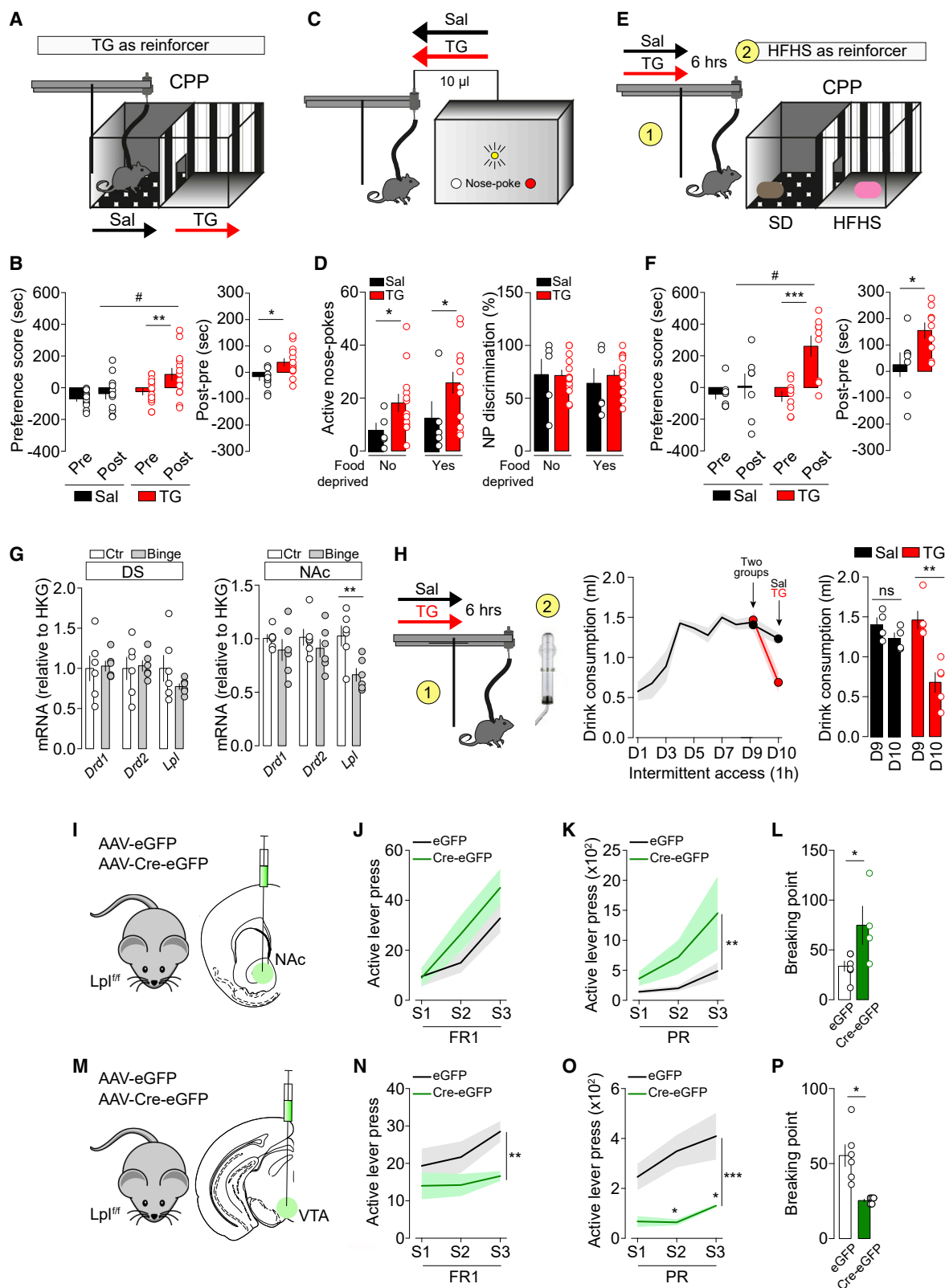


**Figure 5. Central TG Sensing Is Reinforcing and Modulates Food Reward**

(A) Experimental design of the conditioned place preference (CPP) using central TG delivery as reinforcer. On day 1, animals are put in the middle of the cage and explore freely the two compartments of the apparatus for 15 min. The following days of conditioning sessions (1 h each session), the animals learn to associate

(legend continued on next page)

generated mice lacking the *Lpl* gene in DRD2 neurons by crossing *Drd2<sup>Cre/+</sup>* and *Lpl<sup>lox/lox</sup>* mice (*Drd2<sup>Cre/+</sup>::Lpl<sup>+/+</sup>* and *Drd2<sup>Cre/+</sup>::Lpl<sup>f/f</sup>*) (Figure 6A). These mice then received intra-NAc injections of AAV-hSyn-DIO-mCherry to allow Cre-dependent expression of mCherry in DRD2-expressing neurons. *Ex vivo* patch-clamp recordings were then performed on NAc mCherry-positive DRD2-MSNs to measure neuronal modifications triggered by the cell-type-specific deletion of *Lpl* in DRD2 neurons (Figures 6B and 6C). Analysis of active and passive membrane properties (for complete list, see Table S4) revealed that *Lpl* deletion in DRD2-MSNs did not significantly affect resting membrane potential (Figure 6D) or rheobase (Figure 6E), but was associated with a slight increase in membrane resistance (Figure 6F) and a close-to-significant ( $p = 0.051$ ) increase in the delay to first spike (Figure 6G). These results point toward an increased excitability of DRD2-MSNs in *Drd2<sup>Cre/+</sup>::Lpl<sup>f/f</sup>* animals.

Given the critical role of the excitatory glutamatergic cortico-accumbal transmission in controlling the activity of MSNs, we also recorded the occurrence of spiking activity of DRD2-MSNs following stimulation of mPFC fibers (Figure 6B). We found that deletion of *Lpl* in DRD2 neurons was associated with an increased probability to spike in response to cortical stimulation (Figure 6H), further revealing that if their ability to sense TGs is impaired, these neurons become more excitable.

We next explored the behavioral consequences of *Lpl* deletion in DRD2 neurons. Conditional knockout (KO) mice (*Drd2<sup>Cre/+</sup>::Lpl<sup>f/f</sup>*, cKO) displayed enhanced reward-seeking behavior and increased breaking-point values in operant conditioning (Figures 6I and 6J), altered amphetamine-induced locomotor activity (Figure 6K), and decreased cataleptic response to haloperidol (Figure 6L) compared to control mice. Overall, these results clearly establish a key role for LPL onto DRD2-expressing cells as a modulator of DRD2-MSNs excitability and DA-dependent behaviors.

Finally, we tested the integrity of TG sensing in *Drd2<sup>Cre/+</sup>::Lpl<sup>f/f</sup>* mice. Control (*Drd2<sup>Cre/+</sup>::Lpl<sup>+/+</sup>*) and cKO (*Drd2<sup>Cre/+</sup>::Lpl<sup>f/f</sup>*) mice were equipped with intracarotid catheter and perfused with saline or TGs. We found that the decreased locomotor response

caused by brain TG delivery was absent in cKO mice (Figure 6M), thereby further strengthening the close association between LPL in DRD2 neurons and the ability to detect TGs.

Importantly, genetic deletion of *Lpl* in DRD2 neurons did not alter spontaneous locomotor activity, body composition, or basal metabolic efficiency (Figure S6), thus indicating that the above-mentioned behaviors are not the confounding consequence of altered homeostatic functions. Altogether, these data establish a key role for LPL in DRD2-expressing cells in gating DRD2-MSNs excitability and DRD2/DA-dependent behaviors.

### In Humans, Post-Prandial Change in Tryglycerides Are Associated with Brain Responses to Food Cues and Depends on DRD2-Associated Genotype

We reasoned that since *Lpl* mRNA share overlapping expression in common territories of the rodent and human brain (Figure S1), post-prandial TGs might influence brain responses to food cues in these regions in a DRD2-dependent manner. We used fMRI to measure BOLD responses to food and non-food aromas in fasted versus fed nutritional states and tested whether differential responses were associated with post-prandial TGs (Figure 7A) in participants carrying a copy of the A1 allele of the Taq1A polymorphism (Festled et al., 2010; Stice et al., 2008), a mutation known to robustly affect DRD2 signaling (Barnard et al., 2009; Jönsson et al., 1999; Ritchie and Noble, 2003).

We first tested whether internal states or perceptual ratings of the odors differed depending on odorant (food versus non-food), nutritional conditions (hungry, fixed meal, or *ad libitum* meal), or genotype (A1+ versus A1–). Effects are summarized in Figure S7. Next, the effect of time, nutritional condition, genotype, and the interaction among these factors on the concentrations of TGs were tested using a mixed-design ANOVA. There was a significant effect of condition ( $F_{(2,54)} = 8.00$ ,  $p = 0.001$ ) and an interaction between nutritional condition and time ( $F_{(2,54)} = 10.15$ ,  $p < 0.001$ ) on TG levels, but no three-way interactions. *Post hoc* analysis revealed that TG levels significantly increased following the meal in the fixed meal condition

one or another compartment to central delivery of saline (Sal) or triglycerides (TG). After 8 days of conditioning (four sessions in each compartment), animals freely explore the two compartments for 15 min. The analysis considers the time spent in the brain TG delivery- or saline-associated compartments before and after conditioning.

(B) Preference score of CPP and difference of time spent in the conditioned sites between post-test and pre-test between reinforced and non-reinforced compartments. Statistics: \*\* $p < 0.01$  TG-Post versus TG-Pre, # $p < 0.05$  TG-Post versus Sal-Post, post-pre (\* $p < 0.05$  TG<sub>Post-Pre</sub> versus Sal<sub>Post-Pre</sub>).

(C) Experimental design of nose-poke-associated self-administration of saline (Sal,  $n = 5$ ) or triglycerides (TG,  $n = 13$ ).

(D) Active nose-pokes and nose-pokes discrimination (distinction between active and inactive nose-pokes, %) are shown in *ad libitum* and food-deprived conditions. Statistics: \* $p < 0.05$  TG versus Sal.

(E) Experimental design of CPP using palatable food as reinforcer in mice that received a 6-h central perfusion of saline (Sal,  $n = 8$ ) or triglycerides (TG,  $n = 9$ ) prior to conditioning sessions. Conditioning consisted in 8 alternated sessions with standard diet (SD) or high-fat high-sucrose (HFHS) diet access for 30 min.

(F) Preference score of CPP and difference of time spent in the palatable food-associated compartment between post-test and pre-test between reinforced and non-reinforced compartment. Statistics: preference score (\*\* $p < 0.001$  TG-Post versus TG-Pre, # $p < 0.05$  TG-Post versus Sal-Post), post-pre (\* $p < 0.05$  TG<sub>Post-Pre</sub> versus Sal<sub>Post-Pre</sub>).

(G) Quantitative real-time PCR quantifications of *Lpl*, *Drd1*, *Drd2* mRNA abundance relative to HKG in dorsal striatum and NAc of mice after a binge-eating protocol consisting of 9 days of intermittent access to palatable fat and sugar beverage. Statistics: NAc *Lpl* \*\* $p < 0.01$  binge versus control mice.

(H) When animal reached a maximum intake (day 9, D9), on D10 they were centrally infused (6 h) with saline (Sal,  $n = 4$ ) or triglycerides (TG,  $n = 5$ ) before the intermittent access to the palatable drink. The graph shows palatable drink consumption on D9 and D10, prior or after central infusions respectively. Statistics: \*\* $p < 0.01$  D10 versus D9 for TG-group.

(I–P) Viral delivery of eGFP or Cre-eGFP in the NAc (I, NAc-*Lpl<sup>lox/lox</sup>*,  $n = 6$ ; NAc-*Lpl<sup>Δ/Δ</sup>*,  $n = 4$ ) or the VTA (M, VTA-*Lpl<sup>lox/lox</sup>*,  $n = 6$ ; VTA-*Lpl<sup>Δ/Δ</sup>*,  $n = 5$ ) of *Lpl<sup>lox/lox</sup>* mice. Operant behavior performances in fixed ratio sessions (J and N, FR1: fixed ratio 1), progressive ratio (K and O, PR: progressive ratio), and breaking point (L and P). Statistics: \*\*\* $p < 0.001$ , \*\* $p < 0.01$  and \* $p < 0.05$ . For statistical details, see Table S5.



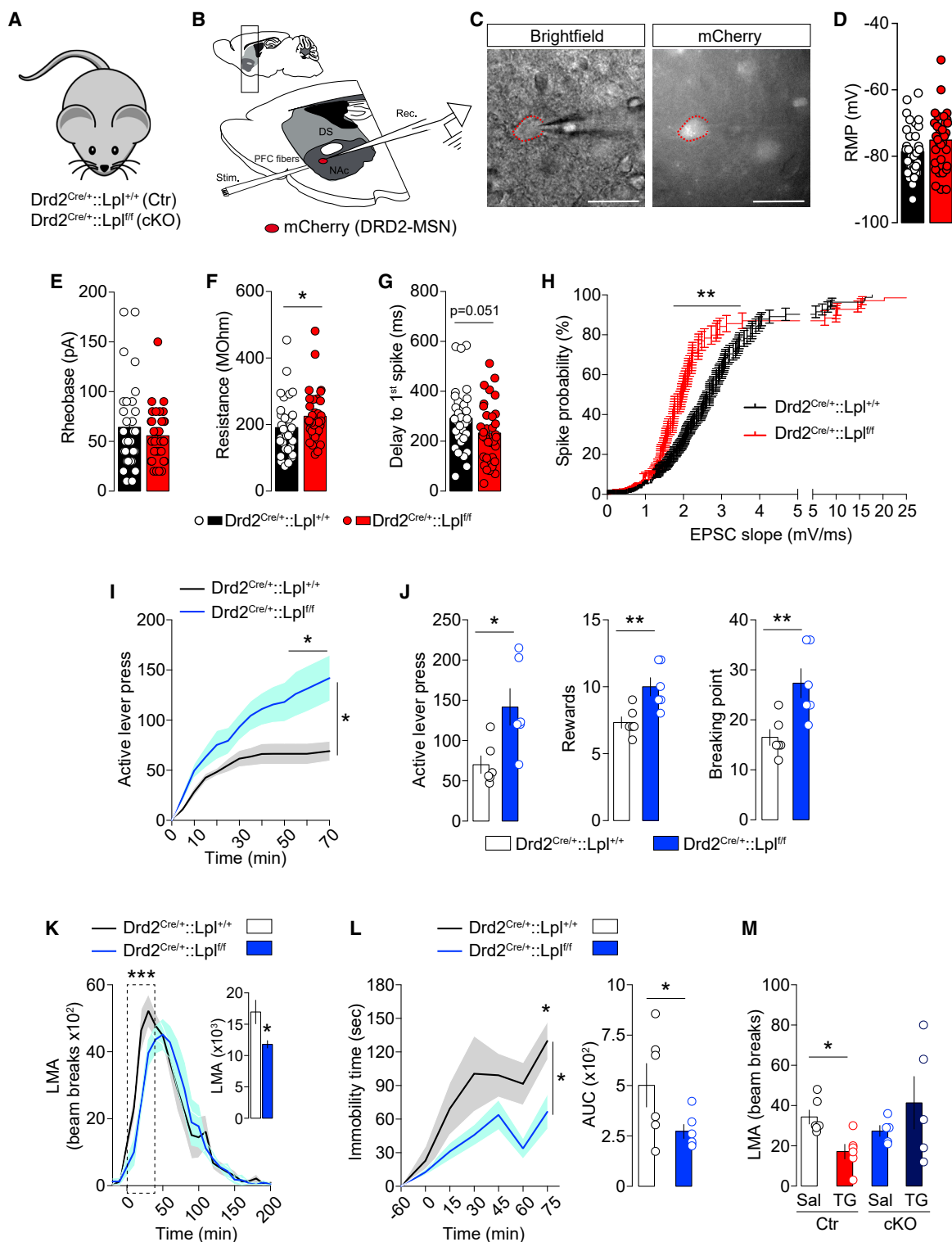


**Figure 6. Lpl in DRD2 Neurons Controls Excitability and Behavioral Responses to DA-Associated Behaviors**

(A) Genetic strategy to delete Lpl from DRD2 neurons: Drd2<sup>Cre/+</sup>;;Lpl<sup>+/+</sup> mice (control, Ctr) and Drd2<sup>Cre/+</sup>;;Lpl<sup>fl/fl</sup> mice (cKO). (B) Drawing illustrates the sagittal slice used for cortical stimulation and patch-clamp recordings in Drd2<sup>Cre/+</sup>;;Lpl<sup>+/+</sup> and Drd2<sup>Cre/+</sup>;;Lpl<sup>fl/fl</sup> transgenic mice, all injected with an AAV-hSyn-DIO-mCherry in the nucleus accumbens (NAc).

(legend continued on next page)

( $p = 0.009$ ), but not in the *ad libitum* meal condition ( $p = 0.08$ ), and that TG levels decreased over the course of the hungry session ( $p = 0.001$ ) (Figure S7). Since plasma TG excursion was only significant in the fixed meal condition, we focused our imaging analysis on the data from the fixed neuroimaging scan.

TG excursion was unrelated to BOLD responses to food versus non-food odors in hungry versus fixed scans in the regions of interest (ROIs) or at the whole-brain level for the group considered as a whole (i.e., collapsing across genotype). However, when genotype (A1+ versus A1−) was included in the model, a significant effect emerged in the vmPFC at 3, 56, and −5 ( $p = 0.04$  following family-wise error [FWE] correction for multiple comparisons across the number of voxels in the ROI and Bonferroni correction for the number of ROI tests performed) (Figure 7B). Importantly, this analysis included FFAs, glucose and insulin excursions, as well as fullness, hunger, and liking ratings as covariates, indicating that post-prandial TGs are unique modulators of vmPFC activity in this experimental setting. Further analysis of independent effects in the A1− and A1+ groups revealed that this interaction arose from a significant positive association in A1+ at 0, 56, and −5 ( $p = 0.02$ ) and a weak non-significant negative association in A1− (Figure 7C). Note also that since the extent of TG excursions did not differ in A1+ versus A1−, this differential effect cannot be attributed to indirect effects of genotype on TG excursions, but rather should result from the effect of this gene variant on DRD2. Collectively, these data strongly support our hypothesis that in humans, circulating TGs are associated with brain response to food cues in the vmPFC in a DRD2-dependent manner.

## DISCUSSION

Excessive consumption of energy-dense food increases the vulnerability to develop uncontrolled craving, compulsive feeding, and ultimately excessive body weight gain (Kenny et al., 2013; Rothmund et al., 2007; Stice et al., 2008; Volkow et al., 2013). However, the possibility of a direct action of circulating TGs on key reward-encoding brain structures has been largely unappreciated. In this work, we demonstrate that circulating post-prandial TGs exert an integrative and multimodal regulatory action onto pre- and post-synaptic neurons of the reward system through an LPL-dependent mechanism.

### Bridging Dietary Inputs to Reward Circuit through Triglyceride Sensing

The presence of TG lipases, including LPL, is required to allow cellular FFA entry upon TG hydrolysis. Here, we provide evidence that in the MCL, *Lpl* mRNA expressions exhibit a certain degree of enrichment in midbrain VTA DA neurons and

striatal DRD1- and DRD2-MSNs (Figures 1A, 1B, and S1), which confer upon these cells the ability to detect and metabolize TGs.

Using brain-specific intracarotid TG delivery, we discovered that nutritional TGs exert time- and dose-dependent actions on VTA DA neurons (long-term exposure) and post-synaptic striatal neurons (short- and long-term exposures). Central TG delivery preferentially dampened DRD2- but not DRD1-related cellular and behavioral responses. This privileged sensitivity of DRD2-expressing neurons to TGs was further supported by (1) *ex vivo*-patch clamp recordings revealing that bath-applied TGs reduced the excitability of DRD2- but not DRD1-MSNs (Figures 3 and S4), and genetic deletion of *Lpl* in DRD2-expressing cells resulted in increased neuronal excitability (Figures 6A–6H); and by (2) *in vivo* recordings where brain TG delivery decreased striatal DRD2-neurons calcium events to environmental cues (Figures 3G–3L).

Consistent with a role for TG sensing in the reward circuit, central TG delivery produced reinforcement on its own (Figures 5A–5D) and modulated the reinforcing aspects of palatable food (Figures 5E–5H). Using loss of function approaches we determined that the action of centrally detected TG relies, at least in part, on the integrity of the LPL in the DA reward circuit and onto DRD2-expressing cells (Figures 5 and 6). Altogether, these results unravel a functional role of LPL-mediated TG sensing onto DRD2 neurons (pre- and post-synaptic neurons) in the control of DA-associated behaviors.

Interestingly, the fact that brain TG delivery could produce positive reinforcement (CPP paradigm) while decreasing motivational drive to lever press for food rewards may appear contradictory at first glance. However, several studies have reported a similar degree of dichotomy between appetitive learning and motivational drive following manipulation of DRD2-MSNs. Indeed, pharmacological inhibition of DRD2-MSNs by activation of DRD2-coupled Gi signaling was sufficient to promote place preference (White et al., 1991). On the other hand, inhibition of DRD2-MSNs in striatal and accumbal regions was reported to decrease motivation to work for food rewards (Soares-Cunha et al., 2016, 2018) while increasing reward reinforcement (Carvalho Poyraz et al., 2016; Durieux et al., 2009; O'Neal et al., 2019).

Hence, the ability of TGs to directly decrease DRD2-MSNs excitability in both dorsal striatum and NAc (Figures 3 and S4) would be predicted to similarly produce two opposite outputs of increased reinforcement and decreased motivation. Whether this mechanism might be instrumental in establishing a set-point of “reward-like sensitivity” is indeed a matter of debate, although it is tempting to speculate that acute and/or chronic brain exposure to circulating TGs could be a fundamental mechanism by which excessive high-fat food intake or

(C–G) Representative picture of a recorded mCherry-positive accumbal DRD2-MSN (C). Histograms indicate the resting membrane potential (RMP in mV, D), the rheobase (in pA, E), the membrane resistance (in MΩ, F) and the delay to first spike (in ms, G) of mCherry-positive accumbal MSNs in both genotypes, *Drd2<sup>Cre/+</sup>::Lpl<sup>+/+</sup>* (black) versus *Drd2<sup>Cre/+</sup>::Lpl<sup>fl/fl</sup>* (red) transgenic mice.

(H) Curves indicate the probability to trigger a spike (in %) in recorded mCherry-positive MSNs following increasing cortical stimulations in both genotypes. Statistics: \* $p < 0.05$  and \*\* $p < 0.01$  *Drd2<sup>Cre/+</sup>::Lpl<sup>fl/fl</sup>* versus *Drd2<sup>Cre/+</sup>::Lpl<sup>+/+</sup>* mice.

(I and J) Operant conditioning performances of *Drd2<sup>Cre/+</sup>::Lpl<sup>+/+</sup>* and *Drd2<sup>Cre/+</sup>::Lpl<sup>fl/fl</sup>* transgenic mice during the active lever press (I). Cumulative active lever press, rewards, and breaking point (J). Statistics: \* $p < 0.05$  *Drd2<sup>Cre/+</sup>::Lpl<sup>fl/fl</sup>* versus *Drd2<sup>Cre/+</sup>::Lpl<sup>+/+</sup>* mice.

(K–M) Locomotor activity (LMA) to amphetamine (3 mg/kg) (K), immobility response to the DRD2 antagonist haloperidol (0.5 mg/kg) during the catalepsy test (L), and spontaneous 6-h locomotor activity (LMA) following central saline or TG delivery (M). Statistics: \*\*\* $p < 0.001$ , \* $p < 0.05$ . For statistical details, see Table S5.

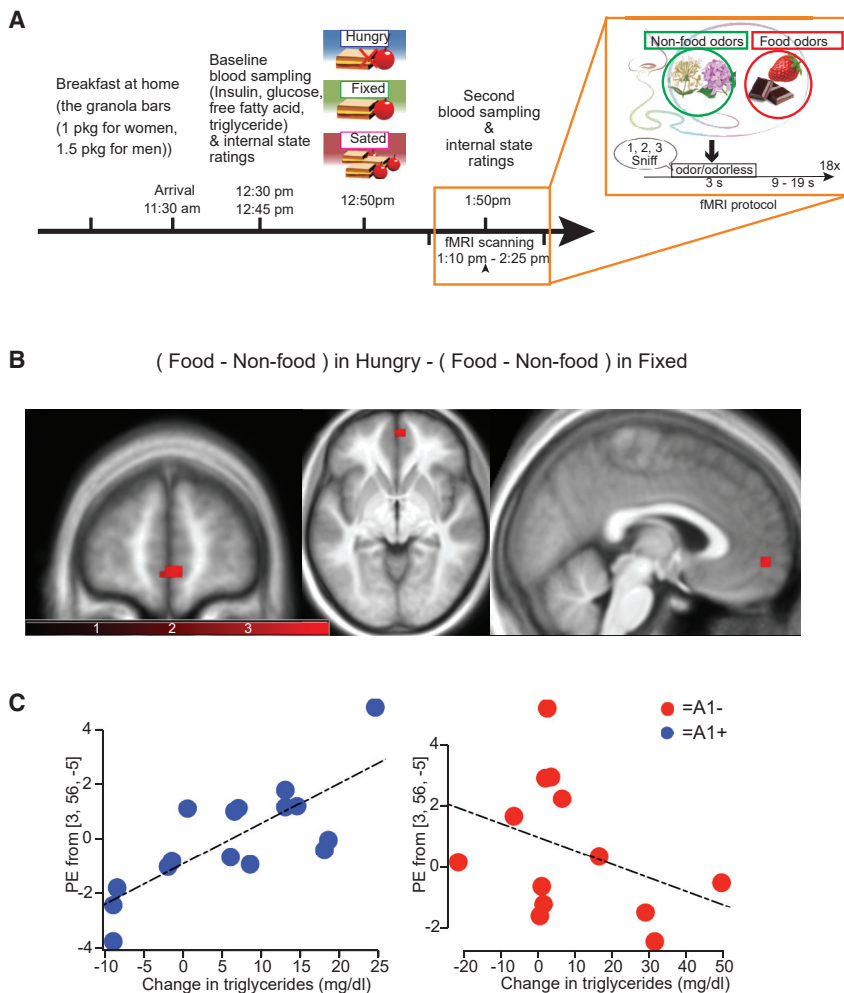


**Figure 7. Post-Prandial TGs Control Human Brain Responses to Food Cues in a DRD2-Dependent Manner (TaqlA Polymorphism Carriers)**

(A) Experimental protocol for fMRI studies and odor stimulation.

(B) Blood oxygen level dependent (BOLD) responses to food versus non-food odors in Hungry versus Fixed conditions correlates with meal-induced changes in TG differentially as a function of genotype in the ventromedial prefrontal cortex (vmPFC) at 3, 56, and -5 ( $p = 0.04$  following FWE correction for comparison across the voxels in the vmPFC ROI and subsequent Bonferroni correction for the number of ROIs tested. Note that this analysis includes all covariates (changes in plasma glucose, insulin and FFA, and changes in internal state and odor perception ratings).

(C) Scatterplots showing the correlation with plasma TG and A1/A2 genotype in the vmPFC. For statistical details, see Table S5.

like system that may drive to a stop signal. This is in line with our results which show (1) reduced cellular excitability of D2R-MSNs following brief application of TG, (2) no *in vivo* impairment in DA-neurons firing following acute delivery of TGs, and (3) reduced *in vivo* firing of DA neurons following long-term delivery of TG.

It is worth mentioning that our current data cannot clearly and univoqually discriminate between a time- and dose-dependent action of TG directly onto VTA neurons and the hypothetical inhibition of midbrain DA neurons as the consequence of inhibited DRD2-projecting neurons to

the VP. Further studies are required to fully depict the exact sequences of such dynamically orchestrated mechanisms.

### Molecular Mechanisms and Physiological Implication of Trygliceride-Mediated Modulation of DRD2 Neurons

We found that central administration of TGs dampens key striatal molecular pathways, notably the MAPK-, mTOR-, and PKA-dependent pathways, indicative of reduced DA-coupled signaling (Figures 2A and 2B). These molecular events are supported by our patch-clamp recordings, which reveal cell-type-specific TG-induced alterations of active and passive membrane properties exclusively in DRD2-MSNs (Figures 3 and S4). In fact, since these signaling pathways play a strong modulatory role on glutamate receptors, voltage-dependent ion channels and transcription factors (for review, see Nagai et al., 2016 and Surmeier et al., 2007), it is formally possible that their modifications, as observed following TG delivery, will alter DRD2-MSNs excitability and neuronal responses. Another non-mutually exclusive hypothesis—by which TGs could modulate DRD2-neurons activity—could involve  $\beta$ -arrestin, mediating DRD2 internalization, and activation of the protein kinase B/Akt,  $\beta$ -arrestin 2, and protein phosphatase 2 (PP2A) complex (Beaulieu et al., 2005). This complex has been shown to operate in striatal DRD2-MSNs

obesity-associated hypertriglyceridemia would ultimately lower reward sensitivity and drive compulsive feeding. Another non-mutually exclusive possibility would be that, as observed in our experiments, sustained TG exposure, by decreasing midbrain DA-neurons firing, would consequently decrease motivational drive and reward sensitivity. Hence, a common general mechanism would be that, by binding to DRD1 (Gs-coupled receptors) and DRD2 (Gi-coupled receptors) receptors, dopamine would lead to activation of DRD1-MSNs and inhibition of DRD2-MSNs, in virtue of their segregated cellular location. By inhibiting DRD2-MSNs, TGs may then result in promoting positive reinforcement, thus bypassing a direct dopamine action onto DRD2-MSNs. These dopamine- and TG-dependent mechanisms may occur on the same cell-types (DRD2-MSNs for instance), but through potentially distinct molecular and metabolic paths, which at the moment remain unknown.

The inhibition of DA-neurons firing within the VTA following long-term TG perfusion agrees with this scenario. For instance, disinhibition of GABAergic ventral pallidal (VP) neurons by TG-inhibited GABAergic DRD2-MSNs would ultimately drive to inhibition of VTA DA neurons as previously described in the literature (Soares-Cunha et al., 2016, 2018). As a consequence, this anatomo-functional interconnectivity would then lead to a backup-

independently of cAMP pathway through the Akt/GSK-3 $\beta$  cascade (Beaulieu et al., 2004, 2005). In our hands, brain TG delivery activated  $\beta$ -arrestin signaling pathway as indicated by the phosphorylation status of both Akt<sup>Ser473</sup> and GSK3 $\beta$ <sup>Ser9</sup> (Figures 2E and 2F) while decreasing canonical DRD2 signaling. Hence, centrally detected TGs could exert a biased action onto DRD2 neurons by decreasing canonical GPCR-coupled cascades while enhancing DRD2- $\beta$ -arrestin signaling.

Of note, synthetic  $\beta$ -arrestin-biased DRD2 ligands (Allen et al., 2011) were shown to oppose amphetamine-induced hyperlocomotion to a similar extent to what we observed with brain TG delivery (Allen et al., 2011).

Altogether, these molecular and cellular adaptations, beside supporting the reduced cellular excitability of DRD2 neurons, also provide a mechanistic explanation for the altered behavioral responses to amphetamine and other dopaminergic agents (raclopride and haloperidol) in the presence of increased circulating TGs.

Importantly, the action of TGs onto DRD2-MSNs activity will inevitably mitigate DRD2-MSNs responsiveness to various inputs including those mediated by DA through its DRD2 receptors.

This is specifically enlightening given that defective DRD2 abundance and signaling has been repeatedly associated with conditions of hypertriglyceridemia such as high-fat feeding or obesity (Adams et al., 2015; Alsiö et al., 2010; Guo et al., 2014; Kenny et al., 2013; Volkow et al., 2008). Interestingly, while these studies provide focal attention onto DRD2, none of them preclude the possibility that DRD2-cells activity would be impaired in pathophysiological conditions associated with overfeeding. In that view, it remains formally possible that the consequence onto DRD2 signaling (i.e., internalization or recycling) might ultimately be the result of altered DRD2-MSNs neural activity.

Finally, we also describe that, in humans, the effect of the meal on brain responses to food versus non-food aromas in the vmPFC was directly proportional to post-prandial TG excursions and that this effect was genotype-dependent, with A1+ carriers showing a strong positive association between changes in BOLD responses and changes in TGs. On the contrary, non-carriers (A1-) exhibited a weak non-significant negative correlation (Figure 7). We did not observe effects in the ventral striatum. However, BOLD responses reflect the activity evoked by inputs into a region, which is consistent with the intimate connection of the vmPFC with the reward system. Importantly, our model co-varied out the potential confounding effects of meal-induced changes in FFAs, glucose, and insulin, as well as changes in ratings of internal state or odor perception. We can therefore conclude that in humans, as we report in mice, post-prandial TGs regulate brain responses to food cues in a DRD2-dependent manner.

In conclusion, this study reveals that dietary TGs can directly alter MCL circuit functions and influence reward reinforcement and food-seeking behaviors by gating DRD2-MSNs activity and associated DA-encoded behaviors. Although we do not fully decipher the precise causal molecular events underlying how dietary lipids gate DRD2-neurons activity, this work provides, for the first time, converging evidence at the behavioral, cellular, molecular, and translational level to directly bridge dietary TG inputs to DRD2 neurons as well as DA-encoded reward events.

These integrative and orchestrated events might provide new avenues for therapeutic innovations in compulsive feeding and obesity-associated pathologies.

### Limitations of Study

Although our study reveals a novel cell-type-specific action of nutritional TGs on the reward system, the molecular underpinnings by which TGs gate the activity of DRD2-expressing neurons remain to be depicted. Indeed, such mechanisms could encompass intracellular lipids metabolism or byproducts signaling, direct membrane G-coupled fatty acid receptors or generation of bioactive lipids. Another functional limitation is the use of DRD2-Cre-mediated Lpl knockdown, which does not fully allow us to specify the involvement of midbrain or striatal DRD2-expressing neuron in TG sensing, as Lpl deletion will occur in both structures. In addition, when trying to isolate the role of post-prandial lipids, we did not consider other energy-related signals that could potentially participate in the overall response. For lipidomic analysis, we chose not to perform multiple comparison analysis, but all raw lipidomic data are available in the Supplemental Information. In our translational approach, the study carried out in humans shows a correlation between brain responses to food cues and plasma TG levels; however, we could not directly test for other reward-driven behaviors nor assess for the isolated action of TGs following intravenous perfusion.

### STAR★METHODS

Detailed methods are provided in the online version of this paper and include the following:

- KEY RESOURCES TABLE
- LEAD CONTACT AND MATERIALS AVAILABILITY
- EXPERIMENTAL MODEL AND SUBJECT DETAILS
  - Animals Studies
  - Human Studies
- METHOD DETAILS
  - Catheter Implantation and Infusion Procedures
  - Viral Production
  - Stereotaxic Procedures
  - Ex Vivo Whole-Cell Patch-Clamp Electrophysiology
  - Measurement of Locomotor Activity
  - Pharmacological Manipulations
  - Catalepsy Test
  - Operant Conditioning System
  - Nose-Poke Operandum for TG Self-administration
  - Conditioned Place Preference (CPP)
  - Binge Feeding Experiment
  - Fiber Photometry and Data Analysis
  - Fluorescent *In Situ* Hybridization
  - Lipidomics
  - In Vivo Electrophysiological Recordings
  - Tissue Preparation and Immunofluorescence
  - Western Blotting
  - Doppler Imaging
  - Whole-Brain c-Fos Immunostaining
  - Isolation of Total RNA and Quantitative RT-PCR
  - Metabolic Efficiency Analysis



- Human Methods and Analysis
- Participant Recruitment
- Genotyping for TaqI A1 Polymorphism
- Food and Non-food Odor Stimuli
- Stimulus Delivery
- Experimental Procedures
- Training Session
- fMRI Scanning Sessions
- fMRI Data Acquisition
- Data Analysis (Human Studies)
- **QUANTIFICATION AND STATISTICAL ANALYSIS**
  - Statistical Analysis
- **DATA AND CODE AVAILABILITY**

## SUPPLEMENTAL INFORMATION

Supplemental Information can be found online at <https://doi.org/10.1016/j.cmet.2020.02.010>.

## ACKNOWLEDGMENTS

We acknowledge funding support from the Centre National de la Recherche Scientifique (CNRS), the Université de Paris, the Bayerische Forschungsförderung, the Allen Foundation Inc., the Nutricia Research Foundation, the Groupe Lipides et Nutrition (GLN), the Modern Diet and Physiology Research Center (MDPRC), the National Research Agency ANR SVSE 1 2011: "Lipobrain" and ANR-16-CE14-0026 "Fat4Brain," and the Fondation pour la Recherche Médicale (FRM). T.S.H. was supported from NIH-NIDA R01DA036612, VA I01BX003759, and a pilot project through P30DK063491. S.L., M.M., M.D.M., E.M., and C.B. received support from the FRM. We thank Rim Hassouna, Ewout Foppen, Anne Sophie Delbes, Raphaël GP Denis, Florence Darlot, Fabien Ducrocq, and Ossie Quehenberger for valuable technical and conceptual help. We thank Dr. Emmanuel Valjent for sharing Drd2-Cre mice for the initial experiment. We thank Olja Kacanski for administrative support, Isabelle Le Parco, Ludovic Maingault, Angélique Dauvin, Aurélie Djemat, Florianne Michel, Maggy Boa, and Daniel Quintas for animals' care and Sabria Allithi for genotyping. We acknowledge the technical platform Functional and Physiological Exploration (FPE) of the Université de Paris, BFA, UMR 8251, CNRS, Paris, France; the viral production facility of the UMR INSERM 1089; and the animal core facility "Buffon" of the Université de Paris/Institut Jacques Monod.

## AUTHOR CONTRIBUTIONS

C.B. designed, performed, and analyzed most of the experiments. E.M. performed transcriptomic meta-analyses and behavioral and molecular studies. E.P., M.D.M., M.M., S.P., S.L., X.F., and L.V. performed and analyzed *ex vivo* patch-clamp electrophysiology. D.M.S., Y.N., M.S., and X.S.D. performed human studies and data analysis. S.T., F.M., and P.F. performed and analyzed *in vivo* electrophysiology recordings. M.A.S. performed the RNA-seq and lipidomics studies. J.C. helped with surgery and behavioral procedures. C. Morel helped perform western blots and dissections. C. Martin designed and performed doppler imaging and fiber photometry experiments. M.C. and S.C. designed and performed self-administration experiments. J.H.-S. and C.C.S. performed the iDISCO analysis. M.H.T., G.G., T.S.H., and S.H.L. secured funding. T.S.H. and D.M.S. provided scientific guidance and experimental design. S.H.L. and G.G. supervised the whole project, interpreted the data, and wrote the manuscript with contribution from all coauthors.

## DECLARATION OF INTERESTS

The authors declare no competing interests.

Received: April 23, 2019

Revised: December 16, 2019

Accepted: February 13, 2020

Published: March 5, 2020

## REFERENCES

- Adams, W.K., Sussman, J.L., Kaur, S., D'souza, A.M., Kieffer, T.J., and Winstanley, C.A. (2015). Long-term, calorie-restricted intake of a high-fat diet in rats reduces impulse control and ventral striatal D2 receptor signalling - two markers of addiction vulnerability. *Eur. J. Neurosci.* **42**, 3095–3104.
- Allen, J.A., Yost, J.M., Setola, V., Chen, X., Sassano, M.F., Chen, M., Peterson, S., Yadav, P.N., Huang, X.P., Feng, B., et al. (2011). Discovery of  $\beta$ -arrestin-biased dopamine D2 ligands for probing signal transduction pathways essential for antipsychotic efficacy. *Proc. Natl. Acad. Sci. USA* **108**, 18488–18493.
- Alsö, J., Olszewski, P.K., Norbäck, A.H., Gunnarsson, Z.E., Levine, A.S., Pickering, C., and Schiöth, H.B. (2010). Dopamine D1 receptor gene expression decreases in the nucleus accumbens upon long-term exposure to palatable food and differs depending on diet-induced obesity phenotype in rats. *Neuroscience* **171**, 779–787.
- Arch, J.R., Hislop, D., Wang, S.J., and Speakman, J.R. (2006). Some mathematical and technical issues in the measurement and interpretation of open-circuit indirect calorimetry in small animals. *Int. J. Obes.* **30**, 1322–1331.
- Babbs, R.K., Sun, X., Felsted, J., Chouinard-Decorte, F., Veldhuizen, M.G., and Small, D.M. (2013). Decreased caudate response to milkshake is associated with higher body mass index and greater impulsivity. *Physiol. Behav.* **121**, 103–111.
- Baik, J.H. (2013). Dopamine signaling in reward-related behaviors. *Front. Neural Circuits* **7**, 152.
- Banks, W.A., Farr, S.A., Salameh, T.S., Niehoff, M.L., Rhea, E.M., Morley, J.E., Hanson, A.J., Hansen, K.M., and Craft, S. (2018). Triglycerides cross the blood-brain barrier and induce central leptin and insulin receptor resistance. *Int. J. Obes.* **42**, 391–397.
- Barnard, N.D., Noble, E.P., Ritchie, T., Cohen, J., Jenkins, D.J., Turner-McGrievy, G., Gloede, L., Green, A.A., and Ferdowsian, H. (2009). D2 dopamine receptor Taq1A polymorphism, body weight, and dietary intake in type 2 diabetes. *Nutrition* **25**, 58–65.
- Beaulieu, J.M., Sotnikova, T.D., Yao, W.D., Kockeritz, L., Woodgett, J.R., Gainetdinov, R.R., and Caron, M.G. (2004). Lithium antagonizes dopamine-dependent behaviors mediated by an AKT/glycogen synthase kinase 3 signaling cascade. *Proc. Natl. Acad. Sci. USA* **101**, 5099–5104.
- Bartoshuk, L.M., Duffy, V.B., Green, B.G., Hoffman, H.J., Ko, C.W., Lucchina, L.A., Marks, L.E., Snyder, D.J., and Weiffenbach, J.M. (2004). Valid across-group comparisons with labeled scales: the gLMS versus magnitude matching. *Physiol. Behav.* **82**, 109–114.
- Beaulieu, J.M., and Gainetdinov, R.R. (2011). The physiology, signaling, and pharmacology of dopamine receptors. *Pharmacol. Rev.* **63**, 182–217.
- Beaulieu, J.M., Sotnikova, T.D., Marion, S., Lefkowitz, R.J., Gainetdinov, R.R., and Caron, M.G. (2005). An Akt/beta-arrestin 2/PP2A signaling complex mediates dopaminergic neurotransmission and behavior. *Cell* **122**, 261–273.
- Ben-Zeev, O., Doolittle, M.H., Singh, N., Chang, C.H., and Scholtz, M.C. (1990). Synthesis and regulation of lipoprotein lipase in the hippocampus. *J. Lipid Res.* **31**, 1307–1313.
- Berland, C., Cansell, C., Hnasko, T.S., Magnan, C., and Luquet, S. (2016). Dietary triglycerides as signaling molecules that influence reward and motivation. *Curr. Opin. Behav. Sci.* **9**, 126–135.
- Berridge, K.C. (2009). 'Liking' and 'wanting' food rewards: brain substrates and roles in eating disorders. *Physiol. Behav.* **97**, 537–550.
- Bertran-Gonzalez, J., Bosch, C., Maroteaux, M., Matamalas, M., Hervé, D., Valjent, E., and Girault, J.A. (2008). Opposing patterns of signaling activation in dopamine D1 and D2 receptor-expressing striatal neurons in response to cocaine and haloperidol. *J. Neurosci.* **28**, 5671–5685.
- Bessenes, D.H., Richards, C.L., Etienne, J., Goers, J.W., and Eckel, R.H. (1993). Spinal cord of the rat contains more lipoprotein lipase than other brain regions. *J. Lipid Res.* **34**, 229–238.
- Cansell, C., Castel, J., Denis, R.G., Rouch, C., Delbes, A.S., Martinez, S., Mestivier, D., Finan, B., Maldonado-Aviles, J.G., Rijnsburger, M., et al. (2014). Dietary triglycerides act on mesolimbic structures to regulate the

rewarding and motivational aspects of feeding. *Mol. Psychiatry* 19, 1095–1105.

Carvalho Poyraz, F., Holzner, E., Bailey, M.R., Meszaros, J., Kenney, L., Kheirbek, M.A., Balsam, P.D., and Kellendonk, C. (2016). Decreasing Striatopallidal Pathway Function Enhances Motivation by Energizing the Initiation of Goal-Directed Action. *J. Neurosci.* 36, 5988–6001.

Cui, G., Jun, S.B., Jin, X., Pham, M.D., Vogel, S.S., Lovinger, D.M., and Costa, R.M. (2013). Concurrent activation of striatal direct and indirect pathways during action initiation. *Nature* 494, 238–242.

Dallman, M.F., Pecoraro, N.C., and la Fleur, S.E. (2005). Chronic stress and comfort foods: self-medication and abdominal obesity. *Brain Behav. Immun.* 19, 275–280.

Davis, J.F., Tracy, A.L., Schurdak, J.D., Tschop, M.H., Lipton, J.W., Clegg, D.J., and Benoit, S.C. (2008). Exposure to elevated levels of dietary fat attenuates psychostimulant reward and mesolimbic dopamine turnover in the rat. *Behav. neurosci.* 122, 1257–1263.

Di Chiara, G., and Imperato, A. (1988). Drugs abused by humans preferentially increase synaptic dopamine concentrations in the mesolimbic system of freely moving rats. *Proc. Natl. Acad. Sci. USA* 85, 5274–5278.

Doyle, J.P., Dougherty, J.D., Heiman, M., Schmidt, E.F., Stevens, T.R., Ma, G., Bupp, S., Shrestha, P., Shah, R.D., Doughty, M.L., et al. (2008). Application of a translational profiling approach for the comparative analysis of CNS cell types. *Cell* 135, 749–762.

Durieux, P.F., Bearzatto, B., Guiducci, S., Buch, T., Waisman, A., Zoli, M., Schiffmann, S.N., and de Kerchove d'Exaerde, A. (2009). D2R striatopallidal neurons inhibit both locomotor and drug reward processes. *Nat. Neurosci.* 12, 393–395.

Eckel, R.H., and Robbins, R.J. (1984). Lipoprotein lipase is produced, regulated, and functional in rat brain. *Proc. Natl. Acad. Sci. USA* 81, 7604–7607.

Epstein, L.H., Temple, J.L., Neaderhiser, B.J., Salis, R.J., Erbe, R.W., and Leddy, J.J. (2007). Food reinforcement, the dopamine D-2 receptor genotype, and energy intake in obese and nonobese humans. *Behav. Neurosci.* 121, 877–886.

Even, P.C., and Nadkarni, N.A. (2012). Indirect calorimetry in laboratory mice and rats: principles, practical considerations, interpretation and perspectives. *Am. J. Physiol. Regul. Integr. Comp. Physiol.* 303, R459–R476.

Farr, S.A., Yamada, K.A., Butterfield, D.A., Abdul, H.M., Xu, L., Miller, N.E., Banks, W.A., and Morley, J.E. (2008). Obesity and hypertriglyceridemia produce cognitive impairment. *Endocrinology* 149, 2628–2636.

Felsted, J.A., Ren, X., Chouinard-Decorte, F., and Small, D.M. (2010). Genetically determined differences in brain response to a primary food reward. *J. Neurosci.* 30, 2428–2432.

Fino, E., Glowinski, J., and Venance, L. (2007). Effects of acute dopamine depletion on the electrophysiological properties of striatal neurons. *Neurosci. Res.* 58, 305–316.

Frank, M.J., and Fossella, J.A. (2011). Neurogenetics and pharmacology of learning, motivation, and cognition. *Neuropsychopharmacology* 36, 133–152.

Gerfen, C.R., Engber, T.M., Mahan, L.C., Susel, Z., Chase, T.N., Monsma, F.J., Jr., and Sibley, D.R. (1990). D1 and D2 dopamine receptor-regulated gene expression of striatonigral and striatopallidal neurons. *Science* 250, 1429–1432.

Goldberg, I.J., Soprano, D.R., Wyatt, M.L., Vanni, T.M., Kirchgessner, T.G., and Schotz, M.C. (1989). Localization of lipoprotein lipase mRNA in selected rat tissues. *J. Lipid Res.* 30, 1569–1577.

Green, B.G., Dalton, P., Cowart, B., Shaffer, G., Rankin, K., and Higgins, J. (1996). Evaluating the 'Labeled Magnitude Scale' for measuring sensations of taste and smell. *Chem Senses* 21, 323–334.

Guo, J., Simmons, W.K., Herscovitch, P., Martin, A., and Hall, K.D. (2014). Striatal dopamine D2-like receptor correlation patterns with human obesity and opportunistic eating behavior. *Mol. Psychiatry* 19, 1078–1084.

Hawrylycz, M.J., Lein, E.S., Guillozet-Bongaarts, A.L., Shen, E.H., Ng, L., Miller, J.A., van de Lagemaat, L.N., Smith, K.A., Ebbert, A., Riley, Z.L., et al. (2012). An anatomically comprehensive atlas of the adult human brain transcriptome. *Nature* 489, 391–399.

Hryhorczuk, C., Florea, M., Rodaros, D., Poirier, I., Daneault, C., Des Rosiers, C., Arvanitogiannis, A., Alquier, T., and Fulton, S. (2016). Dampened Mesolimbic Dopamine Function and Signaling by Saturated but not Monounsaturated Dietary Lipids. *Neuropsychopharmacology* 41, 811–821.

Jackson, D.M., and Westlind-Danielsson, A. (1994). Dopamine receptors: molecular biology, biochemistry and behavioural aspects. *Pharmacol. Ther.* 64, 291–370.

Johnson, P.M., and Kenny, P.J. (2010). Dopamine D2 receptors in addiction-like reward dysfunction and compulsive eating in obese rats. *Nat. Neurosci.* 13, 635–641.

Johnson, B.N., and Sobel, N. (2007). Methods for building an olfactometer with known concentration outcomes. *J. Neurosci. Methods* 160, 231–245.

Jönsson, E.G., Nöthen, M.M., Grünhage, F., Farde, L., Nakashima, Y., Propping, P., and Sedvall, G.C. (1999). Polymorphisms in the dopamine D2 receptor gene and their relationships to striatal dopamine receptor density of healthy volunteers. *Mol. Psychiatry* 4, 290–296.

Karatayev, O., Gaysinskaya, V., Chang, G.Q., and Leibowitz, S.F. (2009). Circulating triglycerides after a high-fat meal: predictor of increased caloric intake, orexigenic peptide expression, and dietary obesity. *Brain Res.* 1298, 111–122.

Kenny, P.J., Voren, G., and Johnson, P.M. (2013). Dopamine D2 receptors and striatopallidal transmission in addiction and obesity. *Curr. Opin. Neurobiol.* 23, 535–538.

Kessler, R.M., Hutson, P.H., Herman, B.K., and Potenza, M.N. (2016). The neurobiological basis of binge-eating disorder. *Neurosci. Biobehav. Rev.* 63, 223–238.

Lein, E.S., Hawrylycz, M.J., Ao, N., Ayres, M., Bensinger, A., Bernard, A., Boe, A.F., Boguski, M.S., Brockway, K.S., Byrnes, E.J., et al. (2007). Genome-wide atlas of gene expression in the adult mouse brain. *Nature* 445, 168–176.

Lerner, T.N., Shilyansky, C., Davidson, T.J., Evans, K.E., Beier, K.T., Zalocusky, K.A., Crow, A.K., Malenka, R.C., Luo, L., Tomer, R., and Deisseroth, K. (2015). Intact-Brain Analyses Reveal Distinct Information Carried by SNc Dopamine Subcircuits. *Cell* 162, 635–647.

Lew, J.Y., Garcia-Espana, A., Lee, K.Y., Carr, K.D., Goldstein, M., Haycock, J.W., and Meller, E. (1999). Increased site-specific phosphorylation of tyrosine hydroxylase accompanies stimulation of enzymatic activity induced by cessation of dopamine neuronal activity. *Mol. Pharmacol.* 55, 202–209.

Lim, J., Wood, A., and Green, B.G. (2009). Derivation and evaluation of a labeled hedonic scale. *Chem Senses* 34, 739–751.

Lindgren, N., Xu, Z.Q., Herrera-Marschitz, M., Haycock, J., Hökfelt, T., and Fisone, G. (2001). Dopamine D(2) receptors regulate tyrosine hydroxylase activity and phosphorylation at Ser40 in rat striatum. *Eur. J. Neurosci.* 13, 773–780.

Michaelides, M., Thanos, P.K., Volkow, N.D., and Wang, G.J. (2012). Dopamine-related frontostriatal abnormalities in obesity and binge-eating disorder: emerging evidence for developmental psychopathology. *Int. Rev. Psychiatry* 24, 211–218.

Nagai, T., Yoshimoto, J., Kannon, T., Kuroda, K., and Kaibuchi, K. (2016). Phosphorylation Signals in Striatal Medium Spiny Neurons. *Trends Pharmacol. Sci.* 37, 858–871.

O'Neal, T.J., Nooney, M.N., Thien, K., and Ferguson, S.M. (2019). Chemogenetic modulation of accumbens direct or indirect pathways bidirectionally alters reinstatement of heroin-seeking in high- but not low-risk rats. *Neuropsychopharmacology*. <https://doi.org/10.1038/s41386-019-0571-9>.

Paradis, E., Clavel, S., Julien, P., Murthy, M.R., de Bilbao, F., Arsenijevic, D., Giannakopoulos, P., Vallet, P., and Richard, D. (2004). Lipoprotein lipase and endothelial lipase expression in mouse brain: regional distribution and selective induction following kainic acid-induced lesion and focal cerebral ischemia. *Neurobiol. Dis.* 15, 312–325.

G. Paxinos, and K. Franklin, eds. (2003). *The Mouse Brain in Stereotaxic Coordinates: Compact, Second Edition* (Gulf Professional Publishing).

Peterson, S.M., Pack, T.F., Wilkins, A.D., Urs, N.M., Urban, D.J., Bass, C.E., Lichtarge, O., and Caron, M.G. (2015). Elucidation of G-protein and  $\beta$ -arrestin

- functional selectivity at the dopamine D2 receptor. *Proc. Natl. Acad. Sci. USA* 112, 7097–7102.
- Picard, A., Rouch, C., Kassis, N., Moullé, V.S., Croizier, S., Denis, R.G., Castel, J., Coant, N., Davis, K., Clegg, D.J., et al. (2013). Hippocampal lipoprotein lipase regulates energy balance in rodents. *Mol. Metab.* 3, 167–176.
- Renier, N., Wu, Z., Simon, D.J., Yang, J., Ariel, P., and Tessier-Lavigne, M. (2014). iDISCO: a simple, rapid method to immunolabel large tissue samples for volume imaging. *Cell* 159, 896–910.
- Ritchie, T., and Noble, E.P. (2003). Association of seven polymorphisms of the D2 dopamine receptor gene with brain receptor-binding characteristics. *Neurochem. Res.* 28, 73–82.
- Rothmund, Y., Preuschhof, C., Bohner, G., Bauknecht, H.C., Klingebiel, R., Flor, H., and Klapp, B.F. (2007). Differential activation of the dorsal striatum by high-calorie visual food stimuli in obese individuals. *Neuroimage* 37, 410–421.
- Ruge, T., Hodson, L., Cheeseman, J., Dennis, A.L., Fielding, B.A., Humphreys, S.M., Frayn, K.N., and Karpe, F. (2009). Fasted to fed trafficking of Fatty acids in human adipose tissue reveals a novel regulatory step for enhanced fat storage. *J. Clin. Endocrinol. Metab.* 94, 1781–1788.
- Salinas, C.B.G., Lu, T.T., Gabery, S., Marstal, K., Alanentalo, T., Mercer, A.J., Cornea, A., Conradsen, K., Hecksher-Sørensen, J., Dahl, A.B., et al. (2018). Integrated Brain Atlas for Unbiased Mapping of Nervous System Effects Following Liraglutide Treatment. *Sci. Rep.* 8, 10310.
- Salvatore, M.F., Calipari, E.S., and Jones, S.R. (2016). Regulation of Tyrosine Hydroxylase Expression and Phosphorylation in Dopamine Transporter-Deficient Mice. *ACS Chem. Neurosci.* 7, 941–951.
- Schultz, W. (2016). Dopamine reward prediction-error signalling: a two-component response. *Nat. Rev. Neurosci.* 17, 183–195.
- Soares-Cunha, C., Coimbra, B., David-Pereira, A., Borges, S., Pinto, L., Costa, P., Sousa, N., and Rodrigues, A.J. (2016). Activation of D2 dopamine receptor-expressing neurons in the nucleus accumbens increases motivation. *Nat. Commun.* 7, 11829.
- Soares-Cunha, C., Coimbra, B., Domingues, A.V., Vasconcelos, N., Sousa, N., and Rodrigues, A.J. (2018). Nucleus Accumbens Microcircuit Underlying D2-MSN-Driven Increase in Motivation. *eNeuro* 5, <https://doi.org/10.1523/ENEURO.0386-18.2018>.
- South, T., and Huang, X.F. (2008). High-fat diet exposure increases dopamine D2 receptor and decreases dopamine transporter receptor binding density in the nucleus accumbens and caudate putamen of mice. *Neurochem. Res.* 33, 598–605.
- Stice, E., Burger, K.S., and Yokum, S. (2015). Reward Region Responsivity Predicts Future Weight Gain and Moderating Effects of the Taq1A Allele. *J. Neurosci.* 35, 10316–10324.
- Stice, E., Spoor, S., Bohon, C., and Small, D.M. (2008). Relation between obesity and blunted striatal response to food is moderated by Taq1A A1 allele. *Science* 322, 449–452.
- Stice, E., Spoor, S., Bohon, C., Veldhuizen, M.G., and Small, D.M. (2008). Relation of reward from food intake and anticipated food intake to obesity: a functional magnetic resonance imaging study. *J. Abnorm. Psychol.* 117, 924–935.
- Sun, X., Veldhuizen, M.G., Wray, A.E., de Araujo, I.E., Sherwin, R.S., Sinha, R., and Small, D.M. (2014). The neural signature of satiation is associated with ghrelin response and triglyceride metabolism. *Physiol. Behav.* 136, 63–73.
- Sun, X., Kroemer, N.B., Veldhuizen, M.G., Babbs, A.E., de Araujo, I.E., Gitelman, D.R., Sherwin, R.S., Sinha, R., and Small, D.M. (2015). Basolateral amygdala response to food cues in the absence of hunger is associated with weight gain susceptibility. *J. Neurosci.* 35, 7964–7976.
- Surmeier, D.J., Ding, J., Day, M., Wang, Z., and Shen, W. (2007). D1 and D2 dopamine-receptor modulation of striatal glutamatergic signaling in striatal medium spiny neurons. *Trends Neurosci.* 30, 228–235.
- Valdivia, S., Cornejo, M.P., Reynaldo, M., De Francesco, P.N., and Perello, M. (2015). Escalation in high fat intake in a binge eating model differentially engages dopamine neurons of the ventral tegmental area and requires ghrelin signaling. *Psychoneuroendocrinology* 60, 206–216.
- Volkow, N.D., Wang, G.J., Telang, F., Fowler, J.S., Thanos, P.K., Logan, J., Alexoff, D., Ding, Y.S., Wong, C., Ma, Y., and Pradhan, K. (2008). Low dopamine striatal D2 receptors are associated with prefrontal metabolism in obese subjects: possible contributing factors. *Neuroimage* 42, 1537–1543.
- Volkow, N.D., Wang, G.J., Fowler, J.S., Tomasi, D., and Baler, R. (2012). Food and drug reward: overlapping circuits in human obesity and addiction. *Curr. Top. Behav. Neurosci.* 11, 1–24.
- Volkow, N.D., Wang, G.J., Tomasi, D., and Baler, R.D. (2013). Obesity and addiction: neurobiological overlaps. *Obes. Rev.* 14, 2–18.
- Vucetic, Z., and Reyes, T.M. (2010). Central dopaminergic circuitry controlling food intake and reward: implications for the regulation of obesity. *Wiley Interdiscip. Rev. Syst. Biol. Med.* 2, 577–593.
- Wang, G.J., Volkow, N.D., Logan, J., Pappas, N.R., Wong, C.T., Zhu, W., Netusil, N., and Fowler, J.S. (2001). Brain dopamine and obesity. *Lancet* 357, 354–357.
- Wang, H., Astarita, G., Taussig, M.D., Bharadwaj, K.G., DiPatrizio, N.V., Nave, K.A., Piomelli, D., Goldberg, I.J., and Eckel, R.H. (2011). Deficiency of lipoprotein lipase in neurons modifies the regulation of energy balance and leads to obesity. *Cell Metab.* 13, 105–113.
- White, N.M., Packard, M.G., and Hiroi, N. (1991). Place conditioning with dopamine D1 and D2 agonists injected peripherally or into nucleus accumbens. *Psychopharmacology (Berl.)* 103, 271–276.
- Wu, Q., and Palmiter, R.D. (2011). GABAergic signaling by AgRP neurons prevents anorexia via a melanocortin-independent mechanism. *Eur. J. Pharmacol.* 660, 21–27.
- Zeisel, A., Hochgerner, H., Lonnerberg, P., Johnsson, A., Memic, F., van der Zwan, J., Haring, M., Braun, E., Borm, L.E., La Manno, G., et al. (2018). Molecular Architecture of the Mouse Nervous System. *Cell* 174, 999–1014.e22.

## STAR★METHODS

## KEY RESOURCES TABLE

REAGENT or RESOURCE	SOURCE	IDENTIFIER
<b>Antibodies</b>		
rabbit anti-phospho-rpS6 Ser <sup>235/236</sup>	Cell Signaling Technology	RRID: AB_331679
rabbit anti-phospho-rpS6 Ser <sup>240/244</sup>	Cell Signaling Technology	RRID: AB_331682
Total rpS6	Cell Signaling Technology	RRID: AB_2238583
rabbit anti-phospho-p70S6K Thr <sup>421</sup> /Ser <sup>424</sup>	Cell Signaling Technology	RRID: AB_2265913
rabbit anti-phospho-p70S6KThr <sup>389</sup>	Cell Signaling Technology	RRID: AB_2269803
rabbit anti-phospho-ERK1/2	Cell Signaling Technology	RRID: AB_331646
rabbit anti-phospho-DARPP-32 Thr <sup>34</sup>	Cell Signaling Technology	RRID: AB_2797914
rabbit anti-phospho-TH Ser <sup>31</sup>	Millipore	RRID: AB_177464
rabbit anti-phospho-TH Ser <sup>40</sup>	Cell Signaling Technology	RRID: AB_2201522
mouse anti-TH	Millipore	RRID: AB_2313764
mouse $\beta$ -actin	Sigma	RRID: AB_476692
rabbit anti-phospho-Akt Ser <sup>473</sup>	Cell Signaling Technology	RRID: AB_2315049
rabbit anti-phospho-Akt Thr <sup>308</sup>	Cell Signaling Technology	RRID: AB_2629447
rabbit anti-phospho-GSK3 $\beta$ Ser <sup>9</sup>	Cell Signaling Technology	RRID: AB_2115201
goat anti-cFos	Santa Cruz Biotechnology	RRID: AB_2106783
rabbit anti-cFos	Synaptic Systems	RRID: AB_2231974
anti-rabbit Cy3 AffiniPure	Jackson ImmunoResearch	RRID: AB_2307443
anti-goat Dylight488	Vector labs	RRID: AB_2336400
IgG-HRP anti-mouse	Dako	RRID: AB_2636929
HRP anti-rabbit	Cell Signaling Technology	RRID: AB_2099233
Rabbit pAb anti c-Fos (Ab-5) (4-17)	Calbiochem	RRID: AB_2106755
anti-rabbit Cy5 AffiniPure	Jackson ImmunoResearch	RRID: AB_2338013
<b>Bacterial and Virus Strains</b>		
AAV 2/9 CBA.nls myc Cre.eGFP	The backbone was kindly provided by Richard Palmiter (Univ. of Washington, Seattle, USA).	N/A
AAV2/9.CMV.GFP	viral production facility of the UMR INSERM 1089 (Nantes, France)	N/A
pAAV.hSyn.eGFP.WPRE.bGH	gift from James M. Wilson	Addgene viral prep #105539-AAV9
pAAV.CMV.HI.eGFP-Cre.WPRE.SV40	a gift from James M. Wilson	Addgene viral prep #105545-AAV9
pAAV-hSyn-DIO-mCherry	a gift from Bryan Roth	Addgene viral prep #50459-AAV8
pAAV.Syn.Flex.GCaMP6f.WPRE.SV40	was a gift from Douglas Kim	Addgene viral prep #100833-AAV9
<b>Diets, food cues</b>		
Chow Diet	Safe diets	A03
High-Fat high-Sucrose	Brogaarden	31797 D12451 Research Diet
Sucrose pellets	TestDiet, Richmond, USA	N/A
Food odour 'chocolate cookie'	Bell Labs Flavors and Fragrances	6002335
Food odour 'strawberry and cream'	Bell Labs Flavors and Fragrances	6106524
Food odour 'honeysuckle'	Chey N-3 from Firmenich, Inc	039831
Food odour 'lilac'	Bell Labs Flavors and Fragrances	31731066
<b>Chemicals</b>		
Haloperidol hypochloride	Tocris	931
SKF38393 hydrobromide	Tocris	0922
Raclopride	Tocris	1810/10

(Continued on next page)



**Continued**

REAGENT or RESOURCE	SOURCE	IDENTIFIER
Intralipid 20%	Fresenius Kabi France	N/A
Amphetamine	Sigma Aldrich	A5880
Deposited Data		
Lpl expression in the mouse human & brain was extracted from Brain Allen Institute <i>in situ</i> -hybridization and microarray data (Hawrylycz et al., 2012)	<a href="http://mouse.brain-map.org/">http://mouse.brain-map.org/</a>	N/A
Single Cell RNA seq analysis of Lpl enrichment was extracted from Zeisel et al., 2018	<a href="http://mousebrain.org/genesearch.html">http://mousebrain.org/genesearch.html</a>	N/A
RNA seq database for Lpl expression was extracted and reanalyzed from Doyle et al. (2008)	<a href="https://www.ncbi.nlm.nih.gov/pubmed/19013282">https://www.ncbi.nlm.nih.gov/pubmed/19013282</a> <a href="https://www.ncbi.nlm.nih.gov/geo/geo2r/?acc=GSE13379">https://www.ncbi.nlm.nih.gov/geo/geo2r/?acc=GSE13379</a>	N/A
Experimental Models: Organisms/Strains		
C57BL/6J mice	Janvier	N/A
B6.129S4-Lpl <sup>tm1ljg/J</sup> (Lpl lox/lox mice)	Jackson Labs	<a href="https://www.jax.org/strain/006503">https://www.jax.org/strain/006503</a>
Tg(Drd2-cre)ER44Gsat/Mmucd mice	Gensat	<a href="http://www.informatics.jax.org/allele/MGI:3836635">http://www.informatics.jax.org/allele/MGI:3836635</a>
Tg(Drd2-EGFP)S118Gsat mice	Gensat	<a href="http://www.informatics.jax.org/allele/MGI:3843608">http://www.informatics.jax.org/allele/MGI:3843608</a>
Drd1a-Cre (Tg(Drd1-cre) EY262Gsat (to generate Drd1a-tdTomato)	Gensat	<a href="http://www.informatics.jax.org/allele/MGI:3836631">http://www.informatics.jax.org/allele/MGI:3836631</a>
Ai14(RCL-tdT)-D mice (to generate Drd1a-tdTomato)	Jackson Labs	<a href="https://www.jax.org/strain/007908">https://www.jax.org/strain/007908</a>
Oligonucleotides		
Drd1 probe for RNA scope	RNAscope® Probe - form Advanced Cell Diagnostic	Mm-Drd1-C2 461901-C2
Drd2 probe for RNA scope	RNAscope® Probe - Cell Diagnostic	Mm-Drd2-C3 406501-C3
Lpl for RNA scope	RNAscope® Probe - Cell Diagnostic	Mm-Lpl 402791
Th for RNA scope	RNAscope® Probe - Cell Diagnostic	Mm-Th-C3 317621-C3
TaqIA A1 forward 5'-CCCTTCCTGAGTGTCATCA-3')	Invitrogen	N/A
TaqIA A1 reverse 5'-CGGCTGGCCAAGTTGTCT-3')	Invitrogen	N/A
Drd1 for RT-PCR quantification forward primer 5'-tctggttacctgatccctca-3'		N/A
Drd1 for RT-PCR quantification reverse primer 5'-gcctcctccctcttcaggt-3'		N/A
Drd2 for RT-PCR quantification forward primer 5'-tgaacaggcggagaatgg-3'		N/A
Drd2 for RT-PCR quantification reverse primer 5'-ctggtgcttgacagcatctc-3'		N/A
Lpl RT-PCR quantification forward primer 5'-CACAGTGGCCGAGAGCGAGAA-3'		N/A
Lpl RT-PCR quantification reverse primer 5'-gctGAGTCCTTTCCCTTCTGCAG-3'		N/A
Rpl19 HKG RT-PCR quantification forward primer 5'-GGGCAGGCATATGGGCATA-3'		N/A
Rpl19 HKG RT-PCR quantification reverse primer 5'-GGCGGTCAATCTTCTTGATT-3'		N/A
Software and Algorithms		
Phenomaster TSE Systems GmbH		N/A
TSE system for operant behavior	TSE Systems GmbH	N/A

(Continued on next page)

**Continued**

REAGENT or RESOURCE	SOURCE	IDENTIFIER
Intellimaze	TSE Systems GmbH	N/A
GraphPad Prism 6	GraphPad Software	RRID:SCR_002798
R software	<a href="https://www.r-project.org">https://www.r-project.org</a>	N/A
ImageJ	NIH	RRID:SCR_003070
Imaris 7.6.5	Bitplane, Zurich, Switzerland	N/A
SPM8 software (Statistical Parametric Mapping, Wellcome Department of Imaging Neuroscience)	Wellcome Trust Centre for Neuroimaging	N/A
TDT Synapse Essentials Software	Tucker-Davis Technologies	N/A
MATLAB R2010b 7.11.0	The MathWorks, Inc.	N/A
NeuroSynth	<a href="http://www.neurosynth.org">www.neurosynth.org</a>	N/A
Other		
Mono Fiberoptic Cannula		MFC_400/460-0.48_5mm_ MF1.25_FLT

**LEAD CONTACT AND MATERIALS AVAILABILITY**

Further information and requests for resources and reagents should be directed to and will be fulfilled by the Lead Contact, Serge Luquet ([serge.luquet@univ-paris-diderot.fr](mailto:serge.luquet@univ-paris-diderot.fr))

This study did not generate new unique reagents.

**EXPERIMENTAL MODEL AND SUBJECT DETAILS****Animals Studies**

All animal experiments were performed with approval of the Animal Care Committee of the University Paris Diderot-Paris 7 (CEB-25-2016) or the University Bordeaux Committee (CEEA 50, number Apafis #3265-2015121811059640v6). Ten-week-old male mice C57BL/6J (25-30 g, Janvier, Le Genest St Isle, France) were individually housed in a room maintained at  $22 \pm 1^\circ\text{C}$  with light from 07:00 to 19:00 h. Regular chow diet (3 438 kcal/kg, protein 19%, lipid 5%, carbohydrates 55%, reference #U8959 version 63 Safe, Augy, France) and water were provided *ad libitum*, unless stated otherwise. All the behavioral experiments were performed during the light cycle, unless stated otherwise. All transgenic mouse lines were obtained from Jackson laboratory or Gensat/MMRRC: Lipoprotein lipase  $Lpl^{lox/lox}$  mice (strain B6.129S4-Lpltm1lg/J, n° 006503), Drd2-Cre mice (STOCK Tg(Drd2-cre) ER44Gsat/Mmucd), Drd2-eGFP mice (Tg(Drd2-EGFP)S118Gsat). Drd1a-tdTomato mice were generated by crossing Drd1a-Cre animals (Tg(Drd1-cre) EY262Gsat, Gensat/MMRRC) with Ai14(RCL-tdT)-D mice (B6;129S6-Gt(ROSA)26Sortm14(CAG-tdTomato)Hze/J, Jackson laboratory).

**Human Studies****Participant Recruitment**

Twenty-nine right-handed participants (age range 18 – 39, M = 26.80, SD = 5.49; BMI range 19.5 – 33.6, M = 23.94, SD = 3.86; male = 16, female = 13) were recruited from the greater New Haven area through the Yale University Interdisciplinary Research Consortium on Stress, Self-Control and Addiction (IRCSSA) P30 Subject's core as well as via flyer advertisement. Participants were screened over the phone to be less than 40 years of age, free of psychiatric disorders, eating disorders, current dieting behavior, alcoholism, use of tobacco or drugs other than alcohol, history of head injury with loss of consciousness, use of daily medication other than monophasic birth control, chemosensory impairments, lactose intolerance or food allergies. We did not impose a BMI upper-limit. Individuals were included so long as they felt comfortable while inserted in the scanner bore. Females provided the date of their last period to ensure that they were not scanned during menstruation or ovulation. All participants provided written informed consent at their first lab visit and the study was approved by the Yale Human Investigations Committee.

**METHOD DETAILS****Catheter Implantation and Infusion Procedures**

Surgery and central infusion were carried out as previously described (Cansell et al., 2014). Mice were anesthetized with isoflurane and received 10 mg/kg intraperitoneal injection (i.p.) of Buprécare® (Buprenorphine 0.3 mg) diluted 1/100 in NaCl 0.9% and 10 mg/kg of Ketofen® (Ketoprofen 100 mg) diluted 1/100 in NaCl 0.9%. Home-made catheters were inserted in the left carotid artery toward the brain. Importantly, no heparin was used during the study to prevent LPL activity changes. Catheters clotting was prevented through regular flushing with small volumes of NaCl 0.9%. Infusions started after a recovery period of 7–10 days by connecting

catheters to a swiveling infusion device allowing animals to move freely and access water and food. After 2 days of habituation to the infusion device, mice received NaCl 0.9% (Sal mice) or TG emulsion (TG mice) (Intralipid 20%) at a rate of 0.1–0.3  $\mu\text{L}/\text{min}$  for 6 h. At the end of the behavioral experiments, catheters viability was assessed with Etomidate injections.

### Viral Production

The plasmid CBA.nls myc Cre.eGFP expressing the myc-nls-Cre-GFP fusion protein (Wu and Palmiter, 2011) was kindly provided by Richard Palmiter (Univ. of Washington, Seattle, USA). Adeno-associated virus serotype 2/9 (AAV2/9) ( $6 \times 10^{11}$  genomes/mL and  $1.7 \times 10^8$  infectious units/ $\mu\text{L}$ ) was produced by the viral production facility of the UMR INSERM 1089 (Nantes, France). Control AAV2/9.CMV.GFP (titer  $\geq 1 \times 10^{11}$  vg/mL) was produced by the viral production facility of the UMR INSERM 1089 (Nantes, France). pAAV.CMV.HI.eGFP-Cre.WPRE.SV40 (titer  $\geq 1 \times 10^{12}$  vg/mL) was a gift from James M. Wilson (Addgene viral prep #105545-AAV9; <https://www.addgene.org/105545/>; RRID:Addgene\_105545). pAAV-hSyn-DIO-mCherry (titer  $\geq 1 \times 10^{13}$  vg/mL, working dilution 1:10) was a gift from Bryan Roth (Addgene plasmid #50459-AAV8; <http://www.addgene.org/50459/>; RRID:Addgene\_50459).

pAAV.Syn.Flex.GCaMP6f.WPRE.SV40 (titer  $\geq 1 \times 10^{13}$  vg/mL, working dilution 1:5) was a gift from Douglas Kim (Addgene viral prep #100833-AAV9; <https://www.addgene.org/100833/>; RRID:Addgene\_100833).

### Stereotaxic Procedures

Mice were anaesthetized with isoflurane and received 10  $\text{mg} \cdot \text{kg}^{-1}$  intraperitoneal injection (i.p.) of Buprécare® (Buprenorphine 0.3 mg) diluted 1/100 in NaCl 0.9% and 10 mg/kg of Ketofen® (Ketoprofen 100 mg) diluted 1/100 in NaCl 0.9%, and placed on a stereotaxic frame (Model 940, David Kopf Instruments, California). Viruses (0.5  $\mu\text{L}$ ) were injected either bilaterally or unilaterally (fiber photometry) into the ventral tegmental area (VTA) (L =  $\pm 0.5$ ; AP =  $-3.4$ ; V =  $-4.4$ , mm), the nucleus accumbens (NAc) (L =  $\pm 1$ ; AP =  $+1$ ; V =  $-4.2$ , in mm) or the dorsal striatum (L =  $+1.5$ ; AP =  $+0.86$ ; V =  $-3.25$ , in mm) at a rate of 0.1  $\mu\text{L}/\text{min}$ . The injection needle was carefully removed after 5 min waiting at the injection site and 2 min waiting half way to the top. Optical fiber for calcium imaging into the striatum was implanted 100  $\mu\text{m}$  above the viral injection site.

### Ex Vivo Whole-Cell Patch-Clamp Electrophysiology

Animals (8–12 weeks old) were terminally anaesthetized using isoflurane. Sagittal striatal slices (350  $\mu\text{m}$ -thick), containing the dorsal striatum and the nucleus accumbens, were cut using a VT1000S vibratome (VT1000S, Leica Microsystems, Nussloch, Germany) in ice-cold oxygenated solution (ACSF: 125 mM NaCl, 2.5 mM KCl, 25 mM glucose, 25 mM  $\text{NaHCO}_3$ , 1.25 mM  $\text{NaH}_2\text{PO}_4$ , 2 mM  $\text{CaCl}_2$ , 1 mM  $\text{MgCl}_2$ , 1 mM pyruvic acid). Slices were then incubated at 32–34°C for 60 min before returning to room temperature in holding ACSF. For whole-cell recordings, borosilicate glass pipettes of 6–8 M $\Omega$  resistance were filled with a potassium gluconate-based internal solution consisting of (in mM): 122 K-gluconate, 13 KCl, 10 HEPES, 10 phosphocreatine, 4 Mg-ATP, 0.3 Na-GTP, 0.3 EGTA (adjusted to pH 7.35 with KOH, osmolarity  $296 \pm 3.8$  mOsm). Signals were amplified using with EPC10-2 amplifiers (HEKA Elektronik, Lambrecht, Germany). All recordings were performed at 32–34°C, using a temperature control system (Bath-controller V, Luigs&Neumann, Ratingen, Germany) and slices were continuously superfused with extracellular solution at a rate of 2 mL/min. Recordings were sampled at 10 kHz, using the Patchmaster v2x32 program (HEKA Elektronik). DRD1-MSNs (Drd1-tdTomato mice), DRD2-MSNs (Drd2-eGFP) and mCherry-expressing MSNs (Drd2<sup>Cre/+</sup>::Lpl<sup>+/+</sup> and Drd2<sup>Cre/+</sup>::Lpl<sup>f/f</sup> mice) were visualized under direct interference contrast with an upright BX51WI microscope (Olympus, Japan), with a 40x water immersion objective combined with an infra-red filter, a monochrome CCD camera (Roper Scientific, the Netherlands) and a compatible system for analysis of images as well as contrast enhancement. Current over voltage (I/V) curves were acquired in current-clamp mode with membrane potentials maintained at  $-70$  mV.

For the bath-applied TG experiments, triolein (4  $\mu\text{M}$ ) was prepared just before use and applied 15–20 min before recording. 20  $\mu\text{L}$  of freshly thawed glyceryl trioleate (T7140 Sigma) was emulsioned in 1 mL of gum Arabic solution (5% in ACSF) by a 4 min probe sonication on ice, leading to a milky white emulsion (20.3 mM glyceryl trioleate) which was stable for several h on ice and readily dispersible in ACSF (final concentration of 4  $\mu\text{M}$ ) for recording. The vehicle solution was obtained by omitting glyceryl trioleate.

For experiments related to synaptic transmission, a concentric bipolar electrode (Phymep, France) was placed on the mPFC afferent glutamatergic fibers to evoke EPSCs at 0.2 Hz, recorded in MSNs under current-clamp configuration with membrane potentials maintained at  $-60$  mV. Only data from fluorescent (mCherry, tdTomato and eGFP) MSNs were included in the present study. The active and passive electrophysiological properties of MSNs were calculated according to and consistent with a previous study (Fino et al., 2007).

### Measurement of Locomotor Activity

Locomotor activity was recorded in an automated online measurement system using an infrared beam-based activity monitoring system (Phenomaster, TSE Systems GmbH, Bad Homburg, Germany).

### Pharmacological Manipulations

During two consecutive days before any procedure (habituation phase) mice were injected in their home-cage with NaCl 0.9% (i.p.). On the test day, animals were perfused for 6 h with NaCl 0.9% or TG and received injections (i.p.) of d-Amphetamine sulfate (3 mg/kg, A5880, Sigma-Aldrich, L'Isle d'Abeau, France), haloperidol hydrochloride (0.5 mg/kg, #0931, Tocris Biosciences, Bristol, United

Kingdom), raclopride (0.6 mg/kg, #1810, Tocris Biosciences, Bristol, United Kingdom) or SKF38393 (10 mg/kg, #0922, Tocris Biosciences, Bristol, United Kingdom). All drugs were dissolved in NaCl 0.9%.

### Catalepsy Test

Animals were centrally infused with saline or TG for 6 h and then injected with haloperidol (0.5 mg/kg) or raclopride (0.6 mg/kg) one h before the catalepsy test. At  $t = 0, 15, 30, 45, 60, 75, 90$  min, animals were taken out of their home cage and placed in front of a 4 cm elevated steel bar, with the forelegs placed upon the bar while the hind legs remained on the ground surface. The time during which animals remained still was measured. Animals that failed to remain on the bar for at least 30 s during the whole test were excluded. A behavioral threshold of 180 s was set so the animals remaining in the cataleptic position for this duration were put back in their cage until the next time point.

### Operant Conditioning System

#### Lever Operandum for Pellets

Mice were food-restricted and maintained at 90% of their initial body weight to facilitate initial learning and performance during the whole operant conditioning. Computer-controlled operant conditioning was conducted in 12 identical conditioning chambers (Phenomaster, TSE Systems GmbH, Bad Homburg, Germany) during the light phase, at the same h every day until the end of the procedure. The mice had intermittent access to an operant wall in their home cages. Each operant wall had two levers located 3 cm lateral to a central pellet dispenser, with the left lever arbitrarily designated as the active lever. The reinforcer was a single 20-mg peanut butter flavored sucrose tablet (TestDiet, Richmond, USA). Operant training was carried out daily with no interruption for 2 h under a fixed-ratio 1 (FR1). When the discrimination score between active and inactive lever press (active lever presses/inactive lever presses) exceeded 2, mice were shifted for 4 consecutive days to 1.5 h sessions under a progressive ratio (PR) [3 lever press more for each subsequent reinforcer ( $r = 3N+3$ ;  $N =$  reinforcer number)].

#### Nose-Poke Operandum for TG Self-administration

##### Nose-Poke (NP) Operandum

Mice were single housed on a 12 h reverse light/dark cycle (lights off 08:00 h) with water and food *ad libitum*. Operant conditioning chambers (Imetronic, Pessac, France) consisted in sound-attenuated boxes equipped with two nose-pokes counterbalanced as active or inactive across left and right. Illumination of a dim house-light signaled the start and the end of each session. 10 days after catheter implantation, mice were first trained to explore the cages with 50  $\mu$ l saccharine 0.1% delivery being contingently presented in a liquid dipper after each active hole visits on a Fixed Ratio 1 (FR-1) reinforcement schedule, then increased to FR-2 until mice reached criterion ( $> 10$  reinforcements in 30 min and  $> 50\%$  discrimination between NP). After saccharine pretraining, mice were moved to TG self-administration sessions of 60 min under a fixed-ratio 2 (FR-2) schedule of reinforcement. Active NP visits delivered 10  $\mu$ l of intracarotid TG accompanied by a 60 s presentation of a cue light above the active NP and followed by a 20 s time out during which nose-poke visits had no consequences. Mice were randomly assigned to self-administer saline ( $n = 5$ ) or TG ( $n = 13$ ). In order to test the role of internal states on TG self-administration, animals were tested under two conditions: food sated or 24 h deprived.

#### Conditioned Place Preference (CPP)

The CPP experiments were performed at the onset of the dark period on an unbiased apparatus. All the compartments were completely cleaned before each session of conditioning. Locomotor activity was recorded with infrared beam-based activity monitoring system and analyzed with the provided software (Phenomaster, TSE Systems GmbH, Bad Homburg, Germany). The least preferred compartment during the exploration phase was designated as the reward-baited compartment (biased protocol). Animals with more than 65% of preference for a compartment on the pre-test day were removed. On day 1, animals were carefully put in the middle of the cage and freely explored the two-compartments apparatus for 15 min. The subsequent days included conditioning sessions of one-h brain TG delivery conditioning alternated with one-h brain saline delivery conditioning. After 8 days of conditioning (4 sessions in each compartment), animals freely explored the two compartments for 15 min. The time spent in the reward-paired compartment before versus after conditioning was the primary outcome variable.

For the high-fat high-sugar (HFHS) conditioning, animals were centrally infused for 6 h in their home cages prior to conditioning sessions, for 10 consecutive days.

#### Binge Feeding Experiment

Animal were implanted with intracarotid catheter and single-housed one week prior to any experiments. Food intake and body weight were measured daily at 10 AM. Intracarotid saline or Intralipid perfusion were performed 6 h prior to intermittent access to drinking solution of high-fat high-sugar solution (Intralipid 20% enriched with sucrose 10%) daily at 10:30 AM during 10 consecutive days for one h.

#### Fiber Photometry and Data Analysis

A chronically implantable cannula (Doric Lenses, Québec, Canada) composed of a bare optical fiber (400  $\mu$ m core, 0.48 N.A.) and a fiber ferrule was implanted 100  $\mu$ m above the location of the viral injection site in the dorsal striatum (DS: L = +1.5; AP = +0.86; V = -3.25, in mm). The fiber was fixed onto the skull using dental cement (Super-Bond C&B, Sun Medical). Real time fluorescence



emitted from the calcium sensor GCaMP6f expressed by neurons with the DRD2 receptor was recorded using fiber photometry as described previously in the literature (Lerner et al., 2015). Fluorescence was collected in the dorsal striatum using a single optical fiber for both delivery of excitation light streams and collection of emitted fluorescence.

The fiber photometry setup used 2 light emitting LEDs: 405 nm LED sinusoidally modulated at 330 Hz and a 465 nm LED sinusoidally modulated at 533 Hz (Doric Lenses) merged in a FMC4 MiniCube (Doric Lenses) that combines the 2 wavelengths excitation light streams and separate them from the emission light. The MiniCube was connected to a Fiberoptic rotary joint (Doric Lenses) connected to the cannula. A RZ5P lock-in digital processor controlled by the Synapse software (Tucker-Davis Technologies, TDT, USA), commanded the voltage signal sent to the emitting LEDs via the LED driver (Doric Lenses). The light power before entering the implanted cannula was measured with a power meter (PM100USB, Thorlabs) before the beginning of each recording session. The irradiance was  $\sim 9 \text{ mW/cm}^2$ . The fluorescence emitted by the GCaMP6f activation in response to light excitation was collected by a femtowatt photoreceiver module (Doric Lenses) through the same fiber patch cord. The signal was then received by the RZ5P processor (TDT). On-line real time demodulation of the fluorescence due to the 405nm and the 465 nm excitations was performed by the Synapse software (TDT). A camera was synchronized with the recording using the Synapse software.

Signals were exported to MATLAB R2016b (Mathworks) and analyzed offline. After careful visual examination of all trials, they were clean of artifacts in these time intervals. The timing of events was extracted from the video. For each session, signal analysis was performed on two-time intervals: one extending from  $-50$  to  $0$  s (home cage, HC) and the other from  $0$  to  $+50$  s (new cage, NC).

From a reference window (from  $-180$  to  $-60$  s), a least-squares linear fit was applied to the 405 nm signal to align it to the 465 nm signal, producing a fitted 405 nm signal. This was then used to calculate the  $\Delta F/F$  that was used to normalize the 465 nm signal during the test window as follows:  $\Delta F/F = (465 \text{ nm signal}_{\text{test}} - \text{fitted } 405 \text{ nm signal}_{\text{ref}}) / \text{fitted } 405 \text{ nm signal}_{\text{ref}}$ . To compare signal variations between the two conditions (HC versus NC), for each mouse, the value corresponding to the entry point of the animal in the new cage was set at zero.

### Fluorescent *In Situ* Hybridization

In order to delineate the expression patterns of *Lpl*, *Th*, *Drd1* and *Drd2* transcripts within the mesolimbic circuitry of the brain, the RNAscope, a commercialized *in situ* hybridization assay was used. Adult male mice ( $n = 3$ ) were euthanized and their brains were immediately extracted and flash frozen in isopentane. Brains were sectioned at  $20 \mu\text{m}$  with a Leica cryostat, and coronal sections were probed for gene expression according to the protocols provided by Advanced Cell Diagnostics. *Th* and *Lpl* expressions were assayed in the VTA; *Drd1*, *Drd2* and *Lpl* expressions were assayed in the both the dorsal striatum (DS) and NAc. Z stacked images were captured with a Zeiss AxioObserver fluorescent microscope, Zeiss Apotome 2.0 and through a 63x objective lens. Three different rostro-caudal coronal sections for each structure (VTA, DS and NAc) were used. 3 images/section were taken from the lateral VTA, whereas 4 images/section were taken for both DS and NAc. Counts were added per section level (according to bregma) and per structure so as to have a representative sample. Cells that exhibited at least 4 puncta (RNA molecules) in addition to DAPI were counted as expressing the respective gene. All error bars represent  $\pm$  SEM.

### Lipidomics

Seven pairs of mice were infused at  $0.2 \mu\text{l/min}$  for 4 h with either saline or triglycerides. Immediately following infusion, mice were euthanized, and had their striatal (dorsal striatum and NAc) brain tissues rapidly extracted and frozen on dry ice. Lipid and protein analyses were performed at the UCSD Lipidomics Core. Relative abundances of individual species per sample were normalized to protein concentration per sample.

### *In Vivo* Electrophysiological Recordings

Adult male mice (10 weeks) perfused for 6 h with TG or saline were anesthetized with chloral hydrate (8%),  $400 \text{ mg/kg}$  i.p. supplemented as required to maintain optimal anesthesia throughout the experiment and positioned in a stereotaxic frame. A hole was drilled in the skull above midbrain DA nuclei (coordinates:  $3 \pm 0.3 \text{ mm}$  posterior to bregma,  $0.5 \pm 0.1 \text{ mm}$  [VTA] lateral to the midline (Paxinos and Franklin, 2003). Recording electrodes were pulled from borosilicate glass capillaries (with outer and inner diameters of 1.50 and 1.17 mm, respectively) with a Narishige electrode puller. The tips were broken under microscope control and filled with 0.5% sodium acetate. Electrodes had tip diameters of  $1\text{--}2 \mu\text{m}$  and impedances of  $20\text{--}50 \text{ M}\Omega$ . A reference electrode was placed in the subcutaneous tissue. The recording electrodes were lowered vertically through the hole with a micro drive. Electrical signals were amplified by a high-impedance amplifier and monitored with an oscilloscope and an audio monitor. The unit activity was digitized at 25 kHz and stored in Spike2 program. The electrophysiological characteristics of DA neurons were analyzed in the active cells encountered when systematically passing the microelectrode in a stereotaxically defined block of brain tissue including the VTA. Its margins ranged from  $-2.9$  to  $-3.3 \text{ mm}$  posterior to bregma (AP),  $0.4$  to  $0.6 \text{ mm}$  mediolateral (ML) and  $4$  to  $5 \text{ mm}$  ventral (DV). Sampling was initiated on the right side and then on the left side. Extracellular identification of DA neurons was based on their location as well as on the set of unique electrophysiological properties that distinguish DA from non-DA neurons *in vivo*: (i) a typical triphasic action potential with a marked negative deflection; (ii) a long duration ( $> 2.0 \text{ ms}$ ); (iii) an action potential width from start to negative trough  $> 1.1 \text{ ms}$ ; (iv) a slow firing rate ( $< 10 \text{ Hz}$  and  $> 1 \text{ Hz}$ ). Electrophysiological recordings were analyzed using the R software (<https://www.r-project.org>). DA cell firing was analyzed with respect to the average firing rate and the percentage of spikes within bursts (%SWB, number of spikes within burst divided by total number of spikes). Bursts were identified as discrete events consisting of a sequence of spikes such that: their onset is defined by two consecutive spikes within an interval  $< 80 \text{ ms}$ .

whenever and they terminate with an inter-spike interval > 160 ms. Firing rate and %SWB were measured on successive windows of 60 s, with a 45 s overlapping period on a total period of 300 s. Responses to TG or Saline acute injections are presented as the Mean of percentage of firing frequency variation from the baseline  $\pm$  SEM. For statistical analysis, maximum of firing variation induced by TG occurring 180 s after the injection are compared to the maximum of firing rate variation induced by saline occurring 180 s after the injection by non-parametric Mann-Whitney paired test.

### Tissue Preparation and Immunofluorescence

Mice were rapidly anaesthetized with pentobarbital (500 mg/kg, i.p., Sanofi-Aventis, France) and transcardially perfused with 4% (weight/vol.) paraformaldehyde in 0.1 M sodium phosphate buffer (pH 7.5). Brains were post-fixed overnight in the same solution and stored at 4°C. 30  $\mu$ m-thick sections were cut with a vibratome (Leica VT1000S, France), stored at  $-20^{\circ}\text{C}$  in a solution containing 30% ethylene glycol, 30% glycerol and 0.1 M sodium phosphate buffer. Sections were processed as follows: Day 1: free-floating sections were rinsed in Tris-buffered saline (TBS; 0.25 M Tris and 0.5 M NaCl, pH 7.5), incubated for 5 min in TBS containing 3%  $\text{H}_2\text{O}_2$  and 10% methanol, and then rinsed three times for 10 min each in TBS. After 15 min incubation in 0.2% Triton X-100 in TBS, sections were rinsed three times in TBS again. Slices were then incubated overnight or 72 h at 4°C with the following primary antibodies: rabbit anti-phospho-rpS6<sup>Ser235/236</sup> overnight (1:500, Cell Signaling Technology), goat anti-c-Fos (1:250, Santa Cruz Biotechnology) or rabbit anti-c-Fos (1:500, Synaptic Systems) for 72 h. Sections were rinsed three times for 10 min in TBS and incubated for 60 min with secondary antibodies anti-rabbit Cy3 AffiniPure (1:1000, Jackson ImmunoResearch) and anti-goat Dylight488 (1:1000, Vector labs). Sections were rinsed twice for 10 min in TBS and once in TB (0.25 M Tris) before mounting.

Acquisitions were performed with a confocal microscope (Zeiss LSM 510) with a color digital camera and AxioVision 3.0 imaging software. Images used for quantification were all single confocal sections. Photomicrographs were obtained with the following band-pass and long-pass filter settings: A488 (band pass filter: 505–530) and Cy3 (band pass filter: 560–615). The objectives and the pinhole setting (1 airy unit, au) remained unchanged during the acquisition of a series for all images. Quantification of immunopositive cells was performed using the cell counter plugin of the ImageJ software taking as standard reference a fixed threshold of fluorescence.

### Western Blotting

Mouse head was cut and immediately immersed in liquid nitrogen for 4 s. The brain was then removed and dissected on ice-cold surface, sonicated in 200  $\mu$ l of 1% SDS supplemented with 0.2% phosphatase inhibitors and 0.1% protease inhibitors, and boiled for 10 min. Aliquots (2.5  $\mu$ l) of the homogenates were used for protein quantification using a BCA kit (BC Assay Protein Quantitation Kit, Interchim Uptima, Montluçon, France). Equal amounts of proteins (15  $\mu$ g) for each sample were loaded onto 10%–12% polyacrylamide gels. Proteins were separated by SDS-PAGE and transferred to PVDF membranes (Millipore). The membranes were immunoblotted with the following antibodies: rabbit anti-phospho-rpS6<sup>Ser235/236</sup> (1:1000, Cell Signaling Technology), rabbit anti-phospho-rpS6<sup>Ser240/244</sup> (1:1000, Cell Signaling Technology), rabbit anti-phospho-p70S6K<sup>Thr421/Ser424</sup> (1:1000, Cell Signaling Technology), rabbit anti-phospho-p70S6K<sup>Thr389</sup> (1:1000, Cell Signaling Technology), mouse  $\beta$ -actin (1:5000, Sigma), rabbit anti-phospho-ERK1/2 (1:2000, Cell Signaling Technology), rabbit anti-phospho-DARPP-32<sup>Thr34</sup> (1:750, Cell Signaling Technology), rabbit anti-phospho-TH<sup>Ser31</sup> (1:1000, Cell Signaling Technology), rabbit anti-phospho-TH<sup>Ser40</sup> (1:1000, Cell Signaling Technology), mouse anti-TH (1:2000, Millipore), rabbit anti-phospho-Akt<sup>Ser473</sup> (1:1000, Cell Signaling Technology), rabbit anti-phospho-Akt<sup>Thr308</sup> (1:1000, Cell Signaling Technology), rabbit anti-phospho-GSK3 $\beta$ <sup>S9</sup> (1:1000, Cell Signaling Technology). Detection was based on HRP-coupled secondary antibody binding detected using ECL as detection system. The secondary antibodies were anti-mouse (1:5000, Dako) and anti-rabbit (1:10000, Cell Signaling Technology). Quantification was performed using the ImageJ software.

### Doppler Imaging

Color Doppler scans of the brain were performed with a Vevo LAZR system (FujiFilm VisualSonics, Toronto, ON, Canada) using the LZ201 transducer (9–18 MHz bandwidth). Mice equipped with a carotid artery catheter were maintained anesthetized with isoflurane. Hair was removed on the head with depilatory cream and mice were positioned prone for imaging. The transducer was positioned to scan a coronal section of the whole head centered on the posterior cerebral artery. Images were acquired continuously. Catheter was connected to an infusion device that delivered NaCl 0.9% or TG emulsion (Intralipid 20%) at rates of 0.1  $\mu$ l/min; 1  $\mu$ l/min or 10  $\mu$ l/min. Images were exported and analyzed using ImageJ software.

### Whole-Brain c-Fos Immunostaining

C57BL/6J male mice received a 6 h saline or Intralipid perfusion and were sacrificed 1 h after amphetamine injection (3 mg/kg). Brains were excised and post fixed in 4% paraformaldehyde overnight at room temperature and transferred stepwise to 100% methanol using the following protocol. 20% methanol (in ddH<sub>2</sub>O) for 1 h, 40% methanol for 1 h, 60% methanol for 1 h, 80% methanol for 1 h, and 100% methanol for 1 h twice. iDISCO staining was performed as described in Renier et al. (Renier et al., 2014) with one exception. All the washing steps after incubation with primary and secondary antibody were extended from one to three days. Incubation time for primary and secondary antibody was 4 days each. The primary antibody was Rabbit pAb anti c-Fos (Ab-5) (4-17) from Calbiochem (1:10,000 dilution), and the secondary antibody was Cy5-anti rabbit from Jackson ImmunoResearch (1:1000 dilution). Brain samples were scanned using an UltraMicroscope II LSFM system (Lavision Biotec, Bielefeld, Germany) in 4.06  $\mu$ m for the c-Fos activation study. Auto-fluorescence was recorded at 545 nm for anatomy information, while the c-Fos signal was acquired

with a 620 nm emission filter. Images were registered to a digital brain atlas using the Elastix software library<sup>11</sup>. A source image  $I_S(x)$  was registered to a target image  $I_T(x)$  by finding a coordinate transformation  $T(x)$  that made  $I_S(T(x))$  spatially aligned with  $I_T(x)$ . We used an affine coordinate transformation for initialization followed by non-rigid b-spline coordinate transformation which was iteratively optimized with respect to the mutual information between the source and the target. Registration parameters for mapping of LSM data were similar to those used in Renier et al. (Renier et al., 2014). Imaris (Release 7.6.5, Bitplane, Zurich, Switzerland) was used to generate Figure 2F. ROI based analysis of the total fluorescence signal for c-Fos heatmap intensities were computed using multiple t tests assuming unequal variance. The heatmaps were generated as described in (Salinas et al., 2018). The statistical analysis was performed using GraphPad Prism (Release 6, GraphPad Software, Inc., United States).

### Isolation of Total RNA and Quantitative RT-PCR

Each sample consisted of the tissue deriving from one mouse brain. Mice were sacrificed by cervical dislocation. The dorsal striatum (DS) and the NAc were quickly dissected out and placed on ice. Each tissue sample was homogenized in TRIzol with 3 mm tungsten carbide beads (QIAGEN cat.No. 69997). Total RNA was extracted with TRIzol Reagent (Life Technologies) according to manufacturer's instructions. The RNA was quantified by using the NanoDrop 1000 spectrophotometer. Between 85 and 500 ng of mRNA from each sample were used for retro-transcription, performed with the Reverse Transcriptase M-MLV (Life Technologies) following the manufacturer's instructions. Quantitative real time PCRs, were performed in a LightCycler 1.5 detection system (Roche, Meylan France) using the LightCycler FastStart DNA Master plus SYBR Green I kit (Roche) in 384-well plates according to the manufacturer's instruction. All reactions were carried out in duplicate (Striatum) or triplicate (Hypothalamus). Results are presented as normalized to the house-keeping gene and the delta-CT method was used to obtain a FC.

### Metabolic Efficiency Analysis

Mice were monitored for whole energy expenditure (EE) or Heat (H), oxygen consumption and carbon dioxide production, respiratory exchange rate ( $RER = VCO_2/VO_2$ , where V is a volume), and locomotor activity using calorimetric cages with bedding, food and water (Labmaster, TSE Systems GmbH, Bad Homburg, Germany).

Ratio of gases was determined through an indirect open circuit calorimeter (for review (Arch et al., 2006; Even and Nadkarni, 2012)). This system monitors  $O_2$  and  $CO_2$  concentration by volume at the inlet ports of a tide cage through which a known flow of air is being ventilated (0.4 L/min) and compared regularly to a reference empty cage. For optimum analysis, the flow rate was adjusted according to the animal body weights to set the differential in the composition of the expired gases between 0.4 and 0.9% (Labmaster, TSE Systems GmbH, Bad Homburg, Germany).

The flow was previously calibrated with  $O_2$  and  $CO_2$  mixture of known concentrations (Air Liquide, S.A. France). Oxygen consumption, carbon dioxide production and energy expenditure were recorded every 15 min for each animal during the entire experiment. Whole energy expenditure was calculated using the Weir equation respiratory gas exchange measurements. Food consumption was measured as the instrument combines a set of highly sensitive feeding and drinking sensors for automated online measurements. Mice had free access to food and water *ad libitum*. To allow measurement of every ambulatory movement, each cage was embedded in a frame with an infrared light beam-based activity monitoring system with online measurement at 100 Hz. The sensors for gases and detection of movement operated efficiently in both light and dark phases, allowing continuous recording.

Mice were monitored for body weight and composition at the entry and the exit of the experiment. Body mass composition (lean tissue mass, fat mass, free water and total water content) was analyzed using an Echo Medical systems' EchoMRI (Whole Body Composition Analyzers, EchoMRI, Houston, USA), according to manufacturer's instructions. Briefly, mice were weighed before they were put in a mouse holder and inserted in MRI analyzer. Readings of body composition were given within 1 min.

Data analysis was performed on Excel XP using extracted raw value of  $VO_2$  consumed,  $VCO_2$  production (express in mL/h), and energy expenditure (kcal/h). Subsequently, each value was expressed by total body weight extracted from the EchoMRI analysis.

### Human Methods and Analysis

The procedures for the human fMRI experiment are described in detail in the Supplemental Information. In brief, 29 participants underwent three days of scanning during which they were instructed to sniff pulses of food and non-food (floral) aromas while their blood oxygen level dependent (BOLD) signal was measured. This comparison isolates BOLD responses to calorie-predictive food cues that are independent from general experiences of pleasantness, and therefore reflect a specific measure of food cue reactivity. Internal state was manipulated across days so that scanning occurred when subjects were fasted (HUNGRY) or fed a standard or *ad libitum* meal (FIXED versus SATIED). Internal state ratings and perceptual ratings of odor stimuli were assessed throughout the sessions and blood samples were acquired at baseline and 30, 60, and 90 min from the start of the meal or equivalent time point on the hungry day. Imaging data were acquired on a Siemens 3.0 Tesla TIM Trio Scanner at the Yale University Magnetic Resonance Research Center using our standard procedures for acquisition and analysis (Sun et al., 2015; Sun et al., 2014). Responses were considered significant corrected for multiple comparisons using family wise error (FWE) correction across the whole brain or across the number of voxels in the NAc or its prefrontal projection region, the ventromedial prefrontal cortex (vmPFC). These regions of interest (ROI) were selected based on the animal findings and were created by searching the Neurosynth database for NAc and vmPFC responses to food cues, followed by extraction of the centroids from the resultant peak responses. 10 mm spheres were then drawn around the centroids to perform small volume correction.

### Participant Recruitment

Twenty-nine right-handed participants (age range 18–39,  $M = 26.80$ ,  $SD = 5.49$ ; BMI range 19.5–33.6,  $M = 23.94$ ,  $SD = 3.86$ ; male = 16, female = 13) were recruited from the greater New Haven area through the Yale University Interdisciplinary Research Consortium on Stress, Self-Control and Addiction (IRCSSA) P30 Subject's core as well as via flyer advertisement. Participants were screened over the phone to be less than 40 years of age, free of psychiatric disorders, eating disorders, current dieting behavior, alcoholism, use of tobacco or drugs other than alcohol, history of head injury with loss of consciousness, use of daily medication other than monophasic birth control, chemosensory impairments, lactose intolerance or food allergies. We did not impose a BMI upper-limit. Individuals were included so long as they felt comfortable while inserted in the scanner bore. Females provided the date of their last period to ensure that they were not scanned during menstruation or ovulation. All participants provided written informed consent at their first lab visit and the study was approved by the Yale Human Investigations Committee.

### Genotyping for TaqI A1 Polymorphism

Saliva samples were obtained from the participants using Oragene Discover collection kits and DNA extraction was performed as directed by the manufacturer (DNA Genotek). TaqI A1 allele status was determined by amplifying a 304 bp region with PCR using forward (5'-CCCTTCCTGAGTGTCA-3') and reverse (5'-CGGCTGGCCAA GTTGTCT-3') primers as described by [Epstein et al., \(2007\)](#). The products of the amplification were digested overnight with the restriction enzyme TaqI. The resulting DNA fragments were tagged with ethidium bromide and separated via gel electrophoresis. The appearance of a 304 bp band indicated the presence of the TaqI A1 allele. Sixteen participants were carriers of the A1 allele of the dopamine D2 receptor (DRD2) gene region (A1+; age range 19–37,  $M = 27.38$ ,  $SD = 5.28$ ; BMI range 19.5–33.6,  $M = 25.04$ ,  $SD = 4.66$ ; male = 9, female = 7), and 13 were non-carriers (A1-; age range 18–39,  $M = 26.08$ ,  $SD = 5.87$ ; BMI range 19.9–25.68,  $M = 22.59$ ,  $SD = 2.00$ ; male = 7, female = 6).

### Food and Non-food Odor Stimuli

Food odors were “chocolate cookie” and “strawberry and cream” odors (6002335, 6106524 from Bell Labs Flavors and Fragrances, Inc.). Non-food odors were “honeysuckle” and “lilac” odors (039831 Chey N-3 from Firmenich, Inc.; 31731066 Lilac 71 from International Flavors and Fragrances, Inc.).

### Stimulus Delivery

Odors were presented by a custom built, MRI compatible olfactometer programmed in Labview (National Instruments). A detailed description of the olfactory stimulation system can be found in a previous publication ([Stice et al., 2008](#)). In brief, mass flow controllers (MKS Instruments) adjust the flow of humidified and temperature-controlled air over stainless steel wells containing an odorant, allowing the air to pick up vaporized odor molecules. The independent odor channels converge into a mixing manifold and exit through 1 of 2 Teflon tubes where the first is dedicated to odors and the second is dedicated to clean air. The trunk terminates in a Teflon manifold (Tegcom) resting on the participant's chest. A vacuum line connected to this manifold creates a closed loop to evacuate odorized as well as odorless (OL) air, preventing head space contamination. The participants receive OL and odor stimuli embedded in a continuous stream of clean, OL air from the manifold through a nasal mask (Philips Respironics). As air exits the mask, it is drawn out through a final Teflon tube by another vacuum line. The mask is also coupled to a pneumotachograph to measure airflow in the nose ([Johnson and Sobel, 2007](#)), which is in turn connected to a spirometer (AD Instruments). The signal from the spirometer is fed into an amplifier (AD Instruments, PowerLab 4SP) and digitally recorded at 100 Hz using Chart 5.5.6 (AD Instruments).

### Experimental Procedures

All participants underwent a training session, and three fMRI scanning sessions (Hungry, Fixed and Sated conditions). All sessions were conducted on separate days and scan order was counterbalanced.

### Training Session

Participants were instructed to refrain from eating or drinking anything other than water for at least an h before the session. Anthropometric measurements were taken at the beginning of the session. Body weight and height were measured using a Detecto 439 balance beam scale with stadiometer at The John B. Pierce Laboratory. BMI was calculated as weight (in kilograms) divided by the squared height (in meters) of the participant ( $BMI = kg/m^2$ ).

Participants were trained to make computerized ratings of their internal state as well as the perceptual qualities of our stimuli on computerized scales. Participants rated the intensity of their feelings of hunger and fullness using adapted cross modal general Labeled Magnitude Scales (gLMS) consisting of a 100 mm vertical line scale with the labels “no sensation” at the lower anchor point and “strongest imaginable sensation” at the upper anchor point ([Bartoshuk et al., 2004](#); [Green et al., 1996](#)). Stimulus ratings consisted of ratings of each stimulus's intensity, liking, wanting to eat, edibility and familiarity. Intensity was measured by adapted cross modal gLMS. Liking was measured using a labeled hedonic scale (LHS) consisting of a 100 mm vertical line scale with the labels “most disliked sensation imaginable” at the lower anchor point, “most liked sensation imaginable” at the upper anchor point, and “neutral” in the middle ([Lim et al., 2009](#)). Wanting to eat, edibility, and familiarity were measured using a 20 mm cross-modal visual analog scale. Wanting to eat labels were “I would never want to consume this” (–10), “neutral” (0) and “I would want to consume this more than anything” (+10). Edibility labels were “not edible at all” at (–10), neutral at (0) and “very edible” at (+10). Familiarity labels were “not familiar at all” (–10), “neutral” (0) and “very familiar” (+10).



After training to make computerized ratings, participants participated in mock scanner training to become familiarized with the task, and to determine whether it would be uncomfortable to be in the scanner with the nasal mask. During mock scanning, the odor stimuli or OL were delivered using the olfactometer. First, each odor was delivered one at a time and participants verbally rated the intensity of each presentation by telling the experimenter approximately where on the gLMS the odor's intensity fell in relation to the scale's labels (e.g., "Very Strong," "A little less than Weak," "Halfway between Moderate and Strong"). An experimenter then manually adjusted the odorant concentration settings on the olfactometer so that each odor was rated moderate in intensity. This resulted in the creation of a personalized dilution profile for each odor and each participant, allowing us to control for individual differences in sensory acuity. Next, participants made internal state ratings as well as perceptual ratings of each of the stimuli using a mouse on a computer monitor viewed via back projection on a headcoil-mounted mirror and then underwent a simulated fMRI run. After completing the ratings, participants underwent odor runs in the mock scanner. At the end of this training session, participants were then given commercially available pre-packaged granola bars (190 kcal per package) for breakfast on the day of fMRI scanning session.

### fMRI Scanning Sessions

All participants were instructed to eat the breakfast bars (1 package for women, 1.5 packages for men) in the morning at home, and then refrain from eating or drinking, with the exception of water, until their session. Participants arrived at the scanning center at 11:45 AM. Starting at 12:15 PM, a Teflon catheter was inserted into an antecubital vein for blood sampling. Baseline blood samples were obtained at 12:30 and 12:45 PM. Five minutes after the baseline blood sampling, participants ate a fixed-portion lunch (1 sandwich and 1 serving of apple slices for women, 1.5 sandwiches and 1 serving of apple slices for men) for the Fixed condition, or an *ad libitum* lunch (3 sandwiches and 4 servings of apple slices for both women and men and instructed to eat as much as they'd like) for the Sated condition, or nothing for the Hungry condition. For a fixed-portion lunch or an *ad libitum* lunch, participants received apple slices (approximately 25 kcal of apple per bag) and their choice of sandwich from the options of tuna, ham, turkey, or avocado served on white bread with cheese, tomato, and mayonnaise. Each sandwich was designed to contain approximately 400 kcal and was cut into quarters before serving to discourage participants from interpreting each entire sandwich as one large "portion." The amount and type of foods consumed at *ad libitum* lunch were recorded without the participants' knowledge.

After eating lunch, participants were escorted to the scanner at approximately 1 PM. The second blood samples were collected at 60 min from time of meal (or no meal) onset. Internal state ratings were obtained concomitant to the baseline and second blood samples were obtained (at 12:45 PM and 1:50 PM). Temporal variability of onset of each blood sampling between each condition was minimized.

Once inside the fMRI scanner, participants underwent four odor runs. Each odor run was 5 min 54 s long. Participants were instructed to breathe in through their nose after receiving the verbal cue "3, 2, 1, sniff" through headphones. Odor or OL delivery always occurred immediately following the auditory cue so that delivery was time-locked to sniff onset. Olfactory stimulation lasted for 3 s followed by a 9–19 s rest period before the next trial. There were 6 repetitions each of food odors, non-food odors, and OL stimuli. Participants were asked to keep their eyes closed during the functional runs, and no behavioral task was required other than to experience the stimuli. Before and after the fMRI scan, participants provided their stimulus ratings in the MRI scanner. At 60 min from meal (or no meal), participants provided internal state ratings for hunger and fullness. The odor runs were interspersed with additional anatomical and functional scans using taste stimuli that are reported in a separate manuscript (Sun et al., 2014).

### fMRI Data Acquisition

Imaging data were acquired on a Siemens 3.0 Tesla TIM Trio Scanner at the Yale University Magnetic Resonance Research Center. High-resolution T1-weighted structural scans were acquired for each participant with the following parameters: TR = 2230 ms, TE = 1.73 ms, flip angle = 9°, matrix = 256 × 256, 1 mm thick slices, FOV = 250 × 250, 176 slices. For fMRI runs, a susceptibility-weighted single-shot echo-planar sequence was used to image regional distribution of the BOLD signal. At the beginning of each functional run, the MR signal was allowed to equilibrate over 6 scans for a total of 12 s, which were subsequently excluded from the analyses. Acquisition parameters were: TR = 2000 ms, TE = 20 ms, flip angle = 80°, FOV = 220, matrix = 64 × 64, slice thickness = 3 mm. Forty contiguous slices were acquired in an interleaved method to reduce the cross-talk of the slice selection pulse.

### Data Analysis (Human Studies)

#### Ratings for Internal State and Stimuli

All statistics were performed in SPSS Version 21.0 (SPSS Inc., Chicago, IL, USA). Internal state ratings for each participant were log transformed. One participant's stimulus ratings from the Hungry, Fixed, and Sated conditions and another's from the Sated condition were omitted due to technical malfunction of equipment during collection. One participant's internal state ratings from the Hungry condition and another's from the Sated condition were also omitted due to technical malfunction. Those missing values were completed by inserting mean values. A mixed-design analysis of variance (ANOVA) was performed to assess the effects of condition, time, and group, as well as interactions between the above, on internal state and stimulus ratings.

#### Food Intake

An unpaired t test was performed to test whether caloric intake from lunch of the Sated condition would differ between groups.

### Blood Collection and Analysis

Samples were centrifuged immediately and kept on ice for the duration of each condition, then frozen at either  $-80^{\circ}\text{C}$  [free fatty acid (FFA) and insulin] or  $-20^{\circ}\text{C}$  (glucose, triglycerides). Plasma levels of insulin were measured with radioimmunoassay kits that utilize the double antibody technique with  $^{125}\text{I}$ -labeled hormone and hormone antiserum (Cat. # HI-14K, EMD Millipore Corporation, Billerica MA). Glucose, FFA and triglyceride concentrations were measured using enzymatic colorimetric techniques (FFA: Cat. # 999-34691, 991034891, 993-35191, Wako Pure Chemical Industries, Ltd., Osaka, Japan. Triglycerides: Cat. # SA1023, RX1023; Glucose: Cat. # SA1014, RX1014, Alfa Wassermann Diagnostic Techniques, West Caldwell NJ).

The effects of time, condition, and group, as well as interactions between the above, on the concentration of triglycerides were tested using a mixed-design ANOVA. We then tested the association between caloric intake and baseline triglyceride concentrations at the Sated session in each group by Pearson's correlation analysis.

### Neuroimaging Data

Neuroimaging data were analyzed using SPM8 software (Statistical Parametric Mapping, Wellcome Department of Imaging Neuroscience) in MATLAB R2010b 7.11.0 (Mathworks, Inc.). Functional images were time-acquisition corrected to the slice obtained at 50% of the TR and realigned to the mean image. Anatomical and functional images were normalized to the standard MNI template brain implemented in SPM8, resulting in voxel sizes of 3 and 1  $\text{mm}^3$ , respectively. Functional time-series data were detrended and then smoothed using a 6 mm FWHM isotropic Gaussian kernel. Motion parameters were included as regressors in the design matrix at the single participant level.

A design matrix was created for each participant for odor runs across all scan days that produced 2 events of interest: 1) Odors (Food + Non-food odors) and 2) OL. Event onsets were defined as the beginning of odor onset and event durations were defined as the 3 s of odor delivery. A 270 s high pass filter was applied to the time series data to remove low frequency noise and slow signal drifts. The general linear model was employed to estimate condition-specific effects at each model. A canonical hemodynamic response function was used to model neural response to events of interest.

To investigate the effect of genotype on the association between postprandial serum triglyceride change (60 min after lunch - baseline) and difference in brain response to food odors (food odor - non-food odor) between conditions [(Hungry - Fixed) and (Hungry - Sated)], individual contrast maps of [(food odor - non-food odor) Hungry - (food odor - non-food odor) Fixed/Sated] were entered into regression models with postprandial serum triglyceride changes as a covariate. The T-map threshold was set at  $p$  uncorrected  $< 0.005$  and a 5-voxel cluster size. Peak voxels of the unpredicted cluster were considered significant at  $p < 0.05$  family wise error (FWE) corrected across the entire brain for multiple comparisons. Next, region-of-interest (ROI) searches were performed using anatomical ROIs. Peaks within these regions were considered significant at  $p < 0.05$  FWE corrected across the individual ROI. All ROI masks (ventral striatum and vmPFC) were selected by searching the Neurosynth database for NAc and vmPFC responses to food cues, followed by extraction of the centroids from the resultant peak responses. 10mm spheres were then drawn around the centroids for small volume correction.

## QUANTIFICATION AND STATISTICAL ANALYSIS

### Statistical Analysis

Except for human study, all statistical comparisons were performed with Prism 6 (GraphPad Software, La Jolla, CA, USA). The statistical tests used are listed along with the statistical values in the Supplemental Tables. In condition of intracarotid catheter implantation, outliers were discarded based on evidence of lost tubing patent and failed perfusion. All the data were analyzed using either Student  $t$  test (paired or unpaired) with equal variances or One-way ANOVA or Two-way ANOVA. Lipidomic results were analyzed by simple comparisons (unpaired  $t$  test). Levels of phospho-proteins were analyzed by both simple comparisons (unpaired  $t$  test) and multiple comparisons (Two-way ANOVA). In all cases, significance threshold was automatically set at  $p < 0.05$ . ANOVA analyses were followed by Bonferroni post hoc test for specific comparisons only when overall ANOVA revealed a significant difference (at least  $p < 0.05$ ). All details related to statistical analyses are summarized in [Table S5](#).

### DATA AND CODE AVAILABILITY

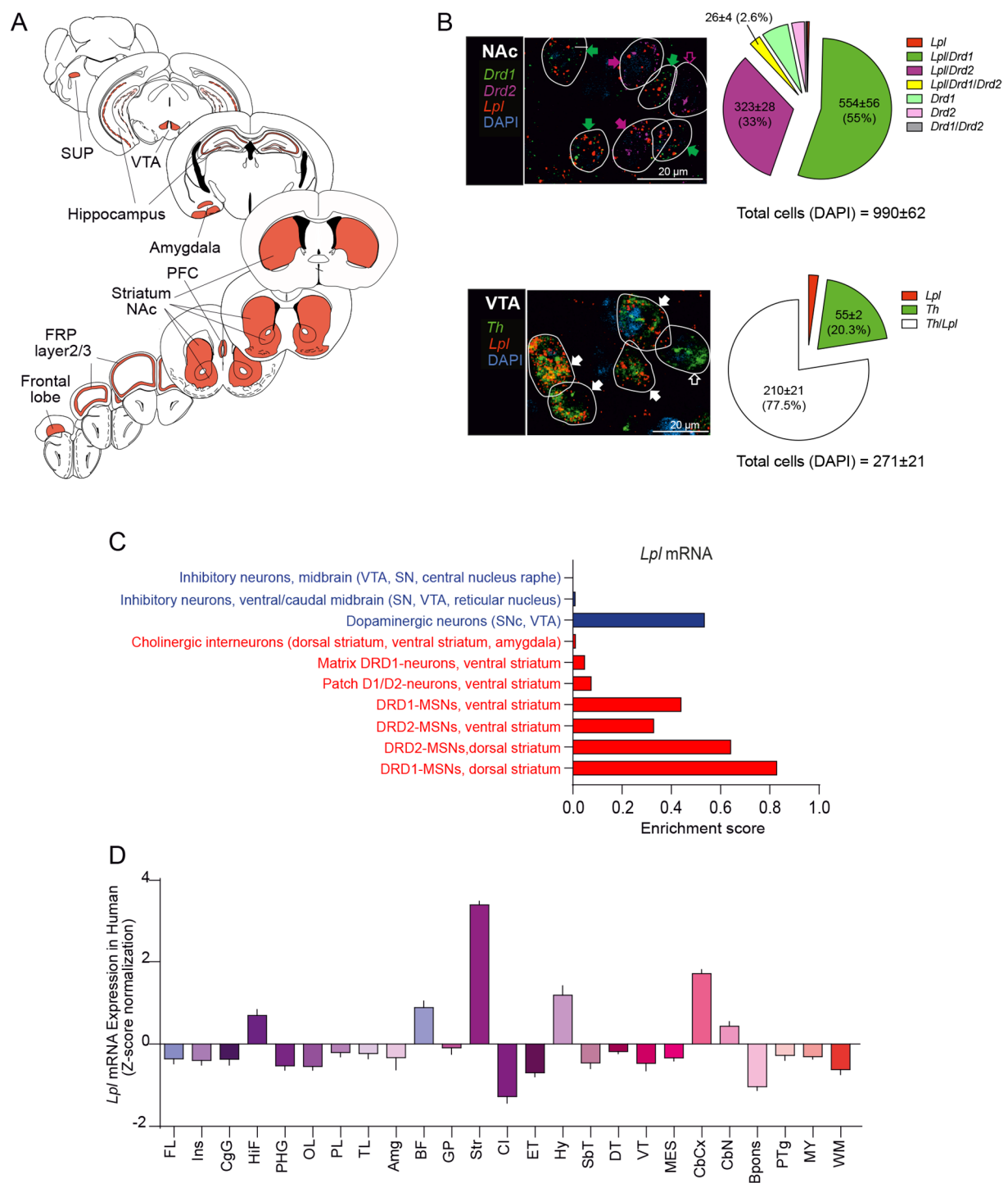
This study did not generate/analyze [datasets/code].

**Supplemental Information**

**Circulating Triglycerides Gate Dopamine-Associated**

**Behaviors through DRD2-Expressing Neurons**

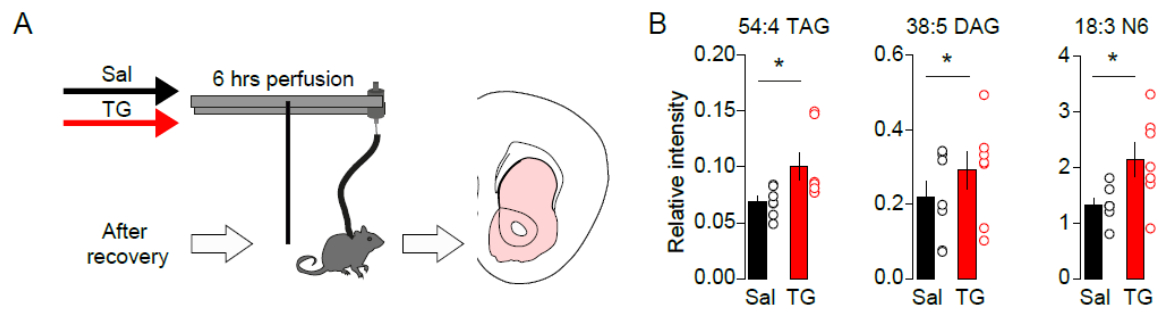
**Chloé Berland, Enrica Montalban, Elodie Perrin, Mathieu Di Miceli, Yuko Nakamura, Maud Martinat, Mary Sullivan, Xue S. Davis, Mohammad Ali Shenasa, Claire Martin, Stefania Tolu, Fabio Marti, Stephanie Caille, Julien Castel, Sylvie Perez, Casper Gravesen Salinas, Chloé Morel, Jacob Hecksher-Sørensen, Martine Cador, Xavier Fioramonti, Matthias H. Tschöp, Sophie Layé, Laurent Venance, Philippe Faure, Thomas S. Hnasko, Dana M. Small, Giuseppe Gangarossa, and Serge H. Luquet**



**Figure S1. Distribution of *Lpl* mRNA in the mesocorticolimbic system. Related to Figure 1. (A)** Central *in situ* hybridization detection of *Lpl* mRNA in C57Bl6/J mouse brain (male) from the Allen Institute. FRP: frontal pole layer, NAc: nucleus accumbens, PFC: prefrontal cortex, VTA: ventral tegmental area, SUP: pontine structures. **(B)** Representative photomicrographs and semi-quantitative analysis of RNAscope fluorescence *in situ* hybridization (FISH) signal for Lipoprotein lipase (*Lpl*, red), tyrosine hydroxylase (*Th*, green), dopamine receptor 1 and 2

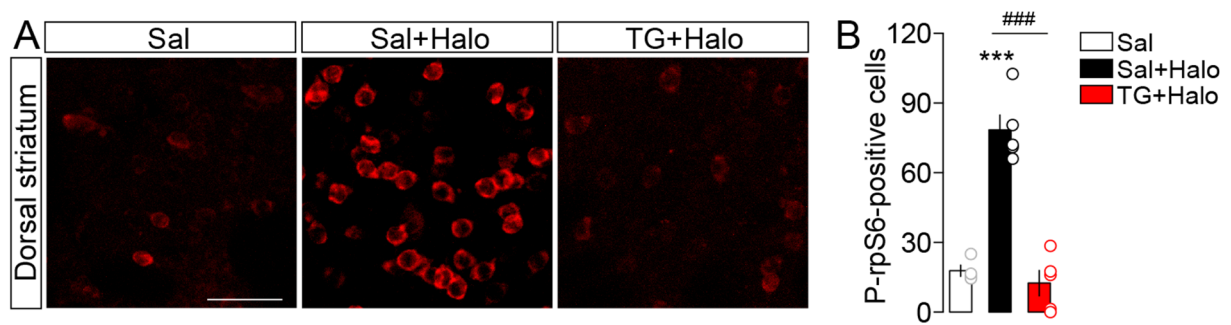


(*Drd1* green, *Drd2* violet) in the ventral tegmental area (VTA) and the nucleus accumbens (NAc). DAPI (blue) was used to identify cells. Scale bars: 20  $\mu$ m. The white lines represent the cellular limits. Filled and empty arrows within representative photomicrographs indicate co-expression or absence, respectively, of *Lpl* according to the presence of *Th* (white arrows), *Drd1* (green arrows) and *Drd2* (violet arrows) transcripts. **(C)** *Lpl* mRNA enrichment score in different midbrain (blue) and striatal (red) cells extracted from single-cell RNA sequencing atlas (Zeisel et al., 2018) (<http://mousebrain.org/genesearch.html>). Data are plotted as function of the enrichment score and filtered by trinarization score >0.95. **(D)** Quantification of *Lpl* expression in human brain structures based on the Allen Institute database. Structures: FL (frontal lobe), Ins (insula), CgG (cingulate gyrus), HiF (hippocampal formation), PHG (parahippocampal gyrus), OL (occipital lobe), PL (parietal lobe), TL (temporal lobe), Amg (amygdala), BF (basal forebrain), GP (globus pallidus), Str (striatum), CI (claustrum), ET (epithalamus), Hy (hypothalamus), Sbt (subthalamus), DT (dorsal thalamus), VT (ventral thalamus), MES (mesencephalon), CbCx (cerebellar cortex), CbN (cerebellar nuclei), Bpons (basal part of pons), PTg (pontine tegmentum), MY (myelencephalon), WM (white matter).



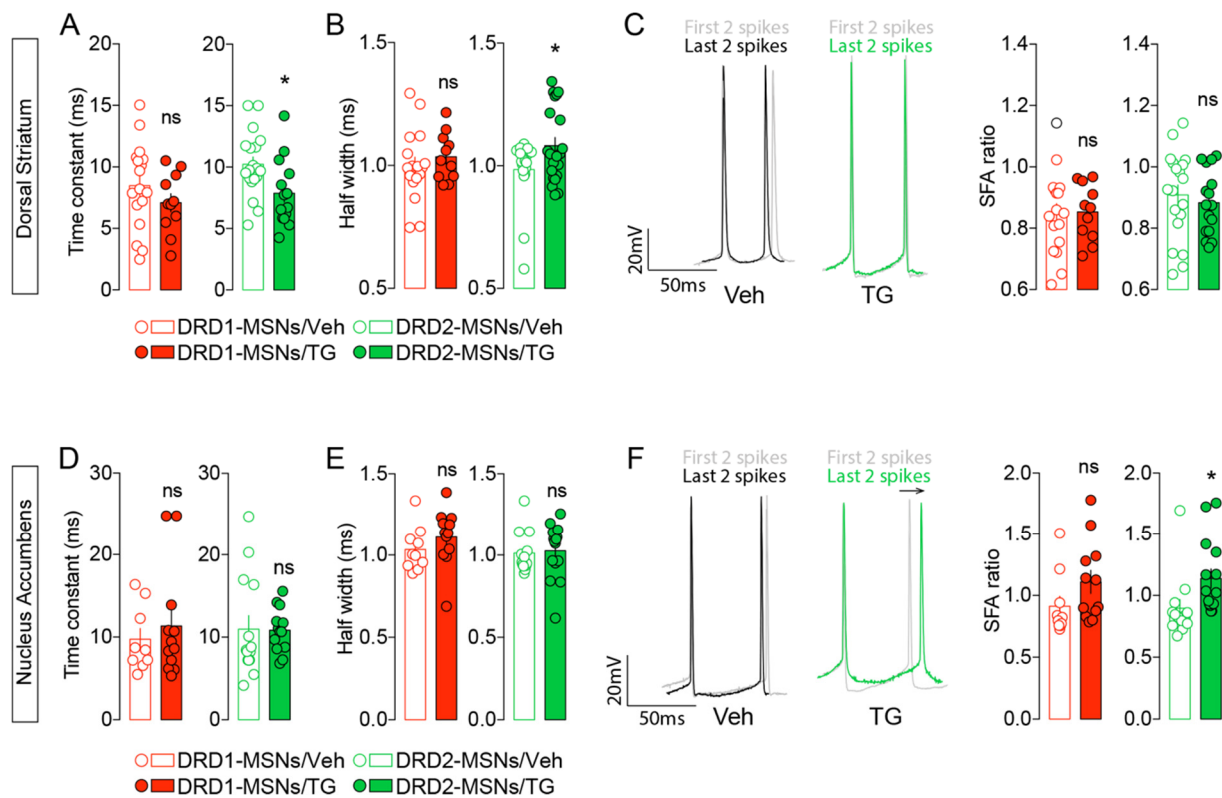
**Figure S2. Lipidomic analysis following central TG delivery. Related to Figure 1.**

**(A)** Experimental design of brain TG delivery technique. Animals were perfused through the carotid for 6-hours (6-hrs) with saline (Sal) or Intralipid™ (TG). Striata were dissected and used for lipidomic analysis. **(B)** Lipidomic analysis of 54:4 TAG, 38:5 DAG and 18:3 N6 FFA contents in the striatum of animals centrally perfused with saline (Sal, n=7) or TG (TG, n=7). Statistics: \* $p < 0.05$  Sal vs TG. For statistical details see Table S5.



**Figure S3. Central TG delivery blunts DRD2-dependent striatal signaling pathways. Related to Figure 2.**

(A) Representative confocal photomicrographs and (B) quantification of phosphor-rpS6<sup>Ser235/236</sup>-positive cells in the dorsal striatum of animals infused with saline and injected with saline (Sal, n=4) or haloperidol (Sal/Halo, n=5) and animals infused with TG and injected with haloperidol (TG/Halo, n=5). Scale bar: 50  $\mu$ m. Statistics (multiple comparisons): (\*\*\*)p<0.001 Sal+Halo vs Sal; (###)p<0.001 TG+Halo vs Sal+Halo). For statistical details see Table S5.





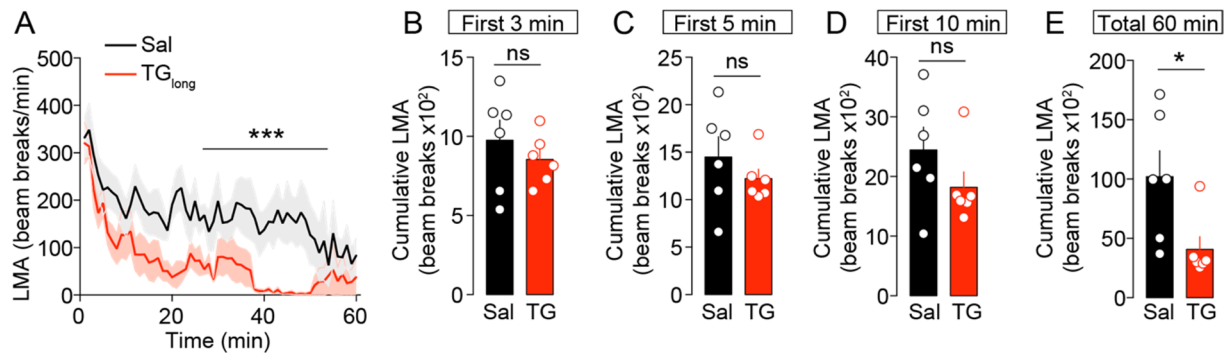


**Figure S5. Effect of central TG delivery on novelty-induced locomotor activity. Related to Figure 3.**

(A) Time course analysis of the locomotor activity (LMA) during the exploratory phase of a novel environment (new cage) following 6-hrs infusion of saline or TG. Cumulative analysis of exploratory activity following 3 (B), 5 (C), 10 (D) and 60 (E) minutes. Statistics (single or multiple comparisons): A (2-Way ANOVA: treatment effect \*\*\*p<0.001), E (\*p<0.05 TG vs Sal). For statistical details see Table S5.

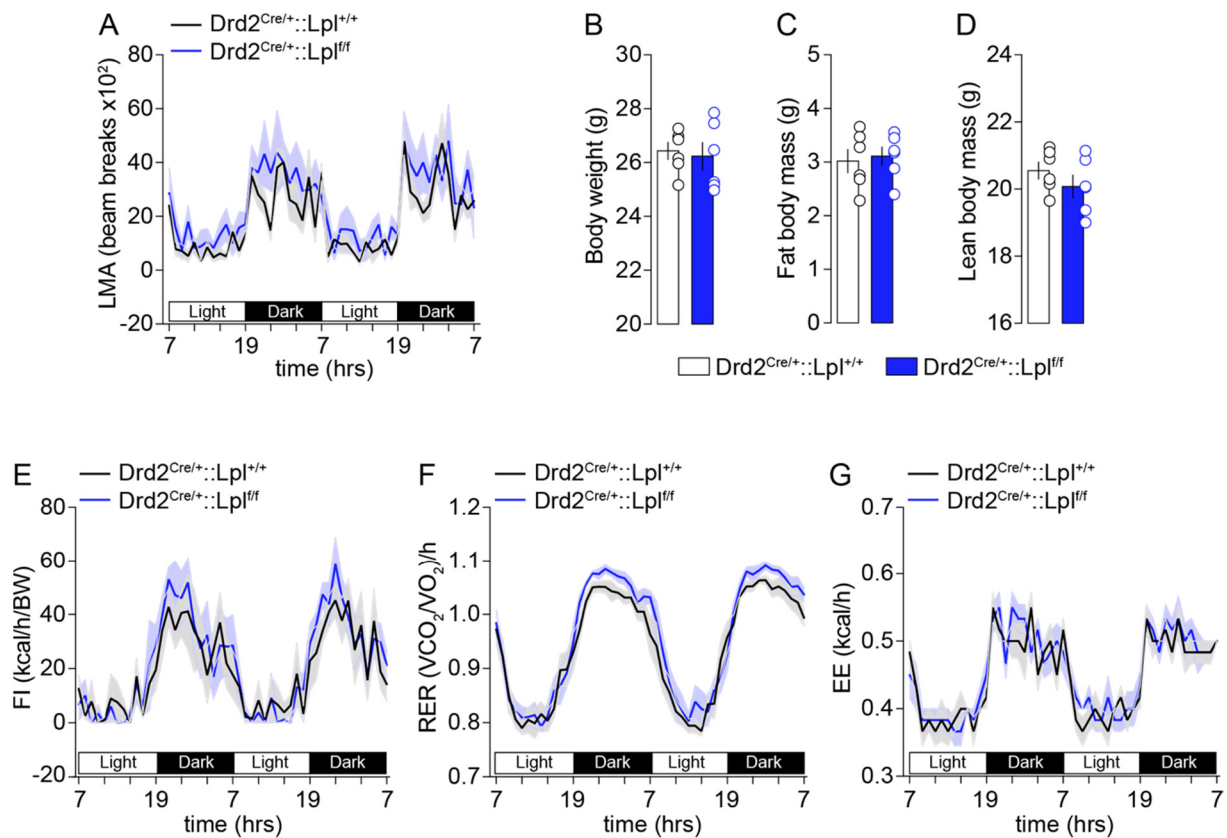


**Figure S6. Intact basal metabolism following genetic deletion of Lpl in DRD2-expressing cells. Related to Figure 6.**

(A) Locomotor activity in control ( $\text{Drd2}^{\text{Cre}/+};\text{Lpl}^{+/+}$ ) and cKO ( $\text{Drd2}^{\text{Cre}/+};\text{Lpl}^{\text{fl}/\text{fl}}$ ) mice during two consecutive days. Histograms indicate body weight (B), fat body mass (C) and lean body mass (D). Food intake (FI, E), respiratory exchange ratio (RER, F) and energy expenditure (EE, G) in control ( $\text{Drd2}^{\text{Cre}/+};\text{Lpl}^{+/+}$ ) and cKO ( $\text{Drd2}^{\text{Cre}/+};\text{Lpl}^{\text{fl}/\text{fl}}$ ) mice during two consecutive days. No differences were observed between experimental groups. For statistical details see Table S5.

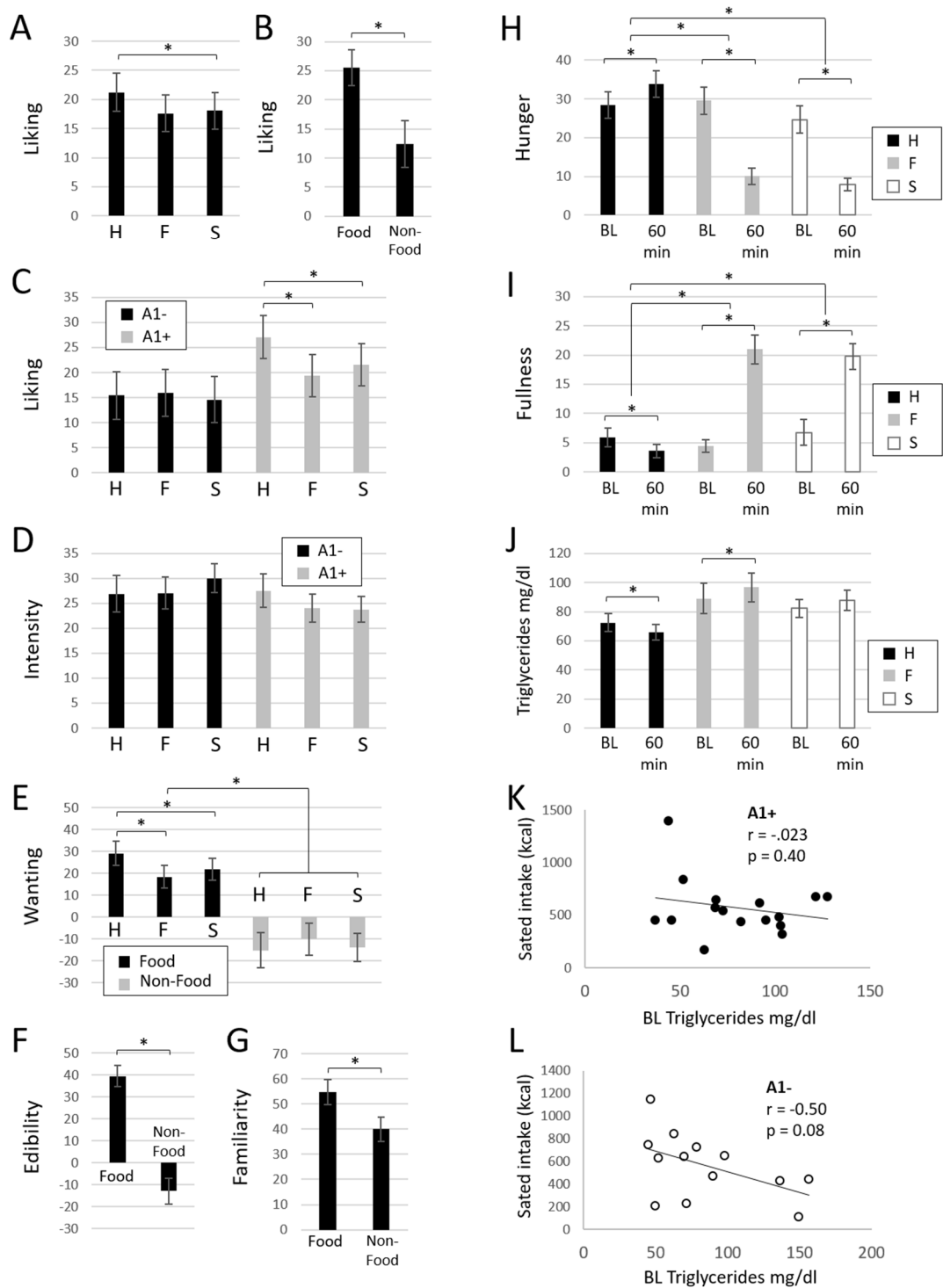


**Figure S7. Metabolic and internal state ratings in humans. Related to Figure 7.**

(A-C) Ratings of odor liking. There were significant effects of condition (A;  $F_{(2,54)}=3.78$ ,  $p=0.029$ ) and odor (B;  $F_{(1,27)}=13.18$ ,  $p=0.001$ ) as well as an interaction between condition and group (C;  $F_{(2,54)}=4.17$ ,  $p=0.031$ ). *Post hoc* tests revealed that liking ratings in Hungry condition

were greater than that in Sated condition ( $p=0.026$ ), and liking ratings for food odor were greater than ratings for non-food odor ( $p=0.001$ ). In the A1+ but not A1- group, liking ratings for all odors were greater in the Hungry condition than in Fixed ( $p=0.003$ ) or Sated ( $p=0.005$ ) conditions. **(D)** Ratings of odor intensity. There was a significant interaction between condition and group ( $F_{(2,54)}=3.21$ ,  $p=0.048$ ). However, post-hoc tests revealed no statistically significant pairwise comparisons. **(E)** Ratings of odor wanting. There was a significant effect of odor ( $F_{(1,27)}=35.72$ ,  $p<0.001$ ) as well as a condition by odor interaction ( $F_{(2,54)}=3.17$ ,  $p=0.05$ ). Post-hoc tests showed that wanting ratings for food odor were greater than that for non-food odor ( $p<0.001$ ), and that for food but not non-food odors, wanting ratings were greater under the Hungry condition than under Fixed ( $p=0.036$ ) or Sated ( $p=0.049$ ) conditions. **(F)** Ratings of odor edibility. There was a significant effect of odor ( $F_{(1,27)}=47.86$ ,  $p<0.001$ ) where edibility ratings for food odors were greater than those for non-food odors. **(G)** Ratings of odor familiarity. There was significant effect of odor on ratings for familiarity ( $F_{(1,27)}=23.32$ ,  $p<0.001$ ) where familiarity ratings for food odors were greater than those for non-food odors ( $p<0.001$ ). **(H)** Ratings of hunger. There were significant effects of condition ( $F_{(2,54)}=50.33$ ,  $p<0.001$ ) and time ( $F_{(1,27)}=26.03$ ,  $p<0.001$ ), as well as an interaction between condition and time ( $F_{(2,54)}=33.05$ ,  $p<0.001$ ). Hunger ratings increased from baseline to 60 min in the Hungry condition ( $p=0.031$ ), but decreased over the same time span in the Fixed ( $p<0.001$ ) and Sated ( $p<0.001$ ) conditions. **(I)** Ratings of fullness. There were significant effects of condition ( $F_{(2,54)}=36.13$ ,  $p<0.001$ ), time ( $F_{(1,27)}=62.70$ ,  $p<0.001$ ), as well as an interaction between condition and time ( $F_{(2,54)}=36.15$ ,  $p<0.001$ ). Fullness ratings decreased from baseline to 60 min in the Hungry condition ( $p=0.004$ ), but increased over the same time span in the Fixed ( $p<0.001$ ) and Sated ( $p<0.001$ ) conditions. **(J)** Circulating plasma triglyceride levels. There was a significant effect of condition ( $F_{(2,54)}=8.00$ ,  $p=0.001$ ) as well as a condition by time interaction ( $F_{(2,54)}=10.15$ ,  $p<0.001$ ). Triglyceride levels decreased from baseline to 60 min in the Hungry condition ( $p<0.001$ ) and increased over the same time span in the Fixed condition ( $p=0.010$ ). There was a trend towards an increase in triglycerides from baseline to 60 min in the Sated condition ( $p=0.055$ ). **(K)** TG level correlations with caloric intake in sated participants as a function of genotype. No relationship was observed in A1+ while a trend **(L)** was evident in A1-. This is despite the fact that there was no significant difference in intake calories from lunch in the Sated condition between groups ( $p=0.91$ ). Nevertheless, we elected to focus imaging analyses on the Fixed scan where intake is held constant. H = Hungry condition, F = Fixed condition, S = Sated condition; BL = baseline; 60 min = 60 min after meal or baseline. Error bars represent standard error of the mean. For statistical details see Table S5.

## Supplementary Tables

Glycerolipid	SAL (relative intensity/mg protein)	TG (relative intensity/mg protein)	p-value
54:4 TAG	0.06899	0.1007	0.0141
60:9 TAG	0.005516	0.008994	0.0189
52:4 TAG	0.0579	0.08414	0.0202
54:5 TAG	0.05881	0.07751	0.0287
38:5 DAG	0.2182	0.2913	0.0332
50:2 TAG	0.1099	0.1594	0.0332
56:6 TAG	0.162	0.2352	0.0379
50:0 TAG	0.3527	0.4922	0.04
56:4 TAG	0.0229	0.03254	0.0459
52:3 TAG	0.1152	0.1581	0.048
60:12 TAG	0.05009	0.08068	0.0481
50:3 TAG	0.01548	0.01944	0.0494
56:5 TAG	0.05221	0.06834	0.0533
52:2 TAG	0.3677	0.4823	0.0536
Total TAG	3.528	4.655	0.0649
54:1 TAG	0.07028	0.08915	0.068
50:1 TAG	0.4231	0.6237	0.0843
60:11 TAG	0.01862	0.02401	0.092
58:6 TAG	0.01411	0.01989	0.0938
48:1 TAG	0.06114	0.07601	0.0998

Free Fatty Acid	SAL (relative intensity/mg protein)	TG (relative intensity/mg protein)	p-value
18:3 N6	1.329	2.143	0.0216
20:3 N9	1.071	1.629	0.0554

**Table S1. Intracarotid TG delivery leads to change in striatal fatty acids and glycolipids content. Related to Figure 1 and S1.** Lipidomics analysis of significant TAG, DAG and FFA changes found in the striata of mice perfused with TG or saline. Raw data for fatty acids and glycolipids are provide in Data S1 & S2



	Dorsal striatum (DS)			
	DRD1-MSNs		DRD2-MSNs	
	Veh (n=15-17)	TG (n=10-11)	Veh (n=18-19)	TG (n=14-21)
<b>RMP (mV)</b>	-75.24 ± 1.43	-76.18 ± 1.27	-73.93 ± 0.77	-81.05 ± 0.63 ***
<b>Rheobase (pA)</b>	150.3 ± 15.64	173.5 ± 21.25	99.17 ± 8.59	124.5 ± 15.69
<b>Resistance (Mohm)</b>	93.49 ± 7.03	102.1 ± 13.0	126.9 ± 9.03	131.1 ± 15.28
<b>AP amplitude (mV)</b>	88.17 ± 4.23	92.93 ± 2.79	94.66 ± 1.57	91.15 ± 2.70
<b>Half width (ms)</b>	0.99 ± 0.03	1.03 ± 0.03	0.98 ± 0.03	1.08 ± 0.03 *
<b>AP threshold (mV)</b>	-34.74 ± 1.54	-36.37 ± 1.51	-38.22 ± 0.96	-36.03 ± 1.29
<b>fAHP amplitude (mV)</b>	15.19 ± 1.47	17.27 ± 1.91	18.12 ± 2.01	16.70 ± 1.18
<b>AP rise time (ms)</b>	0.31 ± 0.02	0.34 ± 0.01	0.27 ± 0.01	0.32 ± 0.01 *
<b>AP decay (ms)</b>	0.92 ± 0.03	0.93 ± 0.05	0.99 ± 0.04	1.05 ± 0.03
<b>SFA ratio</b>	0.848 ± 0.03	0.853 ± 0.03	0.91 ± 0.03	0.88 ± 0.03
<b>Time constant (ms)</b>	8.48 ± 0.85	7.09 ± 0.73	10.23 ± 0.59	7.88 ± 0.72 *

	Statistics (unpaired t-test)	
	DRD1-MSNs (Veh vs TG)	DRD2-MSNs (Veh vs TG)
<b>RMP (mV)</b>	p=0.649, t=0.4602 df=26	*** p<0.0001, t=7.241 df=37
<b>Rheobase (pA)</b>	p=0.379, t=0.8971 df=23	p=0.178, t=1.373 df=36
<b>Resistance (Mohm)</b>	p=0.532, t=0.6338 df=26	p=0.819, t=0.231 df=36
<b>AP amplitude (mV)</b>	p=0.414, t=0.8294 df=26	p=0.289, t=1.076 df=37
<b>Half width (ms)</b>	p=0.471, t=0.7317 df=26	* p=0.039, t=2.133 df=37
<b>AP threshold (mV)</b>	p=0.479, t=0.7175 df=26	p=0.194, t=1.322 df=37
<b>fAHP amplitude (mV)</b>	p=0.391, t=0.8716 df=26	p=0.535, t=0.627 df=37
<b>AP rise time (ms)</b>	p=0.177, t=1.388 df=26	* p=0.021, t=2.401 df=37
<b>AP decay (ms)</b>	p=0.842, t=0.201 df=26	p=0.200, t=1.304 df=37
<b>SFA ratio</b>	p=0.915, t=0.1078 df=26	p=0.556, t=0.5911 df=33
<b>Time constant (ms)</b>	p=0.261, t=1.149 df=26	* p=0.017, t=2.524 df=31

**Table S2.** Bath application of triolein affect DRD2-MSNs activity in the dorsal striatum. Related to Figure 3 and S4. Electrophysiological parameters of DRD1- and DRD2-MSNs in the dorsal striatum (DS) following bath application of triolein.

	<b>Nucleus Accumbens (NAc)</b>			
	<b>DRD1-MSNs</b>		<b>DRD2-MSNs</b>	
	<b>Veh (n=10)</b>	<b>TG (n=12-13)</b>	<b>Veh (n=13)</b>	<b>TG (n=15)</b>
<b>RMP (mV)</b>	-72.90 ± 2.23	-75.83 ± 1.92	-71.77 ± 2.24	-76.73 ± 1.13 *
<b>Rheobase (pA)</b>	90.83 ± 12.02	93.08 ± 14.07	116.0 ± 22.15	103.0 ± 9.63
<b>Resistance (Mohm)</b>	155.6 ± 23.84	205.3 ± 41.42	178.6 ± 27.49	123.4 ± 20.02
<b>AP amplitude (mV)</b>	92.06 ± 1.21	85.71 ± 1.91 *	91.36 ± 1.18	80.77 ± 2.42 ***
<b>Half width (ms)</b>	1.03 ± 0.04	1.11 ± 0.05	1.01 ± 0.03	1.02 ± 0.04
<b>AP threshold (mV)</b>	-38.80 ± 1.70	-34.79 ± 1.45	-35.63 ± 1.36	-34.76 ± 1.01
<b>fAHP amplitude (mV)</b>	14.19 ± 0.97	13.39 ± 0.67	13.89 ± 0.78	15.58 ± 1.46
<b>AP rise time (ms)</b>	0.27 ± 0.02	0.32 ± 0.02	0.26 ± 0.01	0.32 ± 0.01 *
<b>AP decay (ms)</b>	1.14 ± 0.06	1.09 ± 0.06	1.08 ± 0.05	0.99 ± 0.05
<b>SFA ratio</b>	0.91 ± 0.08	1.11 ± 0.09	0.89 ± 0.07	1.14 ± 0.08 *
<b>Time constant (ms)</b>	9.73 ± 1.31	11.34 ± 1.94	10.97 ± 1.63	10.84 ± 0.74

	<b>Statistics (unpaired t-test)</b>	
	<b>DRD1-MSNs (Veh vs TG)</b>	<b>DRD2-MSNs (Veh vs TG)</b>
<b>RMP (mV)</b>	p=0.328, t=1,002 df=20	* p=0.049, t=2.058 df=26
<b>Rheobase (pA)</b>	p=0.908, t=0.1167 df=21	p=0.576, t=0.5656 df=26
<b>Resistance (Mohm)</b>	p=0.336, t=0.9865 df=20	p=0.111, t=1.651 df=26
<b>AP amplitude (mV)</b>	* p=0.014, t=2.673 df=20	*** p<0.0001, t=3.748 df=26
<b>Half width (ms)</b>	p=0.263, t=1.153 df=20	p=0.807, t=0.2469 df=26
<b>AP threshold (mV)</b>	p=0.087, t=1.8 df=20	p=0.603, t=0.5261 df=26
<b>fAHP amplitude (mV)</b>	p=0.498, t=0.6897 df=20	p=0.337, t=0.9784 df=26
<b>AP rise time (ms)</b>	p=0.077, t=1.865 df=20	* p=0.014, t=2.631 df=26
<b>AP decay (ms)</b>	p=0.648, t=0.4681 df=20	p=0.211, t=1.281 df=26
<b>SFA ratio</b>	p=0.125, t=1.558 df=20	* p=0.031, t=2.285 df=26
<b>Time constant (ms)</b>	p=0.529, t=0,6412 df=19	p=0.945, t=0.06918 df=25

**Table S3. Bath application of triolein affect DRD2-MSNs activity in the Nucleus Accumbens. Related to Figure 3 and S4.** Electrophysiological parameters of DRD1- and DRD2-MSNs in the nucleus accumbens (NAc) following bath application of triolein.

	<b>Nucleus accumbens (NAc)</b>	
	<b>mCherry positive DRD2-MSNs</b>	
	<b>Control (n=33)</b>	<b>cKO (n=33)</b>
<b>RMP (mV)</b>	-78.58 ± 1.32	-75.11 ± 1.50
<b>Membrane capacitance (pF)</b>	84.08 ± 6.20	80.23 ± 4.98
<b>Resistance (MOhm)</b>	191.3 ± 14.63	225.1 ± 13.53
<b>Rectification index</b>	0.903 ± 0.007	0.8921 ± 0.006
<b>Rheobase (pA)</b>	64.24 ± 7.50	55.76 ± 4.73
<b>Delay to 1st spike (ms)</b>	292.5 ± 21.62	233.0 ± 20.78
<b>AP threshold (mV)</b>	-38.28 ± 0.72	-38.10 ± 0.77
<b>AP amplitude (mV)</b>	64.03 ± 1.87	62.88 ± 1.36
<b>AP duration (ms)</b>	5.28 ± 0.30	5.33 ± 0.22
<b>fAHP amplitude (mV)</b>	8.23 ± 0.56	7.97 ± 0.54
<b>AP rise (mV/ms)</b>	41.20 ± 2.55	40.02 ± 2.03
<b>AP decay (mV/ms)</b>	21.35 ± 1.95	18.47 ± 0.95

	<b>Statistics (NAc)</b>	
	<b>Unpaired t-test</b>	<b>Mann-Whitney test</b>
<b>RMP (mV)</b>	p=0.088, t=1.734 df=64	
<b>Membrane capacitance (pF)</b>	p=0.629, t=0.4844 df=64	
<b>Resistance (MOhm)</b>		* p=0.047, U=390
<b>Rectification index</b>		p=0.124, U=424
<b>Rheobase (pA)</b>		p=0.703, U=514.5
<b>Delay to 1st spike (ms)</b>	p=0.051, t=1.986 df=64	
<b>AP threshold (mV)</b>	p=0.866, t=0.1695 df=64	
<b>AP amplitude (mV)</b>	p=0.619, t=0.4993 df=64	
<b>AP duration (ms)</b>		p=0.568, U=499.5
<b>fAHP amplitude (mV)</b>	p=0.740, t=0.3333 df=64	
<b>AP rise (mV/ms)</b>	p=0.719, t=0.3614 df=64	
<b>AP decay (mV/ms)</b>	p=0.189, t=1.327 df=64	

**Table S4. *Lpl* expression regulates DRD2-MSNs excitability. Related to Figure 6.**  
Electrophysiological parameters of NAc DRD2-MSNs following genetic deletion of *Lpl*.